TECHNISCHE UNIVERSITÄT ILMENAU

PUCP

Anisotropy and Humidity Effect on Tensile Properties and Electrical Volume Resistivity of Fused Deposition Modeled Acrylonitrile Butadiene Styrene Composites

---

Bachelor: Carlos Ignacio Almenara Cueto

Thesis submitted for the degree of
Master of Science in Material Science and Engineering

Advisor, Ilmenau:
Dr. Ing. Rolf Grieseler
Dr. rer. nat. Thomas Kups
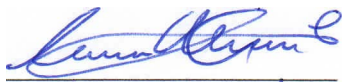
Advisor, Lima:
Dr. Ing. Francisco Rumiche

Supervising Professor, Ilmenau:
Univ.-Prof. Dr. rer. nat. habil. Peter Schaaf

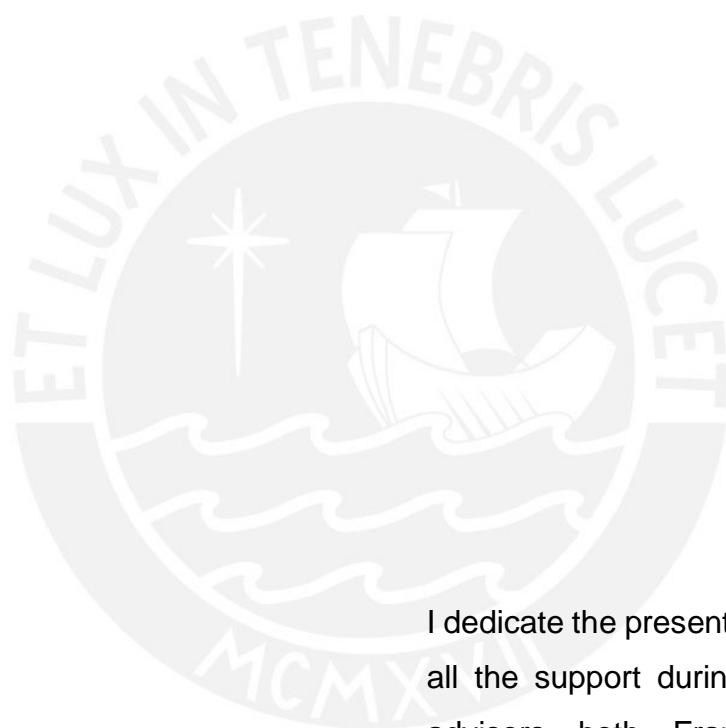**Lima – Perú**
2017

Statement

Hereby, I declare that I have elaborated the present work without any non-specified assistance. The people involved on this research, literature, as well as any other resource used in this thesis, has been completely specified throughout and at the end of the text.

15th July 2017, Lima

Carlos Almenara Cueto

I dedicate the present work to my family for all the support during the master, to my advisors both Francisco Rumiche at Pontificia Universidad Católica del Perú and Rolf Grieseler at Technische Universität Ilmenau, and to the laboratories that support my work: CITE de Materiales PUCP, Sala de Manufactura Digital VEO PUCP and Institut für Mikro- und Nanotechnologien MacroNano®.

Resumen

En la presente tesis, se estudió la influencia de la anisotropía y la humedad en las propiedades mecánicas a la tracción y la resistividad volumétrica de los compuestos de Acrilonitrilo Butadieno Estireno reforzado con Nano Tubos de Carbono y Acrilonitrilo Butadieno Estireno reforzado con Micro Fibras de Carbono impresos en 3D de por Deposición de Material Fundido.

Para estudiar la influencia de la anisotropía, tres diferentes orientaciones de impresión de capa fueron comparadas (0°, 45° and 45°/-45°) esto para una altura de capa de 0.2 mm. Se concluyó que la influencia de la anisotropía es importante para el comportamiento mecánico de el Acrilonitrilo Butadieno Estireno con Micro Fibras de Carbono esto debido a la relación que existe entre la resistencia que realiza el refuerzo y el alineamiento que presentan las fibras respecto a la dirección de tracción. Por otro lado, no se encontraron mayor influencia de la anisotropía en las propiedades mecánicas del Acrilonitrilo Butadieno Estireno con Nano Tubos de Carbono.

En la resistividad volumétrica para el Acrilonitrilo Butadieno Estireno con Nano Tubos de Carbono no se encontró mayor variación en los resultados debido a la anisotropía de las capas. El Acrilonitrilo Butadieno Estireno con Micro Fibras de Carbono no pudo ser ensayado debido a la alta resistividad que el material presentó.

Para estudiar la influencia de la humedad, dos condiciones del filamento se compararon: seco y expuesto a la humedad. Se concluyó que la influencia de la humedad en el filamento es también importante en el comportamiento mecánico a la tracción del Acrilonitrilo Butadieno Estireno con Micro Fibras de Carbono esto debido a que la humedad absorbida por el filamento se elimina a través de burbujas de vapor que explosionan durante la impresión 3D empobreciendo así la adherencia entre la fibra y la matriz polimérica. Por otro lado, no se encontró tampoco mayor influencia en el comportamiento mecánico a la tracción del Acrilonitrilo Butadieno Estireno reforzado con Nano Tubos de Carbono debido a la humedad.

En la resistividad volumétrica, se encontró que la humedad influye más en los resultados que la anisotropía, pero no llega a ser una influencia considerable. Esta influencia se debe principalmente a estructura menos uniforme que presenta el sólido impreso debido a las alteraciones producto de las explosiones de burbujas de vapor para eliminar la humedad absorbida como se mencionó anteriormente.

Abstract

In the present thesis, the influence of anisotropy and humidity in the tensile properties and electrical volume resistivity of Acrylonitrile Butadiene Styrene/Carbon Nanotubes and Acrylonitrile Butadiene Styrene/Micro Carbon Fibers manufactured by Fused Deposition Modeling 3D printing was studied.

To study the influence of the anisotropy three different layer printing orientations were compared (0°, 45° and 45°/-45°) in a layer height of 0.2 mm. It was concluded that the influence of anisotropy is important on Acrylonitrile Butadiene Styrene/Micro Carbon Fibers tensile behavior due to relation that exist between the performance/resistance and the alignment of the reinforcement. On the other hand, no significant influence was found on the Acrylonitrile Butadiene Styrene/Carbon Nanotubes.

On the electrical volume resistivity, no significant variation was found on the Acrylonitrile Butadiene Styrene/Carbon Nanotubes by the anisotropy of the layers. Acrylonitrile Butadiene Styrene/Micro Carbon Fibers could not be essayed because of the high resistance of the composite.

To study the influence of the humidity, two conditions on the filaments of the materials in study were compared: dry and moisture exposed. It was concluded that the influence of humidity is also remarkable on Acrylonitrile Butadiene Styrene/Micro Carbon Fibers tensile behavior because the humidity absorbed by the filaments is removed through vapor bubble blast during the 3D printing that impoverishes the adherence between the fibers and the matrix. On the other hand, no significant influence was again found on the Acrylonitrile Butadiene Styrene/Carbon Nanotubes.

On the electrical volume resistivity, the humidity influences more this attributed to the less uniform structure the specimens printed with moisture exposed filaments have because of the steam explosions mentioned before.

Kurzfassung

In der vorliegenden Arbeit wurde der Einfluss von Anisotropie und Feuchtigkeit in den Zugeigenschaften und dem elektrischen Volumenwiderstand von Acrylnitril-Butadien-Styrol/Kohlenstoffnanoröhren und Acrylnitril-Butadien-Styrol/Mikro Kohlefaser, hergestellt durch Schmelzschichtung Modellieren 3D-Druck, untersucht.

Um den Einfluss der Anisotropie zu untersuchen, wurden drei unterschiedliche Schichtdruckorientierungen (0 °, 45 ° und 45 ° / -45 °) in einer Schichthöhe von 0,2 mm verglichen. Es wurde festgestellt, dass der Einfluss der Anisotropie bei Acrylnitril-Butadien-Styrol/Mikro Kohlefaser zugverhalten aufgrund der Beziehung zwischen der Leistung / dem Widerstand und der Ausrichtung der Bewehrung wichtig ist. Auf der anderen Seite wurde kein signifikanter Einfluss auf die Acrylnitril-Butadien-Styrol/Kohlenstoffnanoröhren gefunden.

Bei dem elektrischen Volumenwiderstand wurde keine signifikante Variation auf der Acrylnitril-Butadien-Styrol/Kohlenstoffnanoröhren durch die Anisotropie der Schichten gefunden. Acrylnitril-Butadien-Styrol/Mikro Kohlefaser konnte wegen der hohen Beständigkeit des Verbundwerkstoffes nicht aufgeschrieben werden.

Um den Einfluss der Feuchtigkeit zu untersuchen, wurden zwei Bedingungen auf den Filamenten der Materialien in der Studie verglichen: trocken und Feuchtigkeit ausgesetzt. Es wurde festgestellt, dass der Einfluss der Feuchtigkeit auch bei Acrylnitril-Butadien-Styrol/Mikro Kohlefaser-Zugverhalten bemerkenswert ist, da die von den Filamenten absorbierte Feuchtigkeit durch Dampfblasenblasen während des 3D-Druckens entfernt wird, was die Haftung zwischen den Fasern und der Matrix verarmt. Auf der anderen Seite wurde auf der Acrylnitril-Butadien-Styrol/Kohlenstoffnanoröhren kein signifikanter Einfluss gefunden.

Bei dem elektrischen Volumenwiderstand beeinflusst die Feuchtigkeit mehr, was auf die weniger einheitliche Struktur zurückzuführen ist. Die mit feuchtigkeitsbelichteten Filamenten bedruckten Proben haben wegen der zuvor erwähnten Dampfexplosionen.

Index

Equations

Figures

Tables

Abbreviations

- **ABS**   Acrylonitrile-butadiene-styrene
- **CF**   Carbon fibers
- **mCF**   Micro or short carbon fibers
- **CNT**   Carbon nano tubes
- **MWCNT**   Multi walled carbon nano tubes
- **ABS/mCF**   Composite with matrix of acrylonitrile butadiene styrene and reinforcement of micro carbon fibers
- **ABS/CNT**   Composite with matrix of acrylonitrile butadiene styrene and reinforcement of carbon nano tubes
- **Wt%**   Percentage in weight
- **3D**   Three dimensions
- **3D Printing**   Three-dimensional printing
- **AM**   Additive Manufacturing
- **FDM**   Fused deposition modelling
- **PNCs**   Nano composite polymers
- **PMCs**   Micro composites polymers
- **H^L**   Layer height of FDM specimens
- **O°**   Layer printing orientation of FDM specimens
- **DSC**   Differential Scanning Calorimetry
- **TG**   Thermogravimetric
- **TGA**   Thermogravimetric Analysis
- **FTIR**   Fourier transformed infrared spectroscopy
- **DTG**   First derivative of the thermogravimetric
- **SEM**   Scanning electron microscope
- **FESEM**   Field emission scanning electron microscope

1. Introduction

Fused deposition modeling (FDM) is one of the most common techniques of Additive Manufacturing (AM) for polymers. Automatized FDM or FDM 3D printing is a digital controlled manufacturing process that allows to build three dimensional solids digitally designed by adding materials layer-by-layer [1].

This modern manufacturing process has a promising potential which lies on the fact of building objects with complex shapes, not much workforce needed and minimal use of harmful chemicals [2][3][4][5] in a life cycle of manufacture with reduced costs, low energy consumption and low CO^2 emissions, in comparison to traditional plastics manufacturing processes [6][7].

The raw materials involved in the process are typically thermoplastic polymer filaments that are extruded thought a nozzle generating a solid according to the driver commands set up.

Since the beginning, most commonly used filaments have been acrylonitrile-butadiene-styrene (ABS) and polylactic acid (PLA), but nowadays highly sought Nylon, polyether ether ketone (PEEK), glycol-modified polyethylene terephthalate (PETG), polycaprolactone (PCL) and polycarbonate (PC) are also used [8][9][10][11][12]. These are materials that in all the cases have shown limitations in mechanical properties, as this is one of the main limitations of the FDM technique [13][14][15].

Recently, industry and academy have started to research composite materials for this automatized manufacturing processes with the objective of fulfilling an important target in materials science and engineering: conceiving a material with great mechanical properties and with the lowest possible weight [16].

This focus of research has recently led FDM 3D printing researchers towards polymer nano- (PNCs) and micro composites (PMCs) because of the singular properties that can be obtained, particularly with reinforcements such as carbon nanotubes [17], graphene [13], nanoparticles of TiO^2 [15], fumed silica [18], nano clays [19], short jute fibers [15], micro glass fibers [20] and micro carbon fibers [14].

11

Scientific literature about ABS based micro- and nanocomposites for FDM 3D printing is still modest, with only few articles from the last years [13][14][15][17]. Even worse is the case of specific ABS micro carbon fiber and carbon nanotube composites publications [14][17].

This is not the case for carbon nanotubes (CNT) and micro or short carbon fibers (mCF), as isolated materials, of which many publications can be found on the literature showing the potential benefits that they can provide to a matrix for improving properties such as: mechanical resistance, thermal conductivity, thermomechanical resistance, electric conductivity, thermal diffusion and damping resistance [21][22][23][24][25].

Recent published papers about carbon nanotubes and micro carbon fiber composites by FDM [14][17] focus specifically on the mechanical resistance comparison and on differential scanning calorimetry analysis (DSC), which is essential for establishing the optimal temperatures of extrusion in the manufacturing process.

In the present thesis, and with the aim of contributing further to the field, the influence of anisotropy and humidity in the tensile properties and electrical resistance of ABS/CNT and ABS/mCF manufactured by FDM 3D printing was studied.

The influence of anisotropy was decided to be evaluated based on the fact that layer printing orientations and the heat introduced on each one of them could influence the internal structure and polymer chains arrangement; which in turn could affect the mechanical behavior, the alignment of the reinforcements and the electrical resistance.

On the other hand, the influence of the humidity was decided to be analyzed because even if recommendations and literature specify the usage of dry filaments, some environments present high moisture, which leads to the absorption of water. This could affect the internal structure and the interaction between the matrix and reinforcements; which could also affect the mechanical behavior, the alignment of the reinforcements and also the electrical resistance.

The analysis was made in five different layer deposition orientation, two layer heights and with or without moisture exposition of the filaments, only in horizontal building orientation, based on previous knowledge reported in many studies [13][14][15][17].

2. Literature Review

2.1 Additive manufacturing and fused deposition modeling

"Additive Manufacturing or also called 3D printing is a modern process of manufacturing by which digital 3D design data is used to build up a component in layers by depositing material" (taken from reference [26]).

The interest in AM is mainly based on the high flexibility that the process involves, avoiding the necessity of a die and tooling for building a different object [27].

Currently the process involves a low rate of production, low quality and high cost for large-scale production, in comparison to traditional polymer manufacturing processes such as injection molding or extrusion [27].

As can be seen in Figure 1, having a large-scale production or zero customization makes the traditional polymer manufacturing cheaper than the AM because the costs of the die and tooling are shared by all the products done. If a customized product is needed and low-scale productions are considered, then the costs of traditional manufacturing die and tooling must be assumed by the few products done making this process much more expensive.
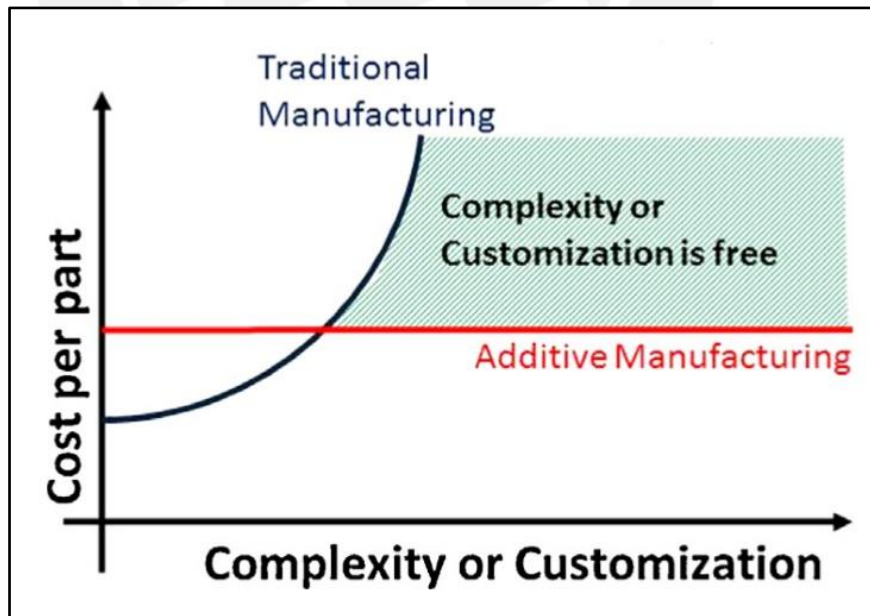
Figure 1. Diagram costs per part versus customization for traditional and additive manufacturing [27]

Conner et al. defined groups of manufacturing according to the volume of production, the complexity of the product and the customization of it. They claimed that AM could redefine the price of value and scale on the future based on a matrix of three axis (Figure 2), where the axis are the potential that flexibility should achieve for a complete manufacturing freedom [27].
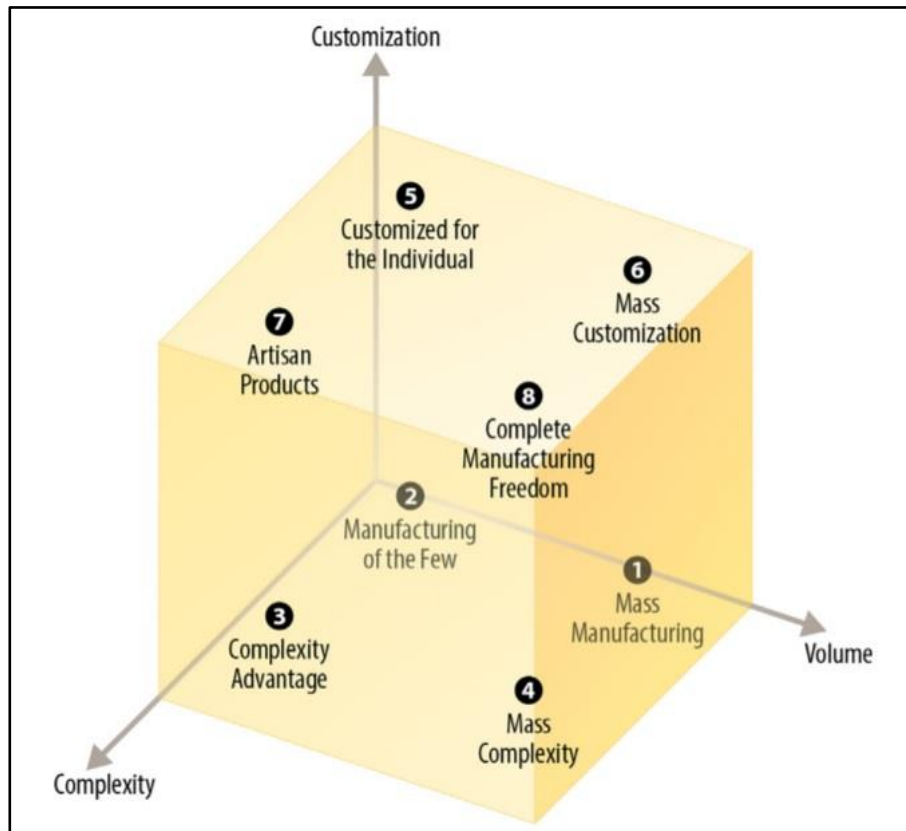
Figure 2. Analysis diagram for complexity, customization and volume of manufacturing [27]

Additive manufacturing is also promising because of the low energy the process involves. The required energy is purely electrical which can be obtained from renewable sources such as solar panels [28].

In a recent study by Gebler et al. it was concluded that this technology can lead to cost reductions, energy savings and reduced CO2 emissions: "The energy and CO_2 emission intensities of industrial manufacturing are reducible by maximally 5% through 3D printing by 2025" [29].

15

Motivated by the advantages these modern manufacturing process can achieve, in the last years many researchers have focused on 3D printing. Recently, efforts have been directed towards finding improvements and diversification of the properties the generic printing materials have, with the introduction of fillers with unique properties and by blending materials exhibiting different properties to generate high performance composites [30][31].

3D printing processes nowadays in the industry are manifold: vat photo polymerization, material jetting, binder jetting, material extrusion, sheet lamination, powder bed fusion and direct energy deposition [26]. Given that the present thesis is based on the study of acrylonitrile butadiene styrene (ABS) based composites for 3D printing by material extrusion, this process is shown in detail.

3D printing by material extrusion is also called fused deposition modeling or FDM because the process involving the heating of the polymer filaments over the melting point to dispense it through a nozzle as an extrusion, which then solidify in the selected orientation in one layer. This process is repeated layer by layer (Figure 3)[5].
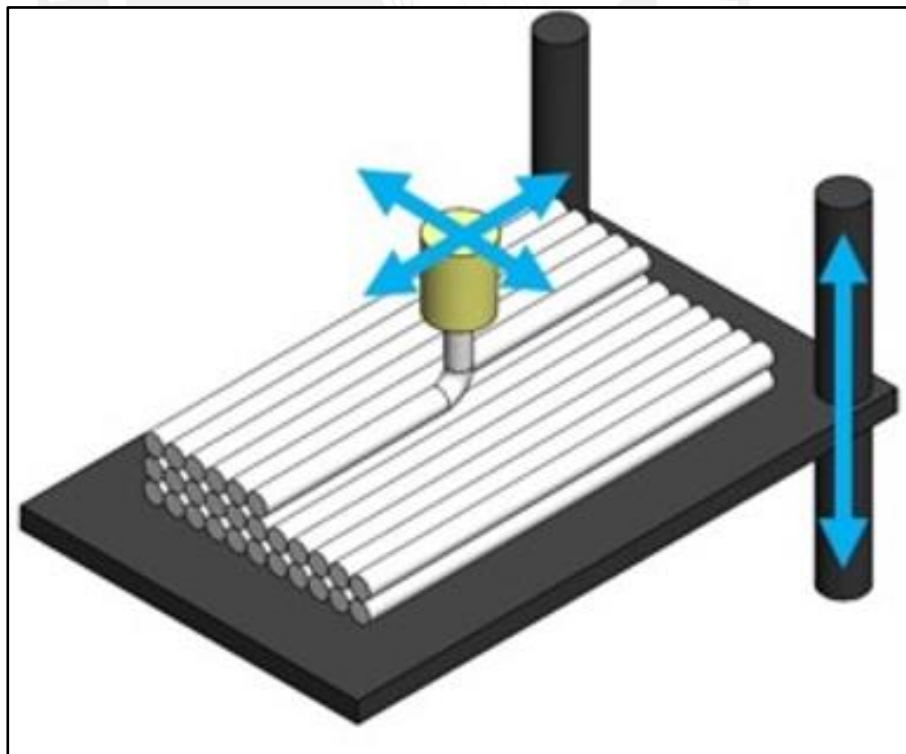
Figure 3. Representation of the fused deposition modeling process [5]

16

The steps to reach a finished product by FDM involves eight stages as described by Gibson et al. (Figure 4) [32]:

1. Drawing a CAD design
2. Converting it into a solid in STL format
3. Transfer the file to the machine by a printer driver
4. Setup the printer and parameters using the same driver
5. Building or manufacturing the product
6. Removing it from the deposition bed
7. Post processing if needed as removing support material and superficial finishing
8. Product is ready for application
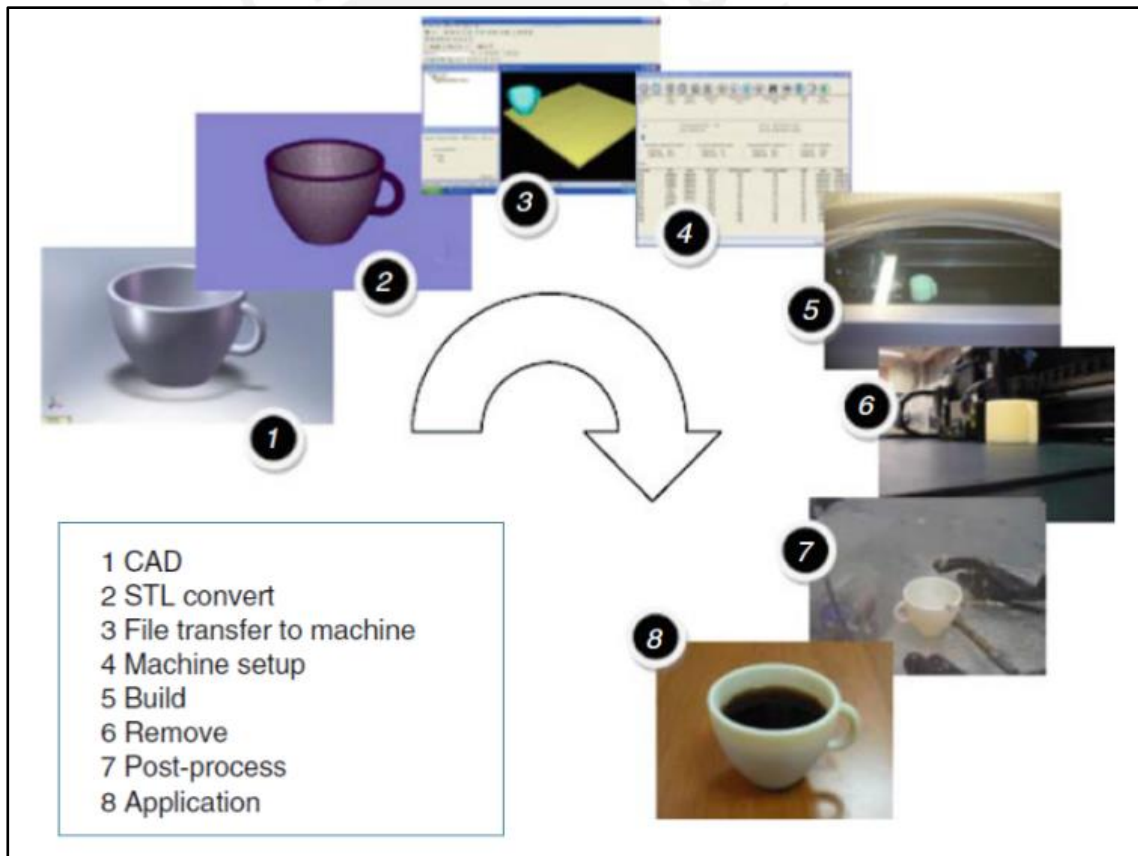
Figure 4. Stages for building a product by 3D printing [32]

To finish this topic review it is important to mention the achievements that this process could reach in medicine. Many investigations with different materials such

as ceramics, plastics and metals are developed on bone tissues, bone regeneration, implants, organs, skin tissues and prosthesis.

The main advantage of the FDM process for building body parts replicas, as already mentioned, is that all the persons are different and customization is really important and, furthermore, should be as fast and as easy as possible [33][34][35][36][37][38].

2.2 Acrylonitrile Butadiene Styrene

Since the scientific discovery of the polymers in 1907 by Leo Baekeland, the interest in these materials have been in continuous growth both for research and applications purposes [39].

Main advantages of polymers are their easy manufacturing, ow density, electrical insulation and immunity to corrosion. On the other hand, their disadvantages are the low elasticity modulus, intermediate to poor chemical resistance, low temperature of degradation and low color stability in many cases [40].

The Acrylonitrile Butadiene Styrene (ABS), topic of the present thesis, is a thermoplastic with an important market share [41]. It is listed as an engineering plastic formed by acrylonitrile, styrene liquids and butadiene gas in a variety of ratios to form a family of resins characterized by their high impact resistance, toughness, rigidity and processability, but low dielectric strength, continuous service temperature and elongation (Table 1) [42].

ABS development was done by grafting styrene-acrylonitrile copolymer (SAN) onto semi cross-linked particles of polybutadiene (PBD). The PBD component of ABS increases the impact strength compared to pure SAN. Later, developments during the 1960s led to a variety of methods to obtain ABS, including bulk, emulsion and suspension polymerizations, although emulsion processes (free-radical polymerization of styrene and acrylonitrile in the presence of PBD or butadiene copolymers) are still the most widely used [41].

A typical ABS formulation contains <15 wt% of butadiene and <20 wt% of acrylonitrile. The morphology of an ABS resin aided by staining the unsaturated sites

of the butadiene component is shown in Figure 5. The form of the unsaturated stains of butadiene can vary with the production process [41].

The immiscibility of PBD with SAN results always in phase separation where PBD is dispersed in the form of small particles into a matrix of styrene-acrylonitrile copolymer (Figure 5). Rubber particles produced by bulk or suspension processes are larger (0.5 to 5 µm) than those produced by emulsion methods (0.1 to 1 µm). Important to notice is that graft polymerization of SAN and PBD provides good interfacial adhesion between the dispersed material and matrix phases [41].

When ABS is mechanically deformed in different manufacturing processes, the PBD particles act to modify the deformation process by either promoting crack formation or shear yielding. As a result, the total energy-to-fail needed for ABS is increased compared to the unmodified SAN [41].

In Figure 5 a scanning electron microscope (SEM) micrograph of a section cut parallel to the surface of a deformed sample of ABS is shown. The arrow in red shows the direction of the applied strain. The dispersed phase or dark region represents the PBD particles and the light-colored background represents the SAN matrix as mentioned before. Cracks appear as dark lines running across the image. These crack structures are orientated perpendicular to the strain direction and pass through several PBD particles [42].

19

Due to the easy processability of ABS, it can be manufactured by extrusion, blow molding, thermoforming, calendaring and injection molding [43]. For example, in the present research all the ABS based raw materials for the FDM 3D printing were filaments manufactured by extrusion forming, in diameters of 1.75 mm as most printers request.

The ABS is classified according to its performance as an intermediate resin, which is higher ranked than commodity resins but lower then engineering resins and high performance engineering resins. It is used for applications like appliance housing, refrigerator liners, safety helmets, tubing, telephone handsets and luggage [44].

As first general reference, representative properties of a medium-impact grade ABS are shown in Table 1 [41][45]:

Table 1. Representative properties of ABS (medium-impact grade) [41][45]

Property (ASTM)	Values
Density (D792)	1.03 – 1.06 g/cm^3
Tensile strength (D638)	41 – 52 MPa
Tensile modulus (D638)	2.1 – 2.8 GPa
Elongation to break (D638)	5 – 25 %
Flexural strength (D790)	76 – 90 GPa
Flexural modulus (D790)	26-28 GPa
Impact strength notched Izod (D265)	160 – 320 J/m
Heat deflection temperature (D648)	102 – 107 kPa

With these reference data, ABS can be plotted in Ashby charts for selectivity and material selection [41][45]. One of the basics and very important chart is the strength versus density plot (Figure 6) where the ABS properties has been situated in the diagram with green lines [46].

The analysis of these chart should be made as guidelines displayed recommends: if a line is traced from 0 vertex to any material, the slope will describe the relation between the maximum strength reached and its density.
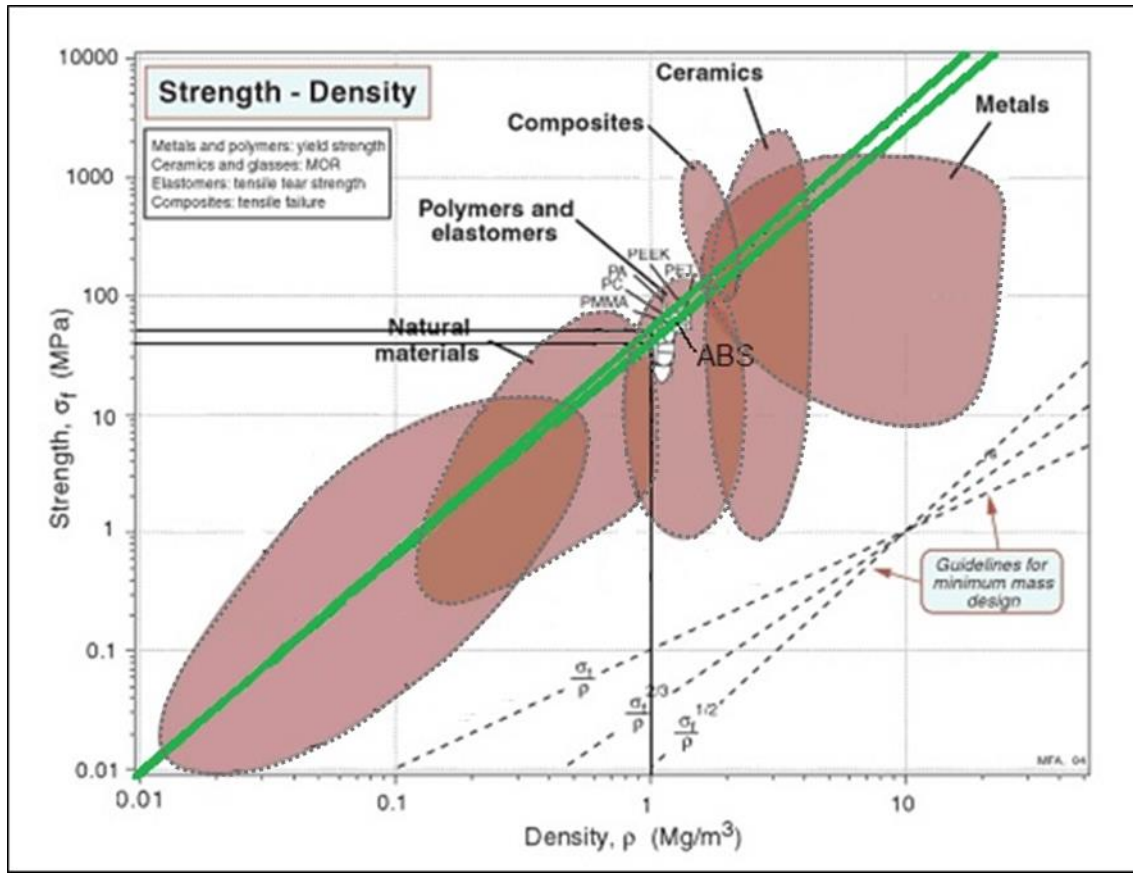
Figure 6. Ashby strength-density chart for material selection with ABS properties highlighted [46]

Also, a comparison using an Ashby chart can be done in final strength versus elastic modulus. The ABS Young's modulus is around 1.5 and 2 GPa [45]. This comparison is situated in the chart in Figure 7 where ABS data is displayed in green as well [47].
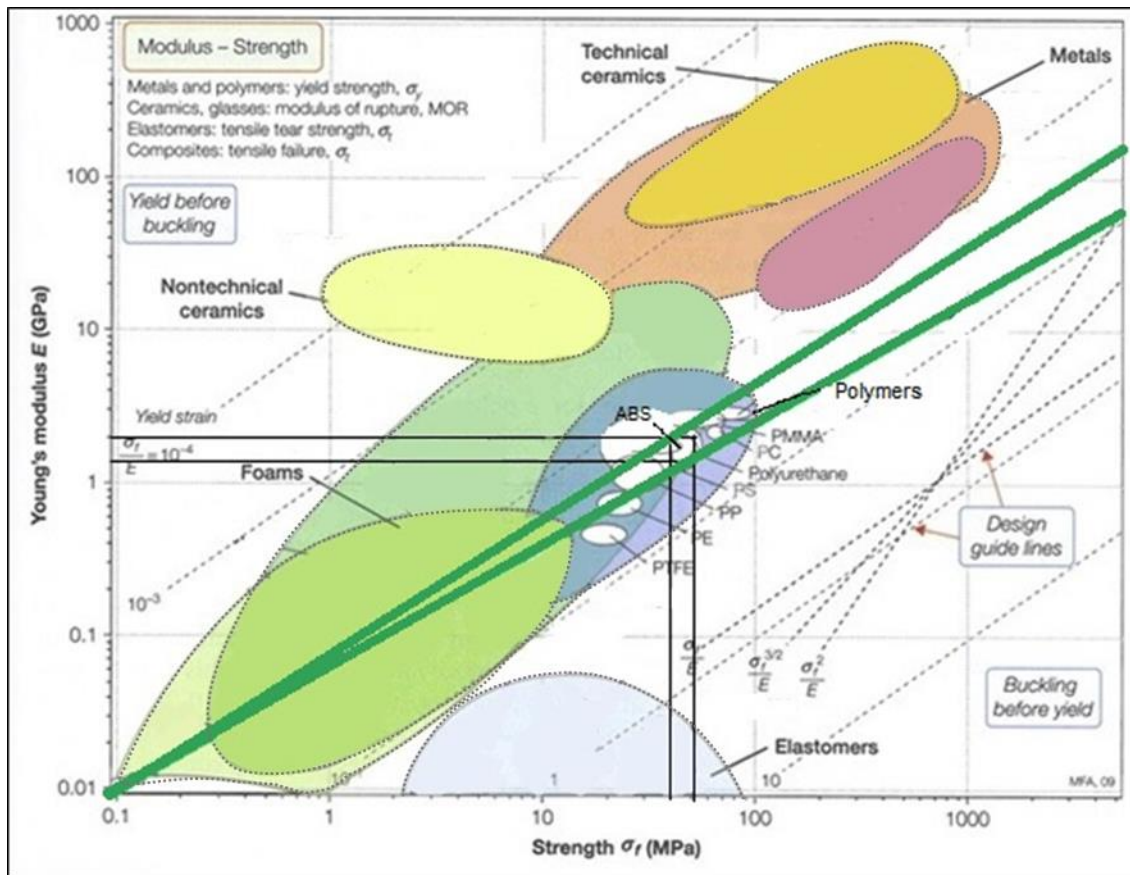
Figure 7. Ashby E modulus-strength chart for material selection with ABS properties highlighted [47]

With this general view of ABS, deeper and recent research works have been conducted looking for improvement on the mechanical behavior of this unreinforced thermoplastic polymer.

Many based ABS composites have been studied in the last years but not in the field of fused deposition modeling (FDM) by 3D printing [48].

When evaluating FDM 3D printing four points must be considered: production rate, quality, cost and flexibility [49]. This process can be described as one with low rate of production, intermediate surface quality which can be improved with a finishing of the printed object in acetone, low cost and sustainable process as well as with a high flexibility.

In the properties database of some polymers registered by Bryan Ellis and Ray Smith [47], pure extruded ABS can reach the properties described in Table 2.

23

Table 2.Extruded ABS properties values [47]

Property	Values	Observation
Volumetric and Calorimetric Properties		
Density	1.06 g/cm^3	ISO 1183
Melting temperature	230° - 250°	-
Glass-transition temperature	88° - 120°	-
Vicat softening point	92° - 101°	50 K h^{-1}, 50 N, ISO 306
Mechanical Properties		
Tensile modulus	1600 – 2700 MPa	1 mm min^{-1}, ISO 527
Tensile strength yield	35 – 45 MPa	50 mm min^{-1}, ISO 527
Flexural modulus	1800 – 2400 MPa	2 mm min^{-1}, ISO 178
Flexural strength yield	52 – 85 MPa	5 mm min^{-1}, ISO 178
Electrical Properties		
Surface/Volume resistance	0.01 – 1 x 10^{15} Ω.cm	IEC 93, Type S
Dissipation factor (power)	0.009 / 100 Hz	
	0.007 – 0.01 / 1 MHz	IEC 250

The same authors [41] summarize the properties values reached for a carbon fiber fabric composite with an ABS matrix made by injection molding in Table 3.

Table 3. ABS/Carbon fiber composites properties value [41]

Property	Values	Observation
Volumetric and Calorimetric Properties		
Density	1.12 g/cm^3	ASTM D792
Melting temperature	210° - 260°	-
Glass-transition temperature	100° - 110°	-
Mechanical Properties		
Tensile modulus	12409 – 13788 MPa	ASTM D638
Tensile strength yield	80 MPa	ASTM D638

Flexural modulus	6000 MPa	ASTM D790
Flexural strength yield	100 MPa	ASTM D790
Electrical Properties		
Surface/Volume resistance	$10^3 - 10^6$ Ω.cm	ASTM D257

It can clearly be seen that including carbon fibers lead to increase the tensile resistance and modulus, also this study shows that the surface/volume electrical resistance is clearly reduced going from an insulating material to a semiconductor one.

It must be understood, that this results are from a blend of a carbon fiber fabric and results cannot be compared with short carbon fibers composites because of the arrangement and performance that each one have.

2.3 Nano and micro composites in 3D printing

Recently, many Aditive Manufactruing companies have developed new materials, including new composites, for FDM. Most of these composites have a polymer matrix such as ABS or PLA (Polylactic Acid), even though this modern manufacturing technique is not exclusive for polymers matrix composites [49]. To set the present thesis into the current scientific context, investigations on micro and nano reinforcements for filaments for FDM are described briefly in the following section.

2.3.1   FDM carbon nanotubes composites

Carbon nanotubes (CNTs) are 1-D nanomaterial with the length as the only no nanometric dimension which are well known for their electric, thermal, damping, tensile properties and even fire resistance properties [50][51]. Since the beginning of this century, many researchers focus on study how CNTs could be used to improve different properties in polymer matrix composites, focusing on both mechanical [52] and electrical properties [53].

In latest investigations on CNTs/polymer composites, the target has been the study of the influence of the CNTS dimensions, oxidation states and concentration of the

25

reinforcement for the composites improvement. Wang et al. [52] concluded that electrical and thermal conductivity depends on the lengths of the CNTs, obtaining better conductivity for longer nanotubes. The mechanical resistance on the other hand does not depend on the CNTs length. Gardeas and Lagoudas [53] studied the electrical conductivity behavior varying the concentration of CNTs as well as their oxidation state. The conclusion of the investigation shows an improvement by 10 orders of magnitude concerning the electrical conductivity varying the reinforcements of pristine CNTs from 0.3wt% to 0.6wt% and by 6 orders of magnitude using as reinforcements oxidized CNTs in the same concentration range. Also an increase up to 5.5% was observed in the thermal conductivity using pristine CNTs while oxidized and fluorinated CNTs provide less enhancement.

3DX Tech©, a manufacturer of 3D printing composite filaments (www.3dxtech.com), without published results describes these composite filaments as having a consistent surface resistance, low particle contamination and minimal contributions to outgassing contamination. The typical applications described by the company include semi conductive and industrial applications such as HDD components, wafer handling, conveying, metering and sensing applications [54].

An investigation from the University of Tennessee was aimed to compare the tensile and thermal properties of PLA and MWCNTs/PLA composites (0.1, 0.2 and 0.5wt% of reinforcement) made by AM in a Lulzbot Mini Printer at layer orientations of 45°/-45°. This research concluded that PLA can reach moderate but not significant increase in mechanical properties with the additions of MWCNTs as reinforcement (Figure 8) [55].
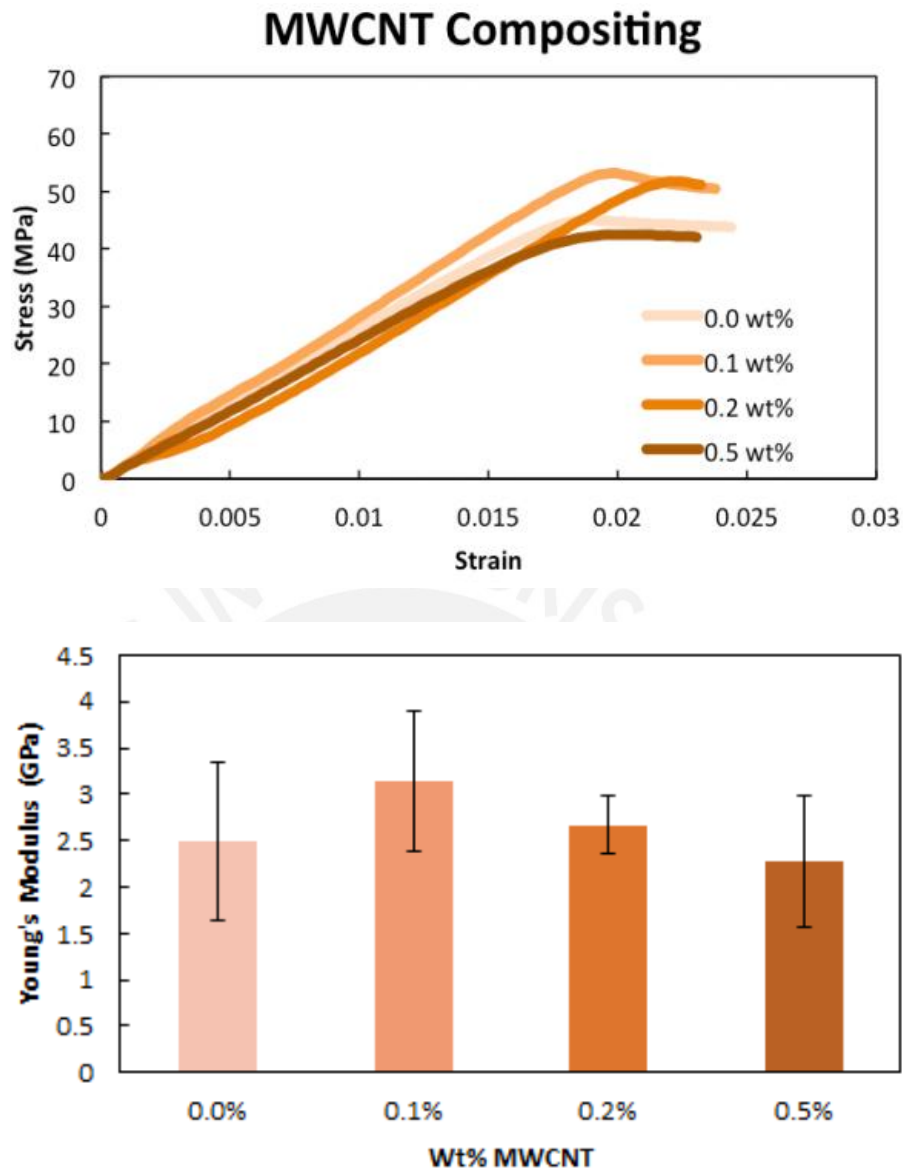
Figure 8. Tensile Stress and Young´s Modulus of PLA and MWCNTs/PLA composites of 0.1, 0.2 and 0.5 wt% [55]

For thermal properties DSC analysis was made showing that the addition of MWCNTs does not change the glass temperature, also no melt temperature was found because of the amorphous structure of PLA [55]. Results of DSC analysis are shown in Figure 9.
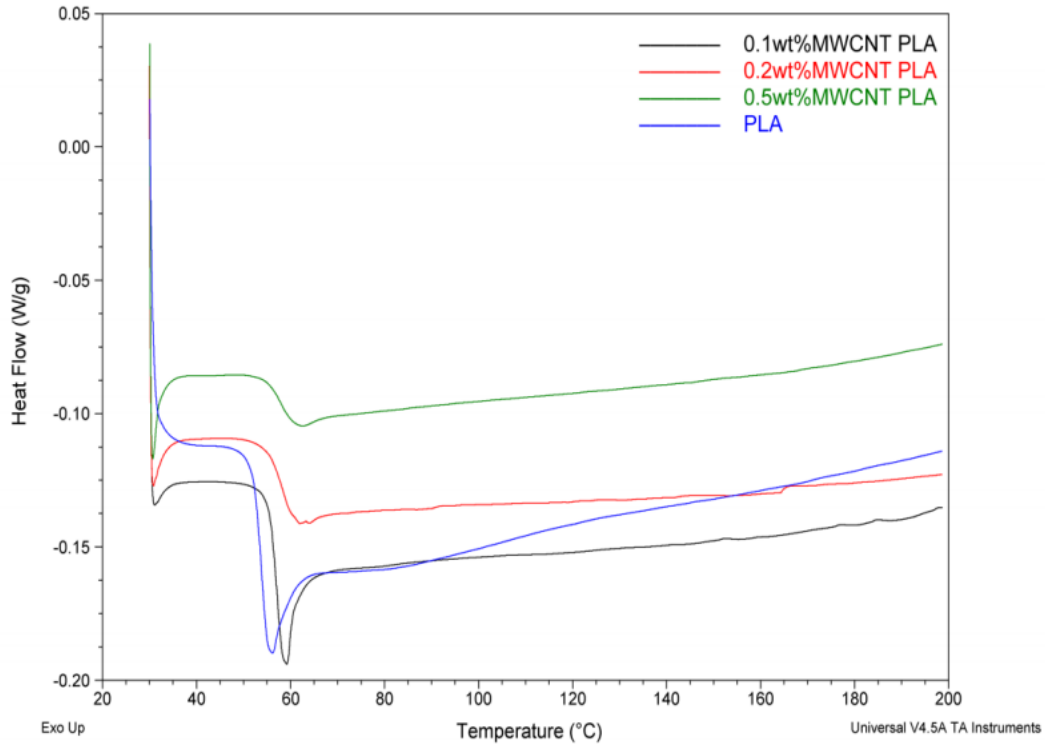
Figure 9. DSC curves of PLA and MWCNTs/PLA composites of 0.1, 0.2 and 0.5 wt% [55]

In Figure 10 SEM images of fracture surfaces are shown which led to the conclusion that due to the increase of bright spots on the surface of the composites a clustering of nanoparticles took part. This clustering indicates a good mixing in the PLA and indicates that even this failure mode did not lead to a loss in mechanical properties [55].
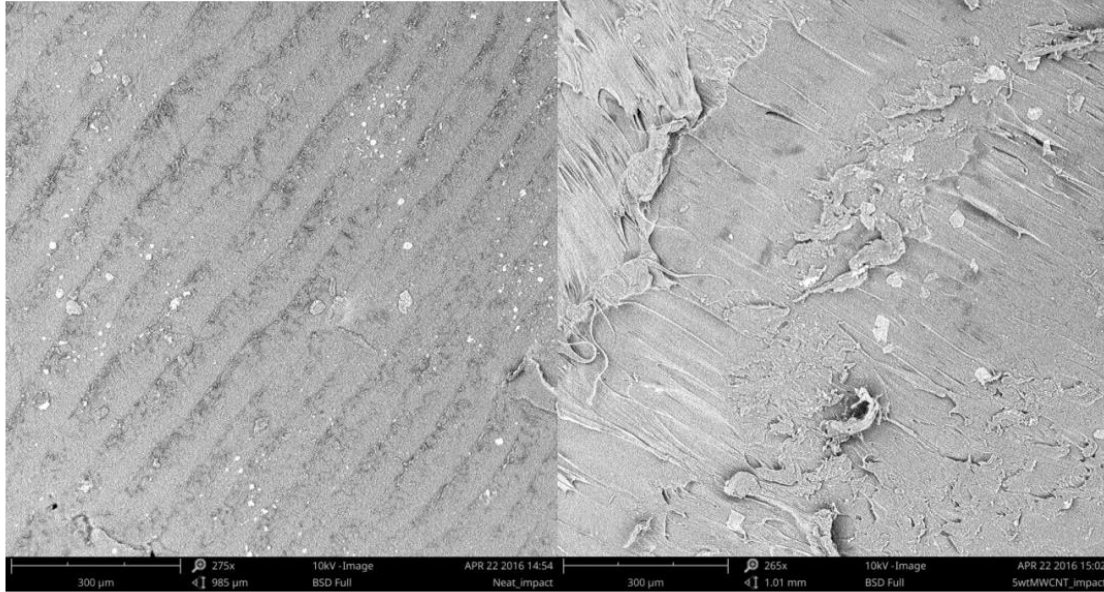
Figure 10. Fracture surface of PLA (on the left) and MWCNTs/PLA 5wt% (on the right) [55]

Nowadays many research groups are focusing their studies on this field as much as commercial producers of the 3D printing filaments.

2.3.2 FDM short carbon fiber composites

In the search for improvement or new properties for 3D printing products, researches also have been recently made in short fibers with the only restriction that the dimensions must be able to extrude [56].

A recently research from Texas Tech University compares the mechanical properties of short carbon fiber reinforced ABS, these short carbon fibers dimensions were 100-150 µm in length and 7.2 µm in diameter. The mechanical analysis was carried out to investigate the tensile and flexural properties concluding that the highest mean value of 42 MPa was found for 5wt% of reinforcement, as can be seen in Figure 11. It is also remarkable how the behavior changes with more addition of reinforcement showing a change in the failure mechanism of the ABS and carbon fiber reinforced ABS with 15wt% that have almost no ductility at failure force [57]. A SEM image is shown in Figure 12 where carbon fibers can be seen.
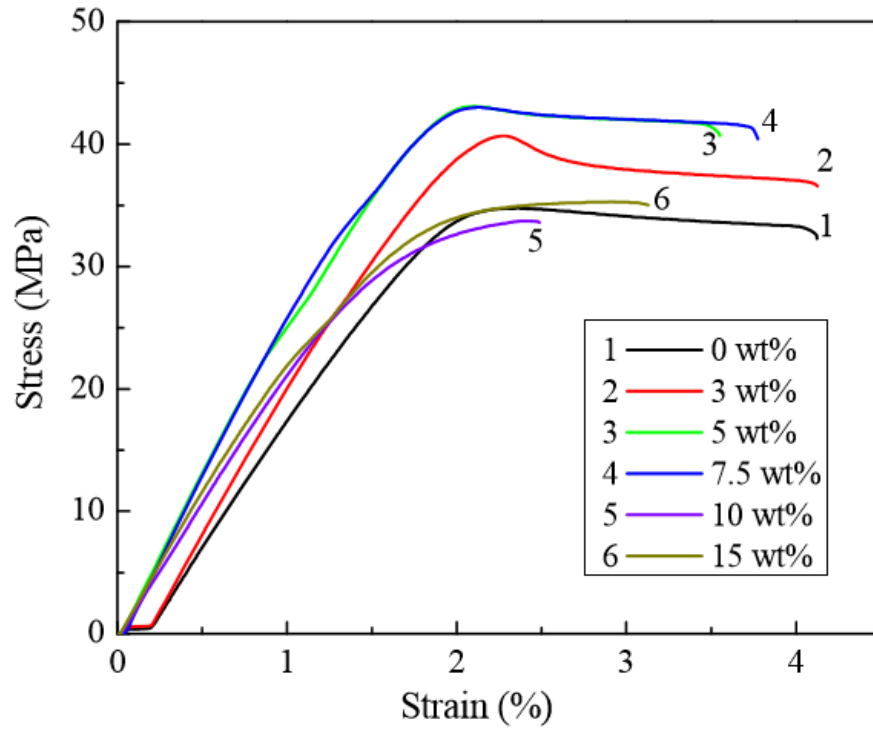
Figure 11. Stress-stain diagrams for ABS and ABS/short carbon fiber composites of 3, 5, 7.5, 10 and 15 wt% [57]
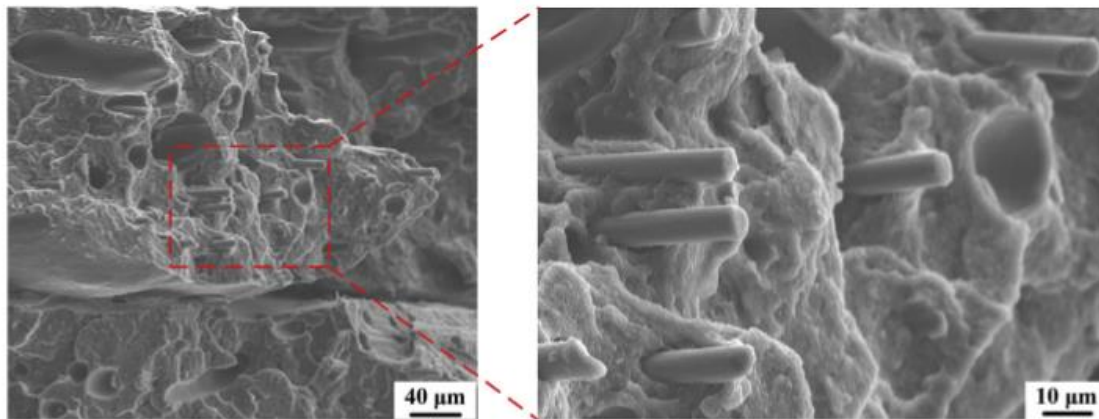
Figure 12. SEM image of 10 wt% ABS/short carbon fiber composite failure surface [57]

3. Theoretical Framework

3.1 Objectives

This thesis work is focused on investigating ABS matrix nano and micro composites as well as pure ABS as a basis of comparison for 3D printing by fusion deposition modeling (FDM), the objectives of the present thesis are outlined as follows:

3.1.1 Main objective

The main objective is to analyze how the deposition set-up or anisotropy and the humidity influence the tensile properties and the electrical resistivity of the fused deposition modeled Acrylonitrile Butadiene Styrene composites in study (FDM ABS/CNT and FDM ABS/mCF). Also pure ABS was analyzed as a base of comparison.

3.1.2 Specific objectives

- Determine the optimal parameters for the 3D printing of ABS and composites.

- Perform the structural and mechanical characterization of the ABS composites filaments for FDM 3D printing identifying their tensile properties and composition.

- Analyze the influence of the layer height and layer orientation of printing on the tensile properties of the ABS and composites.

- Analyze the influence of the reinforcements on electrical resistance of the ABS and composites.

- Analyze the influence of water absorption from moisture exposure on the tensile properties and electrical resistance of the ABS and composites.

- Analyze the influence of the layer height of printing as well as the influence of the water absorption from moisture exposure on the roughness and surface finishing of the ABS and composites.

4. Experimental Details

4.1 Materials

The materials used in this thesis work were: pure ABS, ABS reinforced with carbon nanotubes (ABS/CNT) and ABS reinforced with micro carbon fibers (ABS/mCF).

These materials were analyzed before and after the FDM 3D printing process during this study, having first the raw materials (FDM 3D printing filaments) and afterwards the final products (3D printed specimens).

The raw materials, FDM 3D printing filaments, were acquired from the company 3DXTech® as (www.3dxtech.com):

- commercial bright white 3DXTech™ ABS for the pure ABS
- 3DXNano™ ESD ABS as the composite ABS/CNT
- 3DXMax™ CFR ABS as the composite ABS/mCF

For the pure ABS, the company describes the bright white 3DXTech ABS as a filament prepared with MG-94 premium ABS with virgin resin and colorants, precision extruded and vacuum-sealed with desiccant to protect it from moisture. It is recommended for use with any FDM printers which requires filaments with diameters of 1.75 or 2.85 mm. For example, the printer used in the present thesis is a MakerBot Replicator 2X which work with diameters of 1.75 mm [58].

The recommended print conditions given are: extrusion temperature of 220-240°C, bed temperature of 100-110°C and a bed preparation with 3DXTech Polyimide Tape or ABS / Acetone Slurry [58]. In Figure 13 two tensile specimens made by FDM in layer heights of 0.2 mm (left) and 0.4 mm (right) both in 45° layer orientation and with the pure ABS filament described are shown.

Figure 13. FDM pure ABS tensile specimens

For the ABS/CNT, the company describes the 3DXNano™ ESD ABS as a composite filament made with MG-94 Premium ABS and then compounded according to a proprietary formulation of multi-wall carbon nanotubes and process/dispersion modifiers giving a filament with excellent printing characteristics and consistent electrostatic discharge (ESD) properties. It is recommended for the use with any FDM printers which requires filaments with diameters of 1.75 or 2.85 mm [59].

The company states that the target surface resistance varies between 10^7 and 10^9 Ω making this and advanced ESD-Safe compound designed for use in critical applications that require electrostatic discharge protection and a high level of cleanliness [59].

The recommended print conditions given are the same: extrusion temperatures of 220 - 240°C, bed temperature of 100-110°C and a bed preparation with 3DXTech Polyimide Tape or ABS / Acetone Slurry [59]. In this case the company specifies the melt viscosity is higher than pure ABS, being sometimes necessary to print at higher temperatures to allow the resin flow properly. In Figure 14 a filament of 1.75 mm diameter from the material described is shown.

33

Figure 14. ABS/CNT FDM filament (3DXNano™ ESD ABS)

For the ABS/mCF, the company describes the 3DXMax™ CFR ABS as a composite filament made with premium Sabic MG-94 ABS and 15wt% high-modulus carbon fiber (not carbon powder or milled carbon fiber). It is recommended for use with any FDM printers which requires filaments with diameters of 1.75 or 2.85 mm [60].

The company states the material is a high-performance carbon fiber reinforced ABS filament, ideal for anyone that desires a structural component with high modulus, excellent surface quality, dimensional stability, light weight and ease of printing [60].

The recommended print conditions given are the same: extrusion temperatures of 220 - 240°C, bed temperature of 100-110°C and a bed preparation with 3DXTech Polyimide Tape or ABS / Acetone Slurry [60]. In this case the company stipulates that is necessary a nozzle with a minimum 0.4 mm diameter orifice. In Figure 15 a filament of 1.75 mm diameter from the material described is shown.

Figure 15. ABS/mCF FDM filament (3DXMax™ CFR ABS)

4.2 Methodology and equipment

All ABS composites, ABS/CNT and ABS/mCF, were compared to the pure ABS to study the effect of the reinforcement. The selected parameters of the FDM 3D printing for the present thesis were the humidity absorbance and anisotropy in layer height of 0.2mm and the printing orientations of 0°, 45°, and 45°/-45°. The parameters in study were selected from a previous study made only with filaments exposed to moisture [61] and based on the current knowledge to follow the purpose of the present research.

Regarding the manufacturing process, the first step was the determination of the optimal parameters of printing for each material. The parameters selected were the temperature of extrusion and the speed of extrusion based on the materials specifications, published literature on the topic and the DSC-TG analysis performed in each filament.

With this knowledge, a first production of FDM 3D printed specimens was made in all the layer heights and printing orientations in study for each ABS based material,

35

with the filament exposed to the moisture for approximately three to four weeks (21 to 28 days).

Simultaneously, the water absorbed from the moisture exposed of each ABS based material filament was measured by a weight comparison and compared with the maximum absorption each material can reach to saturate, according to the ASTM standards [62].

Finally, a second production of FDM 3D printed specimens was made also in all the layer heights and printing orientations in study for each ABS based material dried filament. This drying was made following the ASTM standards for polymers which recommend a drying of 24 hours in a muffle at 50°C [62].

The selection of the printing orientations was based on the results from a previous study at PUCP [61] where a comprehensive set of orientations of printing was studied for the same materials filaments with the intention of analyzing the interaction between the reinforcements and the matrix.

A summary of all the materials in study is given in Table 4.

Table 4. Filaments and FDM 3D printed materials in study

Materials	Conditions	
Filaments (raw material)	Acrylonitrile Butadiene Styrene without any reinforcement (ABS)	
	Acrylonitrile Butadiene Styrene + Carbon Nanotubes (ABS/CNT)	
	Acrylonitrile Butadiene Styrene + short Carbon Fibers (ABS/mCF)	
FDM 3D Printed (final product)	ABS	Humidity = moisture exposed and dry
		Layer height = 0.2 mm
		Printing orientation = 0°, 45° and 45°/-45°
	ABS/CNT	Humidity = moisture exposed and dry
		Layer height = 0.2 mm

		Printing orientation = 0°, 45° and 45°/-45°
	ABS/mCF	Humidity = moisture exposed and dry
		Layer height = 0.2 mm
		Printing orientation = 0°, 45° and 45°/-45°

Each material filaments and all specimens manufactured were mechanical tested to determine the tensile properties (see section 4.2.5) and in the failure zone a structural characterization was performed by SEM, FESEM (4.2.6) and LSM (4.2.7) to determinate the interaction of the nano and micro reinforcement with the ABS matrix in all the cases. Figure 16 shows each material filaments and corresponding tensile specimens.
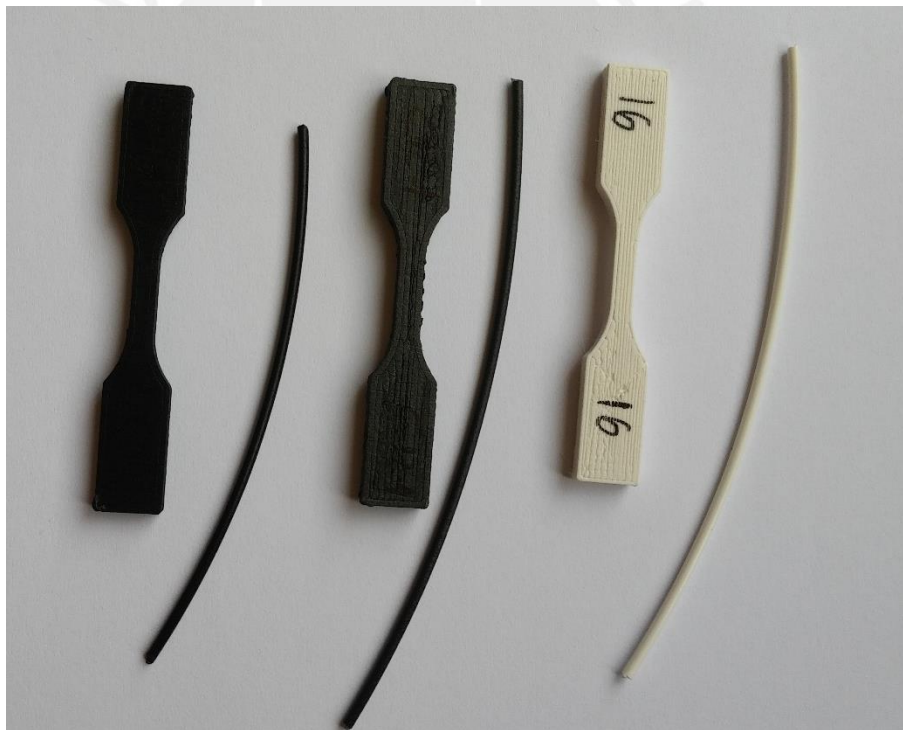
Figure 16. FDM filaments and FDM tensile specimens of ABS/CNT, ABS/mCF and ABS (from left to right)

To analyze the influence of the reinforcement on the electrical conductivity, a resistance essay was made on the manufactured specimens analyzing also the influence of the anisotropy and humidity (see section 4.2.8).

All these experiments were carried out at room temperature in the facilities of the polymer materials laboratory at Pontificia Universidad Católica del Perú and the Institute for Micro- and Nanotechnology (MacroNano®) laboratory at Technische Universität Ilmenau.

4.2.1 Differential Scanning Calorimetry and Thermogravimetric Analysis (DSC/TGA)

DSC/TGA was performed on the ABS composites samples with a mass of about 10 mg. The test was made under a nitrogen flow of 25 ml/min to have an inert atmosphere, and heated from 30ºC to 600ºC at a rate of 10ºC/min [13][17][55].

The first derivative of the thermo gravimetric data curve (DTG) was used to measure the concentration in weight of the reinforcements given the high degradation temperatures of the reinforcements compared to the one for ABS, which is around 430°C [39][50][57]. The equipment used was a Netzch 449 F3 Jupiter STA (*Figure 17*).

Figure 17. DSC/TG Netzch 449 F3 Jupiter STA

4.2.2 Fourier Transform infrared analysis (FTIR)

Filament samples were tested in the FTIR spectroscope with the aim of analyzing absorbance or transmittance spectrum from the infrared light applied verifying the polymer in study and identifying the effect of the reinforcements [43][44][68].

The FTIR spectra were recorded with the OPUS 7.0 software in a Bruker tensor27 spectrometer, using the Attenuated Total Reflection (ATR) mode, in a range of 400 – 4000 cm^{-1} with a resolution of 2cm^{-1}. The background was measure before testing the sample.

The equipment used was a FTIR spectroscope Tensor 27/ ATR Platinum – Brukerbalance, shown in Figure 18.

Figure 18. FTIR spectroscope Tensor 27/ ATR Platinum – Brukerbalance

4.2.3 Water absorption

The water absorption was analyzed on the three ABS based filaments following the recommendations of the ASTM standard test method for water absorption of plastics D570 [62].

The filament weight was measured in the dried state (24 hours at 50°C), and after 2 and 24 hours submerged in water at room temperature and superficially dried (Figure 19). Percentage of water absorbed is determined using the difference in weight

measured for the samples submerged in water and the dry specimens. The equipment used was a balance Mettler Toledo XS.

Figure 19. Imaging of the water absorption analysis (filaments water immersion and filaments weight)

4.2.4 FDM 3D printing and optimal printing parameters

The methodology described for 3D printing by FDM is similar for all the ABS based filaments in study. There do exist certain differences for the production processes of each material but all of these different parameters are summarized in the results for each material (see sections 5.2).

The specific methodology used in the present study for the 3D printing by FDM (Figure 20) involves the digital design of the object or specimens in .STL format with the Autodesk Inventor®. Afterwards, the driver Simplify 3D® was used to control and communicate with the 3D printer to set the different printing parameters. Finally, a MakerBot Replicator 2X® FDM 3D printer was used to print the samples (Figure 21).
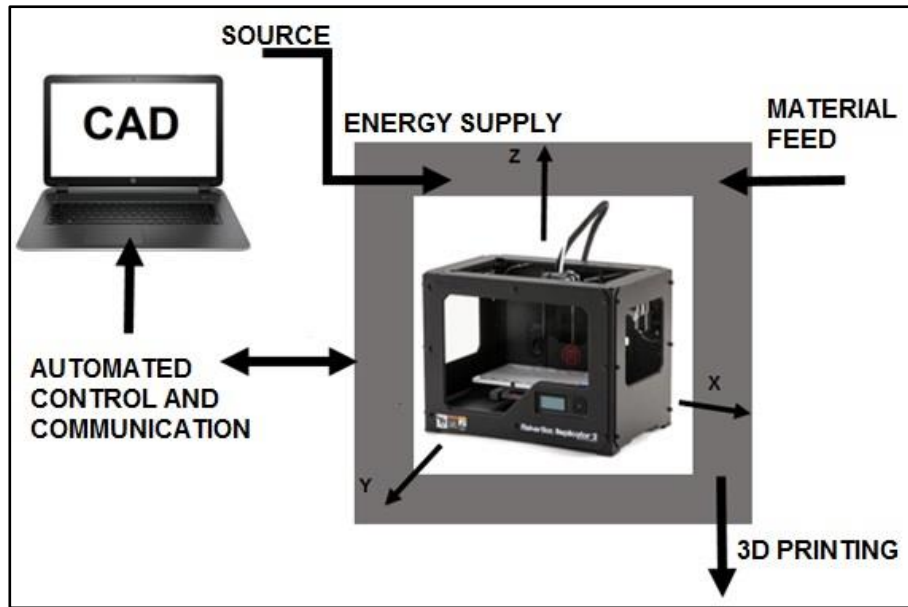
Figure 20. Diagram of the 3D printing by FDM process
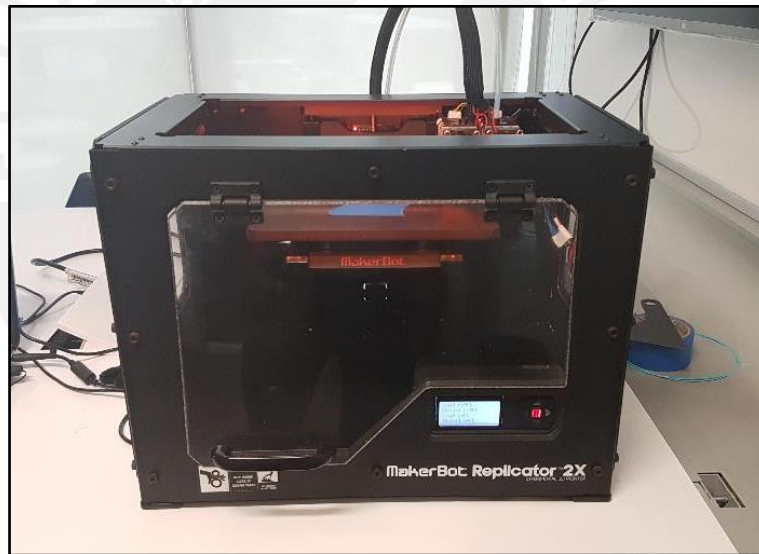
Figure 21. MakerBot Replicator 2X® FDM 3D printer

4.2.5 Tensile test

Tensile properties of the three ABS based filaments in study and 3D printed specimens were analyzed based on the ASTM standard test method for tensile properties of plastics D638 [63]. To determine the length of the filaments for the tensile test ASTM standard test method for tensile properties of fiber reinforced polymer matrix composite bars D7205 was used as support [64].

41

Specimens recommended in the standards for 3D printed materials are Type V which were modeled, printed and measured at 1 mm/min for the different variables studied based on the standards. Dimensions recommended for type V are shown in Figure 22.
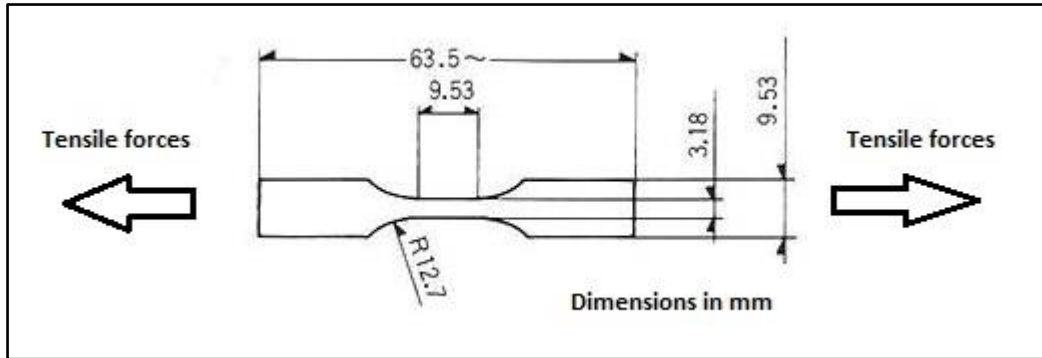
Figure 22. ASTM D638 type V tensile specimen

The filaments were tested at the same speed of deformation for a free length between the anchors of 40 times the diameter and a total length sufficient for adequate anchorage.

The equipment used was an Universal Tensile Machine Zwick/Roell Z050 (Figure 23, Figure 24).

Figure 23. Tensile test in FDM ABS/CNT specimen

Figure 24. Tensile test in ABS filament

4.2.6 Scanning Electron Microscope and Field-Emission Scanning Electron Microscope (SEM/FESEM)

Structure and reinforcements were analyzed by a scanning electron microscope (SEM) and field emission scanning electron microscope (FESEM).

The analysis was made with a Quanta 650 - FEI SEM microscope at Pontificia Universidad Católica del Perú at 10 kV recommended for insulating and semiconductor materials for better resolutions avoiding the accumulations of electrons in the surface analyzed [55][56][57]. At Technische Universität Ilmenau a Hitachi S4800 FESEM microscope was used for better resolutions also at 10 kV following the same recommendations (Figure 25).

Figure 25. SEM FEI Quanta 650 and SEM/FESEM Hitachi S4800 (from left to right)

4.2.7 Laser Scanning Microscope (LSM)

Failure and layers roughness were observed by using an OLS 300 Olympus confocal laser scanning microscope. LSM is based on an optical laser system which focus in a selected depth range allowing the caption of 3D surfaces, depth and intensity. In Figure 26 the equipment used is shown.
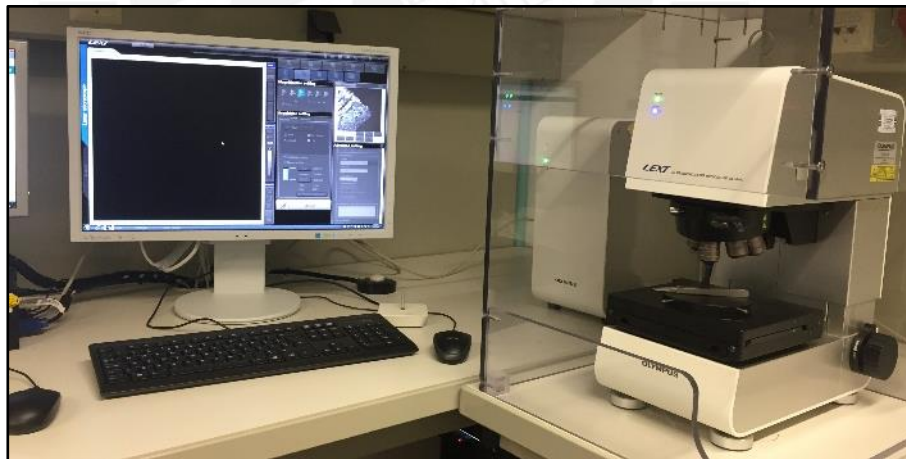
Figure 26. OLS 300 Olympus confocal LSM

4.2.8 Plastics volume resistivity test

To calculate the volume resistivity of the materials in study, ASTM D257[65] for measuring DC Resistance or Conductance in Insulating Materials was used on the FDM samples.

44

A NI SCB-68 device was fed with 10 V supply and resistance measurement was obtained by measuring the voltage across resistor support as electrical diagram shows (Figure 27).
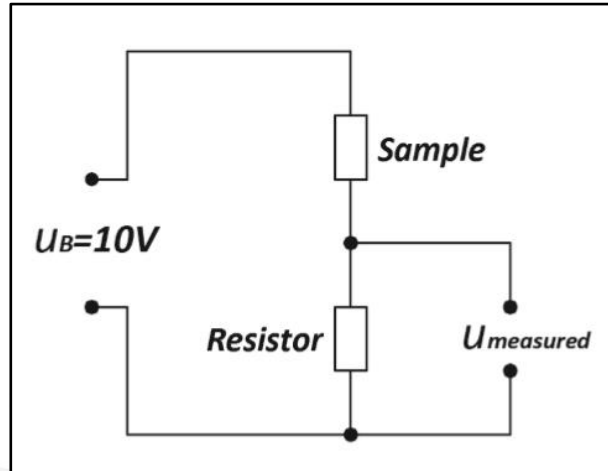
Figure 27. Electrical diagram for the volume resistivity test

Cooper plates of 10 x 8 mm and cables of d=0.4 mm were used with tin welding, resistance of these connectors was depreciated (Figure 28).

The measuring time for each specimen was 10 min. Two specimens for each printing orientation were analyzed.
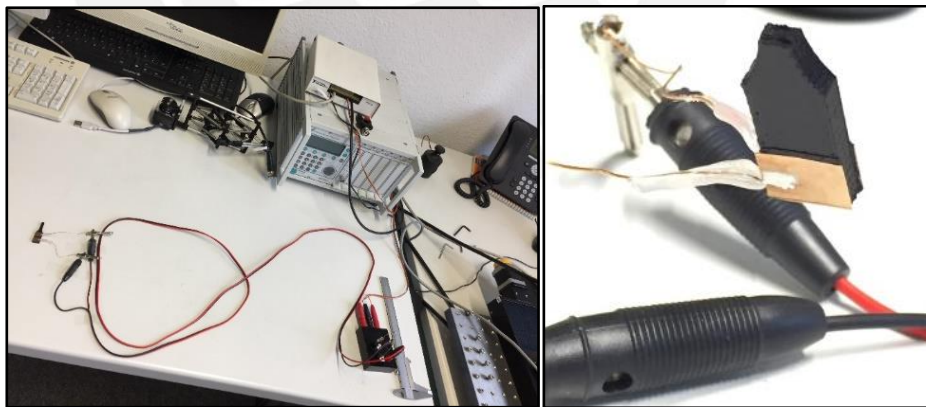
Figure 28. Volume resistivity test equipment

From the diagram shown on , Equation 1 was derived to calculate the electrical resistivity the material in analysis have.

Equation 1. Electric diagram derivation equation

$$u_B = I.\left(R_{sample} + R_{resistor}\right)$$
$$u_m = I.R_{resistor}$$
$$u_B = I.R_{sample} + u_m$$
$$R_{sample} = \frac{u_B - u_m}{I}$$
$$R_{sample} = \left(\frac{u_B - u_m}{u_m}\right).R_{resistor}$$

Where:

- R sample= Resistance of the sample
- R resistor= Resistance of the support resistor
- u_B= Voltage of input = 10V
- u_m= Voltage measured on the terminals of the support resistor
- I= Current flowing on the resistor and sample

Equation 2 was used to calculate the sample volume resistivity.

Equation 2. Volume Resistivity

$$Rv = R_{sample} \cdot \frac{A}{d}$$

Where:

- Rv: Volume resistivity or specific resistance
- R sample: Resistance of the sample
- d= thickness
- A= Area of the cooper conductive plates

5. Results and Discussion

5.1 Characterization of the Filaments

5.1.1 Structural characterization of the ABS based filaments

The ABS, ABS/CNT and ABS/mCF filaments were structurally and mechanically characterized.

The structural characterization was made by FTIR, DSC/TG, SEM and FESEM analysis:

FTIR analysis was made on the filaments in order to confirm the polymer structure with the characteristic peaks the spectrum shows and to analyze the influence of the carbon reinforcements on the infrared absorbance.

As shown in Figure 29 and Figure 30, the spectrum of ABS, ABS/CNT and ABS/mCF present the same characteristic peaks from ABS according to the Bruker Optik GMBH data base. Notice that the presence of carbon nanotubes or micro carbon fibers in the polymer matrix results in a higher absorbance along all the spectrum even when all ABS characteristic peaks are preserved.
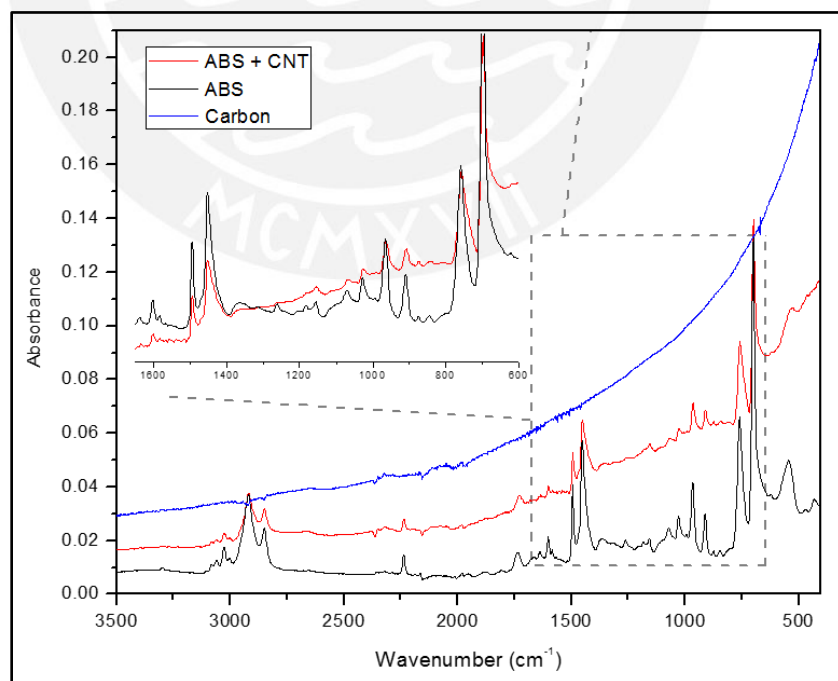
Figure 29. FTIR of ABS (black), ABS/mCF (red) and carbon (blue)
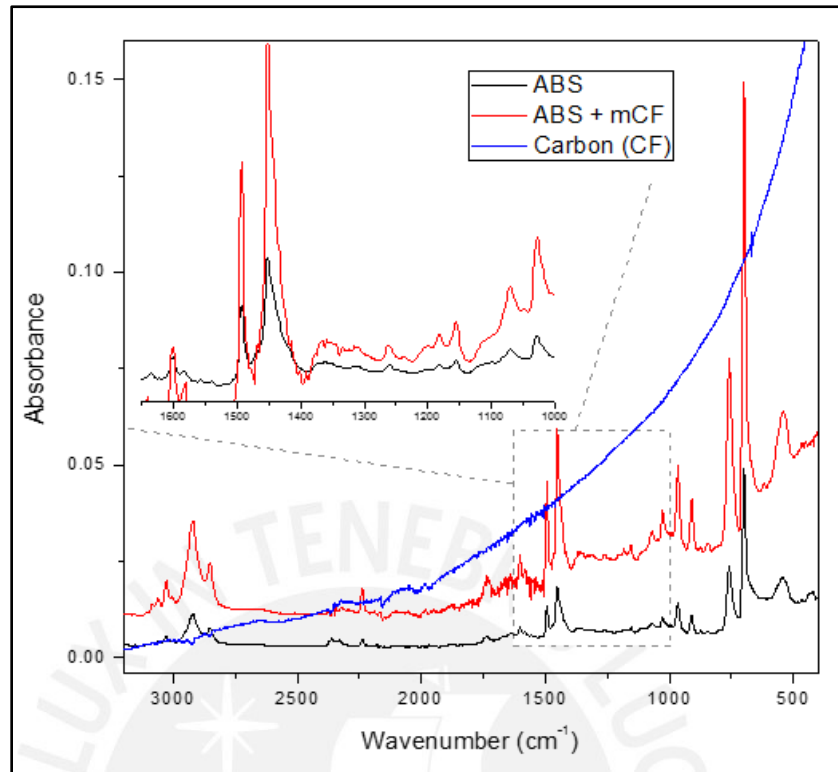
Figure 30. FTIR of ABS (black), ABS/mCF (red) and mCF (blue)

In both analyses a spectrum of pure carbon was displayed in order to analyze the influence of the carbon reinforcements on the infrared absorbance. As can be seen, carbon absorbs along all the wavenumber in a typical exponential form with a higher absorbance for the smaller wavenumbers and a minor absorbance on the bigger wavenumbers [68].

It is also important to notice that the micro carbon fibers influence in the ABS band intensities as can be seen in Figure 30, unlike the carbon nanotubes reinforcement (Figure 29). The differences concern mainly the bands located in the 1040-1620 cm^{-1} range. These changes may result from the interactions of the carbon fiber surface functional groups and the polymer matrix.

With this analysis only the presence of carbon reinforcements can be confirmed but no characterization of the reinforcements can be made, based on the fact that no new characteristics peaks can be seen.

DSC/TG analysis was made on the composite filaments, ABS/CNT and ABS/mCF, to determinate from the first derivative data curve (DTG) the percentage in weight of the nano and micro reinforcement for each case. this with the knowledge of the ABS decomposition temperature around 430°C and the carbon reinforcements stability at this temperature [13][17][55] (see section 4.2.1).

DTG diagram from ABS/CNT (Figure 31) shows a weight loss of about 90% to the ABS matrix and a non-volatile residue at this temperature of 10 wt% which corresponds to the carbon nanotubes, according to the material description (see section 4.1). The ABS was decomposed in an isothermal at 425.9°C; temperature that was selected from a first DSC/TG essay on the material.
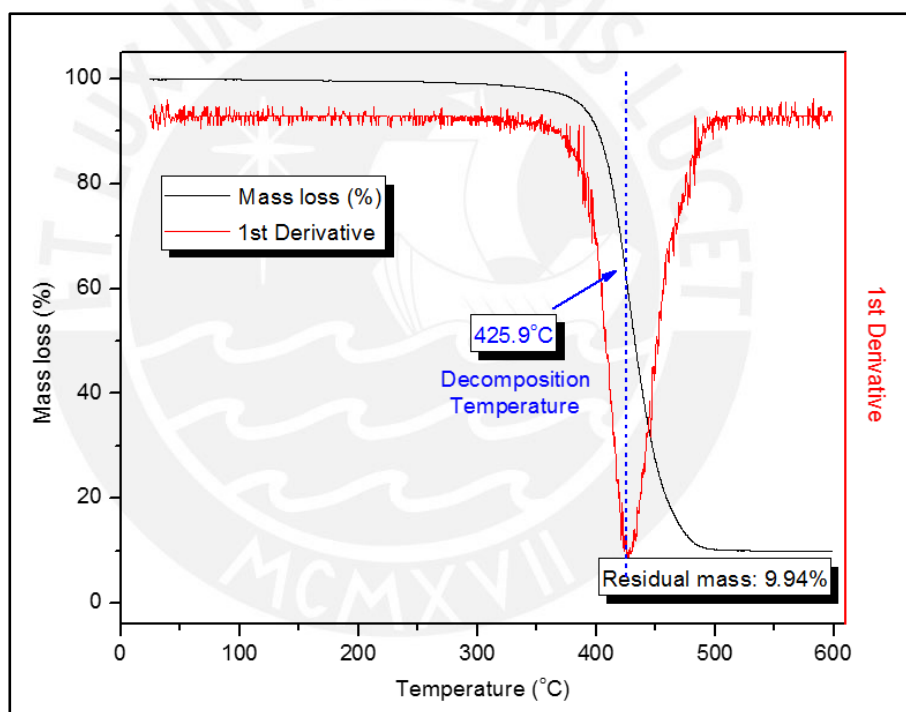
Figure 31. DTG analysis of ABS/CNT filament

DTG diagram from ABS/mCF (Figure 32) shows a weight loss of about 85% to the ABS matrix and a non-volatile residue at this temperature of 15 wt% which correspond to the micro carbon fibers (mCF), according to the material description (see section 4.1). The ABS was decomposed in an isothermal at 430.5°C; temperature that was selected from a first DSC/TG essay on the material.
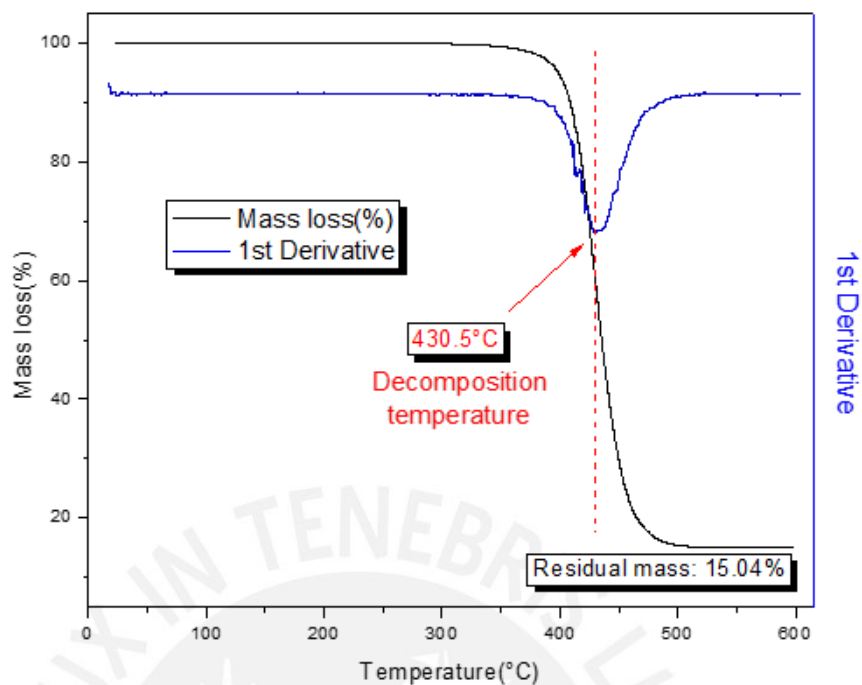
Figure 32. DTG of ABS/mCF filament

SEM and FESEM analysis was conducted on the composite filaments, ABS/CNT and ABS/mCF, to confirm the nano and micro reinforcement for each case (see section 4.2.6).

On the ABS/CNT, FESEM microscopy was used to confirm that the 10wt% of reinforcement corresponds to the CNT because of the highest resolution needed. The scanning was made on a piece of filament confirming the nature of the reinforcement as can be seen in Figure 33.
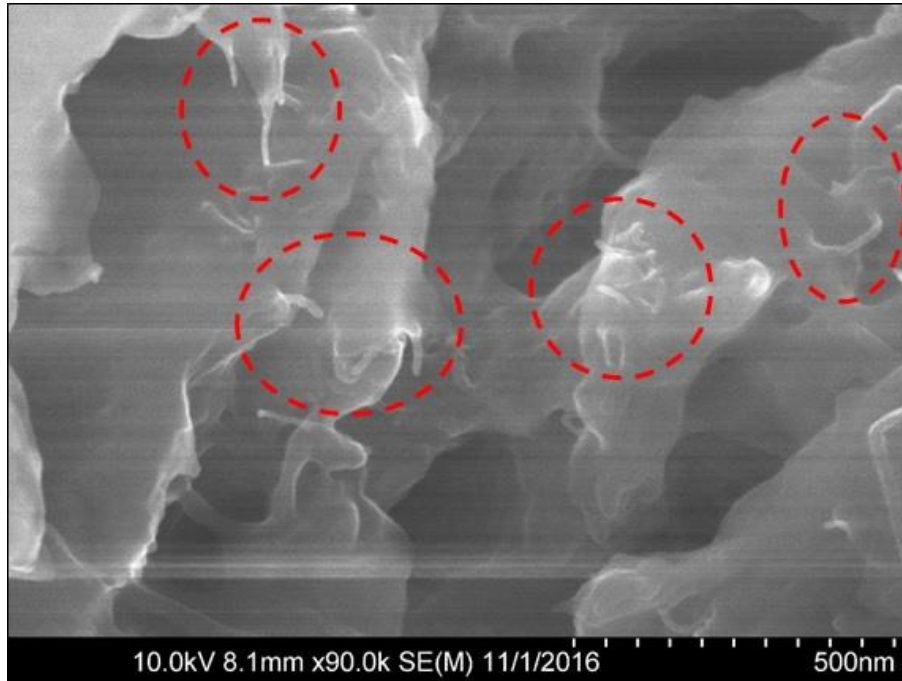
Figure 33. FESEM analysis of ABS/CNT (CNT tangles pointed in red)

Also some dimensional values from the carbon nanotubes were registered during the FESEM imaging. As can be seen on Figure 34, two nanotubes dimensions were analyzed in detail presenting in one of them dimensions of around 20 nm for the diameter and 297 nm for the exposed length (on the left), and in the other dimensions of around 8 to10 nm for the diameter and 87 nm for the length (on the right).
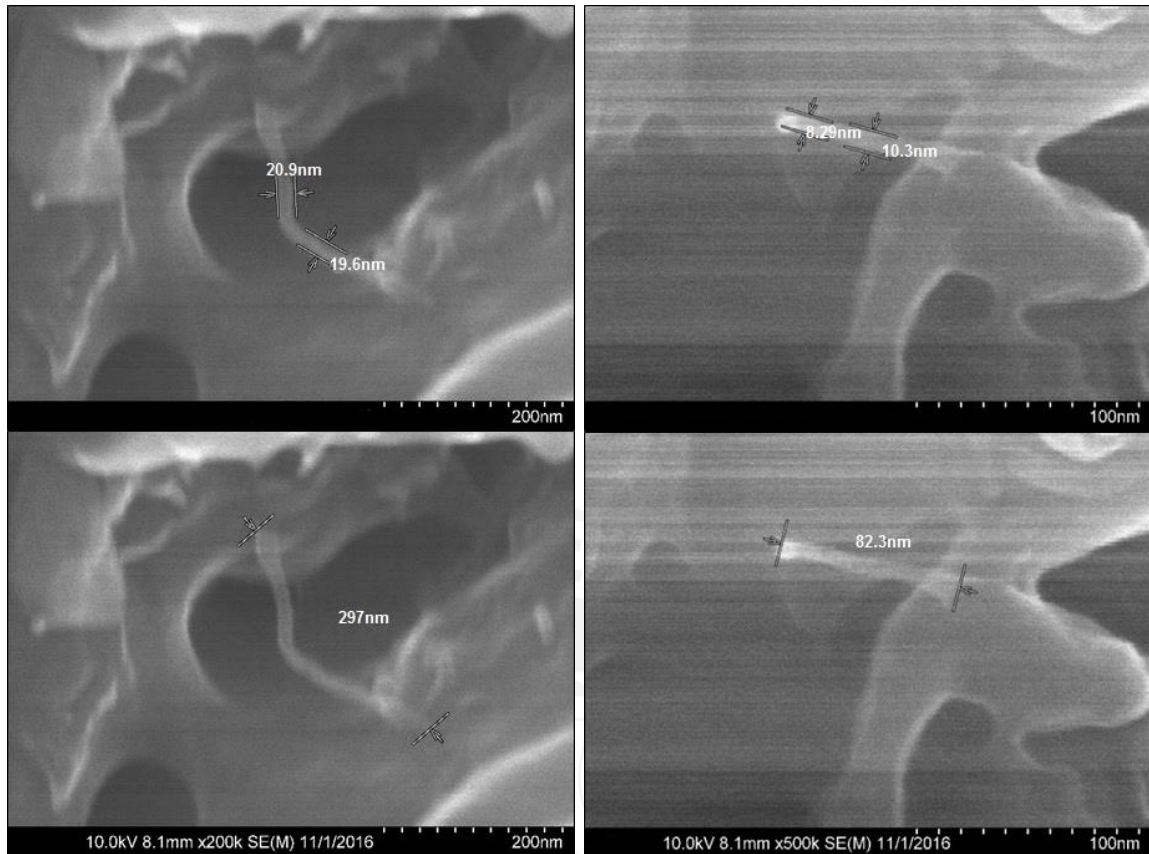
Figure 34. CNT dimensions from FESEM analysis

On the ABS/mCF, SEM microscopy was used to confirm that the 15wt% of reinforcement corresponds to the mCF. The scanning was made on the residue from the DSC/TG analysis confirming the micro fibers reinforcement as can be seen in Figure 35. Also some values from the dimensions of the micro fibers were taken characterizing the fiber with diameters around 7 μm and length around 100 μm as can be seen in Figure 36.
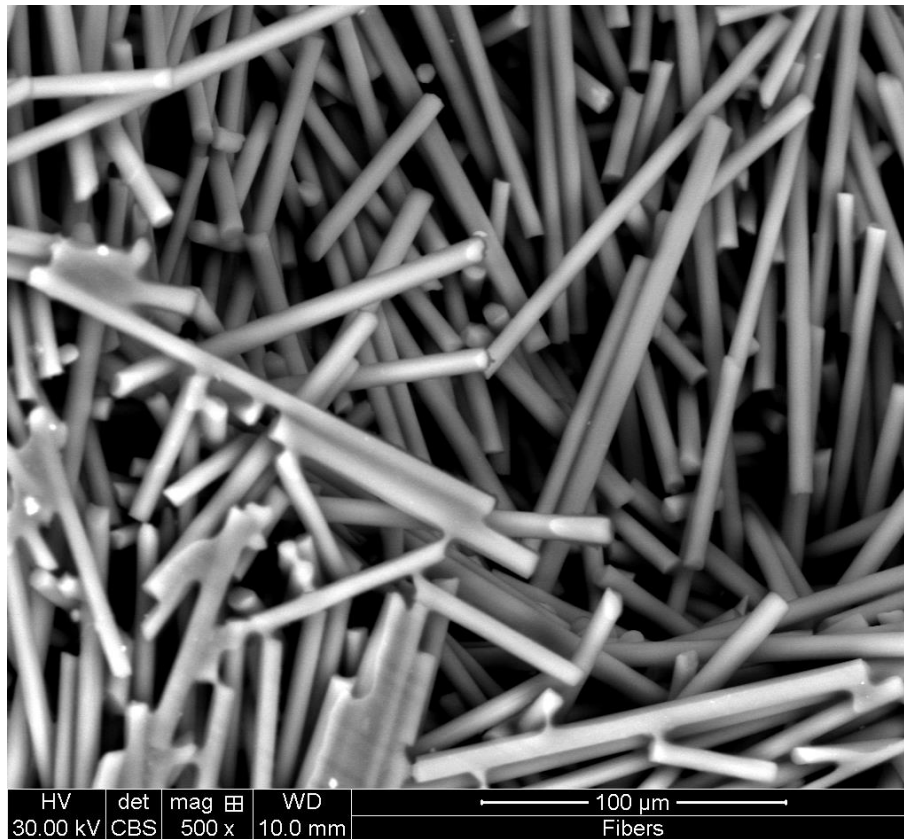
Figure 35. mCF from DSC/TG analysis
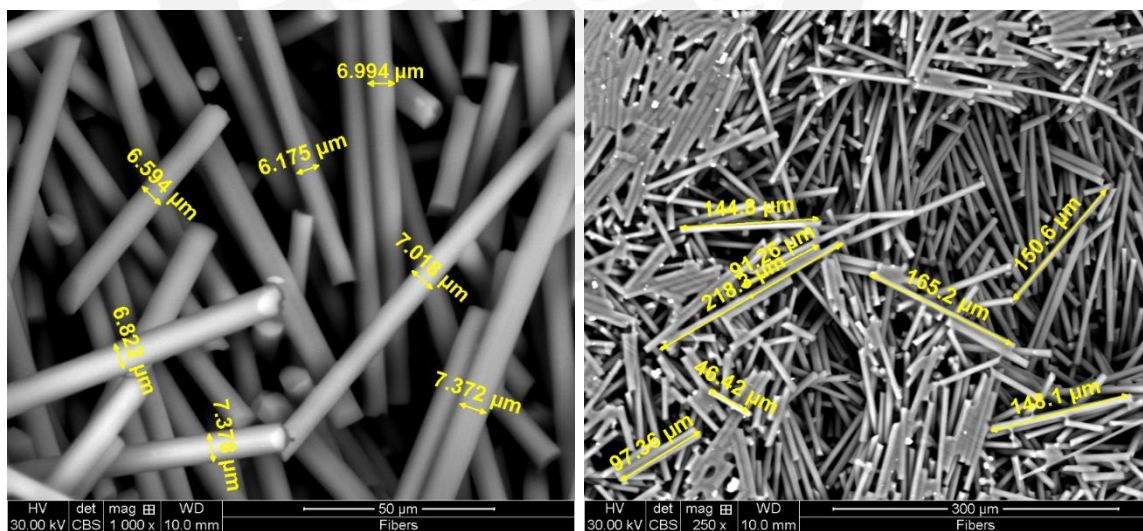
Figure 36. mCF dimensions from DSC/TG analysis

53

5.1.2 Mechanical characterization of the ABS based filaments

The mechanical characterization was made by means of tensile tests on the filaments.

The filaments were tested according to ASTM D638 [63] which stipulate a speed of testing of 1mm/min (see section 4.2.5). These results also will serve as base of comparison for the FDM 3D printed samples.

ABS filament maximum strength was 34.9 MPa which compared with literature values corresponds to ABS extruded values [47]. On the composite filaments in study, the ABS/CNT reach a maximum strength of 33.38 MPa losing around 4% compared to the ABS resistance, on the other hand ABS/mCF reach a maximum strength of 37.69 MPa increasing the resistance of the ABS on around 8% (Figure 37).

The tensile modulus on the pure ABS filament was 1686 MPa which also corresponds to the ABS extruded values [47]. On the composite filaments in study, the ABS/CNT had a tensile modulus of 1794 MPa increasing the rigidity in comparison to the ABS in around 6%, the ABS/mCF also increase the rigidity but in this case the increase was of around 152% presenting a tensile modulus of 4254 MPa (Figure 38). The main reason of the significant increase of the ABS/mCF tensile modulus is related to the performance and the adherence of the high modulus micro carbon fibers as reinforcement on the ABS matrix. Results obtained are almost the same as those reported by the producer company confirming the technical specifications [60].

The elongation reached for the pure ABS was 5.56% and even if this results had a big fluctuation, both composites could not reach similar values because of the obstacle that the reinforcements represent for the unfolding of the polymer chains and also because reinforcements tend to increase the flow index [13][14][15][17][18][20][21][22]. ABS/CNT reached 1.89% and ABS/mCF a mean of 1.23% (Figure 39).

According to the literature, nanoreinforcement on polymers matrix cannot change dramatically mechanical properties [13][17][18], but micro reinforcements could [41]. In

54

the present thesis, the ABS/mCF filament in study do not present a dramatic change in the mechanical properties in comparison to the values reported for carbon fibers composites, even if the tensile modulus increase more than 150%. This could be attributed to the poor adherence of the fibers product of the low pressure the manufacturing process involves, the dimensions of the fibers and the arrangement [70].
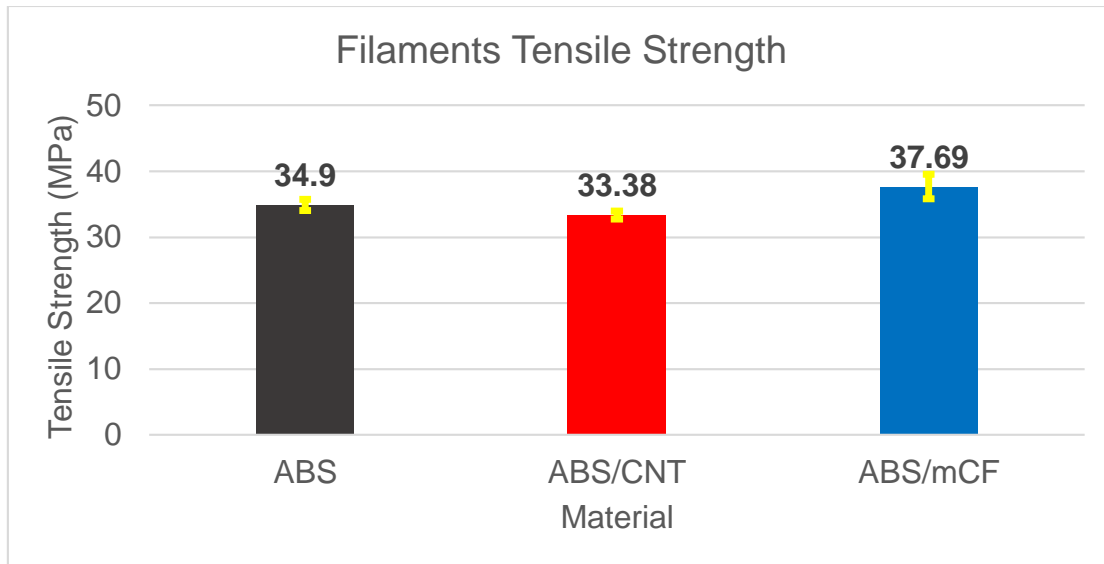
Figure 37. Tensile strength of ABS (black), ABS/CNT (red) and ABS/mCF (blue) filaments
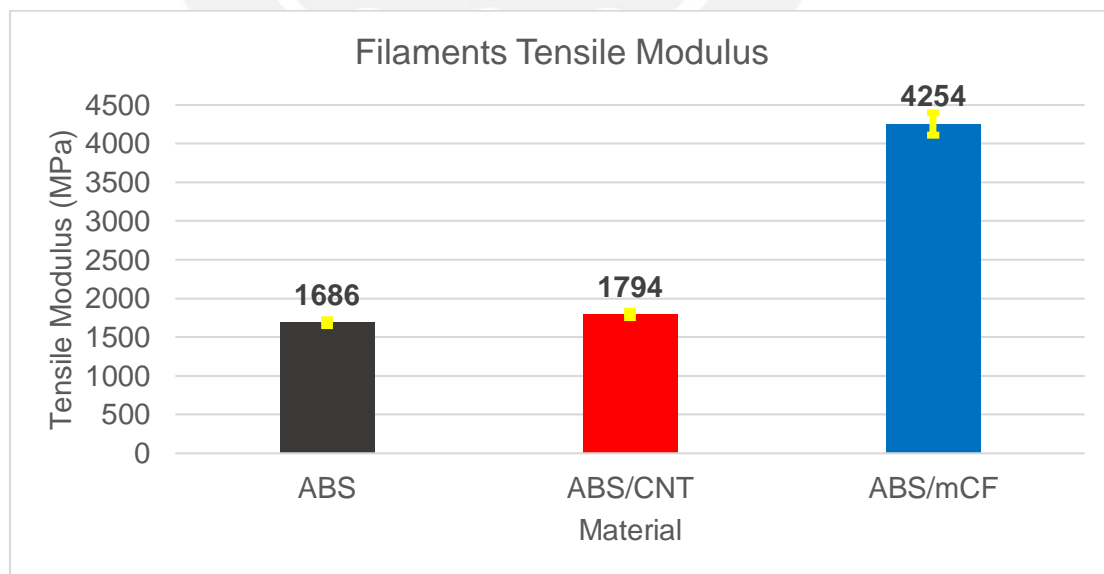
Figure 38. Tensile modulus of ABS (black), ABS/CNT (red) and ABS/mCF (blue) filaments

55
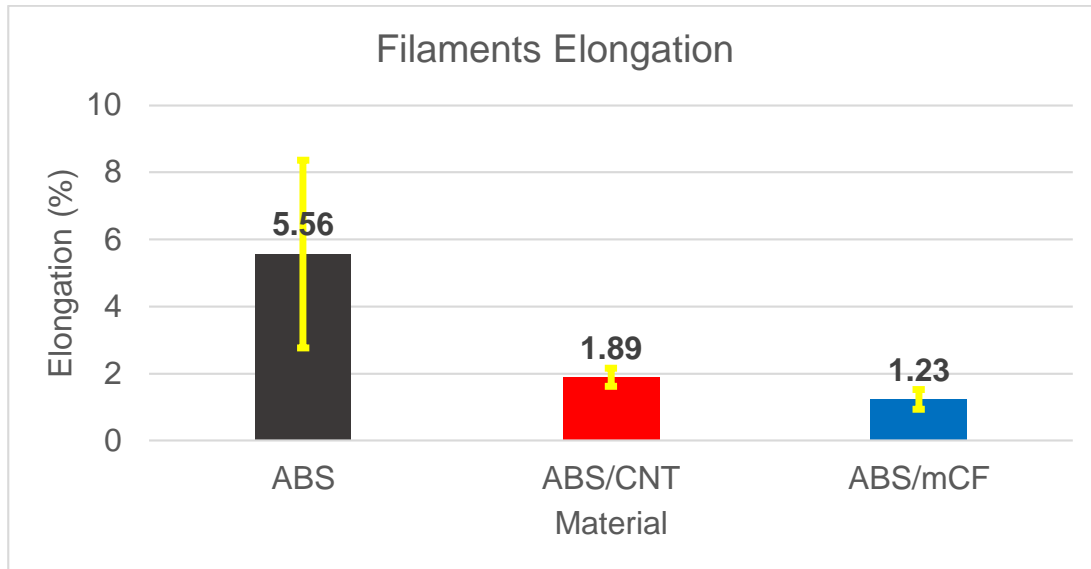
Figure 39. Elongation of ABS (black), ABS/CNT (red) and ABS/mCF (blue) filaments

5.2 Determination of FDM testing parameters

Fused deposition modeling works under the principle of extrusion manufacturing and according to a programed arrangement of deposition. With the aim of finding the optimal parameters for the best tensile properties, the preparation parameters were calculated.

In the advanced drivers used for FDM 3D printing, such as Simply3D® (used in the present thesis), the parameters that must be introduced are: from the extrusion process the speed of extrusion, thread diameter and temperature of extrusion; and according to the programed arrangement the layer height or thickness, layer printing orientation, outline perimeter shell and infill of the solid. For an easy removal also the bed of deposition should be heated.

To determine the optimal parameters a visual and tensile strength analysis was conducted in ranges according to the literature and technical specifications of the filaments.

The temperature of extrusion was determined as the mean of the range the specifications suggest based on non-significant variation of the tensile behavior on specimens printed with different temperatures. It is also important to notice that the

56

temperature of extrusion depends on the nozzle temperature and this can vary in some degrees during the printing.

The temperature of the bed of deposition was selected according to recommendations from the printer and filaments provider.

Speed of printing was selected focusing on the efficiency and based on a good adherence from the first layer deposited as the literature suggest and the first printings confirm.

One outline perimeter shell was selected based on the literature and for a better modelling of the solid, in this case the tensile specimens.

The layer thickness, infill and orientation of modeling were selected based on the objective of this study and with the maximum diameter the printer nozzle can extrude.

Based on what was mentioned above, a testing parameters set was elaborated, which is presented in Table 5.

Table 5. Testing parameters for ABS based materials FDM

FDM parameters	ABS	ABS+CNT	ABS+mCF
Extrusion temperature (°C)	230	245	230
Bed temperature (°C)	100	100	100
Layer height or thickness (mm)	0.2/0.4	0.2/0.4	0.2/0.4
Layer printing orientation (°)	0°, 90°, 45°, 0/90°, 45/-45°	0°, 90°, 45°, 0/90°, 45/-45°	0°, 90°, 45°, 0/90°, 45/-45°
Speed of printing (mm/min)	1200	1200	1200
Outline perimeter shell	1	1	1
Infill (%)	100	100	100

5.3 Layer orientations and layer height selection

The complexity and the resources the process involves, especially for printing specimens with dry filaments, make it recommendable to have a previous study in order to determinate the layer printing orientations and layer height which are relevant looking for the greatest tensile mechanical properties and surface finishing by a roughness analysis.

This previous study was made for each ABS composite and in both cases compared with pure ABS in order to determinate how the reinforcement works. The main reason of this previous analysis is to determinate which orientations and layer height will be as important as to study in detail with dried filaments.

The analysis was made with filaments moisture exposed for four weeks (28-30 days) and results are presented by separate for each ABS composite and in both cases compared with the pure ABS.

5.3.1 Selection by tensile analysis

To study in detail only the potential layer printing orientations and layer height on the ABS based composites in study, a previous analysis was made in the typically used layer heights and layer printing orientations for FDM manufacturing such as 0.2 mm and 0.4 mm layer heights and 0°, 90°, 45°, 0°/90° and 45°/-45° layer printing orientations.

With this premise a tensile test analysis was made in five samples for each configuration and the mean of the three more representative tests are shown in the following diagrams (Figure 40 to Figure 48) as the ASTM standards specify [63].

In the tensile strength, results presented show clearly that samples deposited with 0.2 mm layer height have always a higher maximum strength than the ones with 0.4 mm layer height this due to the higher energy introduced per sample which creates a better adhesion between the threads deposited.

On the ABS/CNT (Figure 41), the highest tensile resistance was found for layer heights of 0.2 mm and orientations of printing of 0°, 45° and 45°/-45°.

On the ABS/mCF (Figure 42), the highest tensile resistance was found for layer heights of 0.2 mm and orientations of printing of 0°, 45° and 45°/-45°, but it should be noted that the resistance reached by the ABS/mCF FDM samples is very poor in comparison to the unfiled ABS and their raw material filament (see section 5.1). This loss of resistance is analyzed in detail on the influence of humidity (see section 5.4).

Figure 40. Tensile strength of FDM ABS for the selection of the parameters to study (0.4mm layer height in gray and 0.2mm layer height in black)

Figure 41. Tensile strength of FDM ABS/CNT for the selection of the parameters to study (0.4mm layer height in pink and 0.2mm layer height in red)
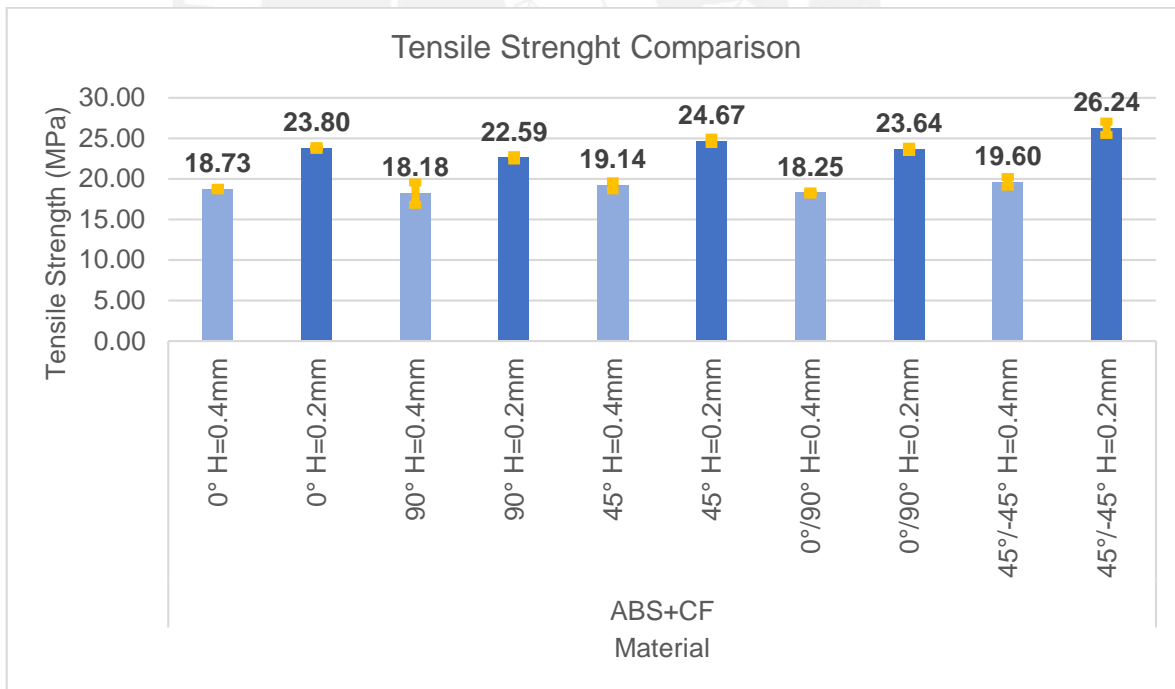
Figure 42. Tensile strength of FDM ABS/mCF for the selection of the parameters to study (0.4mm layer height in light blue and 0.2mm layer height in blue)

60

In the tensile modulus, the variability of the results is higher being in many cases impossible to affirm which layer height or layer printing orientations evidence a better behavior. But overall, the 0.2 mm layer height samples show a more rigid behavior than the 0.4 mm ones.

On the ABS/CNT (Figure 44), roughly it can be seen that samples with a layer height of 0.2 mm have a higher modulus than that for 0.4 mm samples and that the layer printing orientations of 0°, 45° and 45°/-45° stand out from the others.

On the ABS/mCF (Figure 45), roughly it can be see that layer height of 0.2mm have a highest modulus than the 0.4 mm samples and that the layer printing orientations of 90°, 0°/90° and 45°/-45° stand out from the others, but again it cannot be safely concluded.
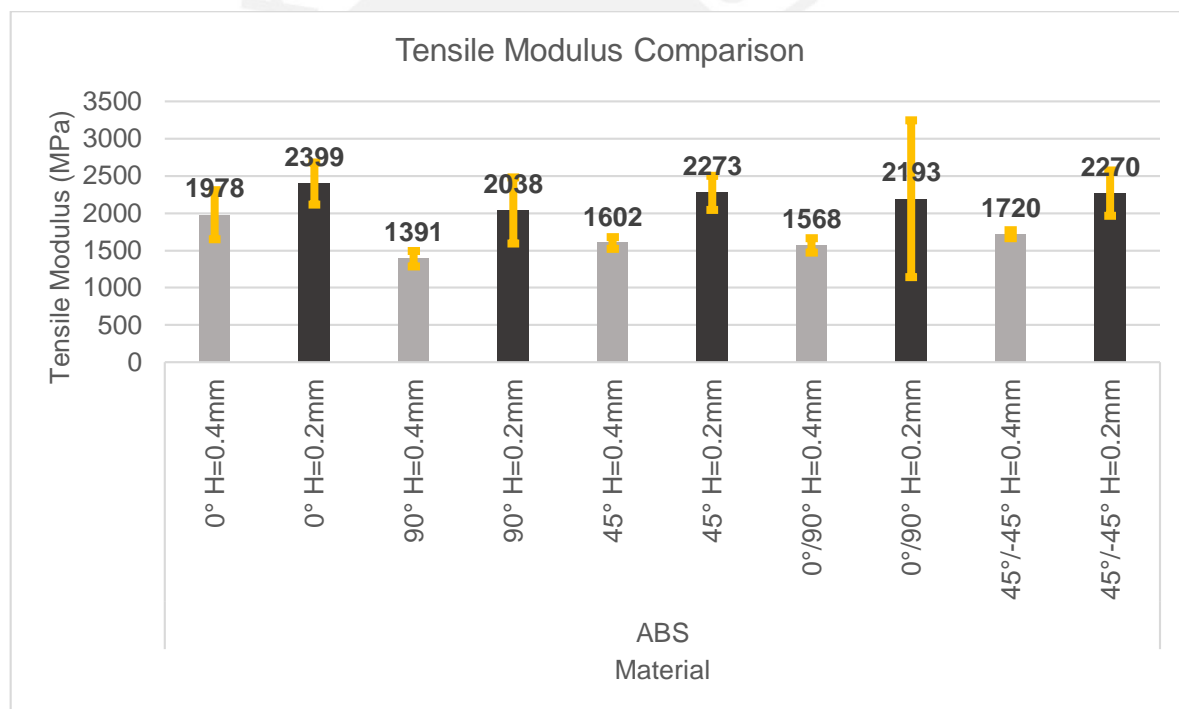
Figure 43. Tensile modulus of FDM ABS for the selection of the parameters to study (0.4mm layer height in gray and 0.2mm layer height in black)
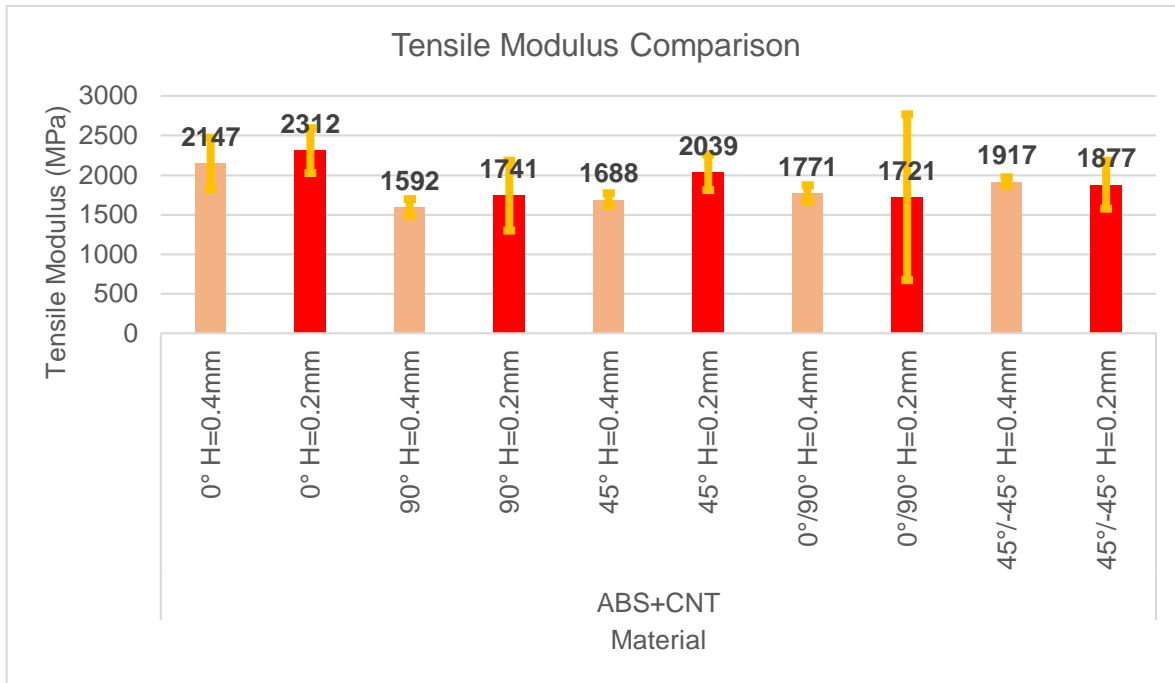
Figure 44. Tensile modulus of FDM ABS/CNT for the selection of the parameters to study (0.4mm layer height in pink and 0.2mm layer height in red)
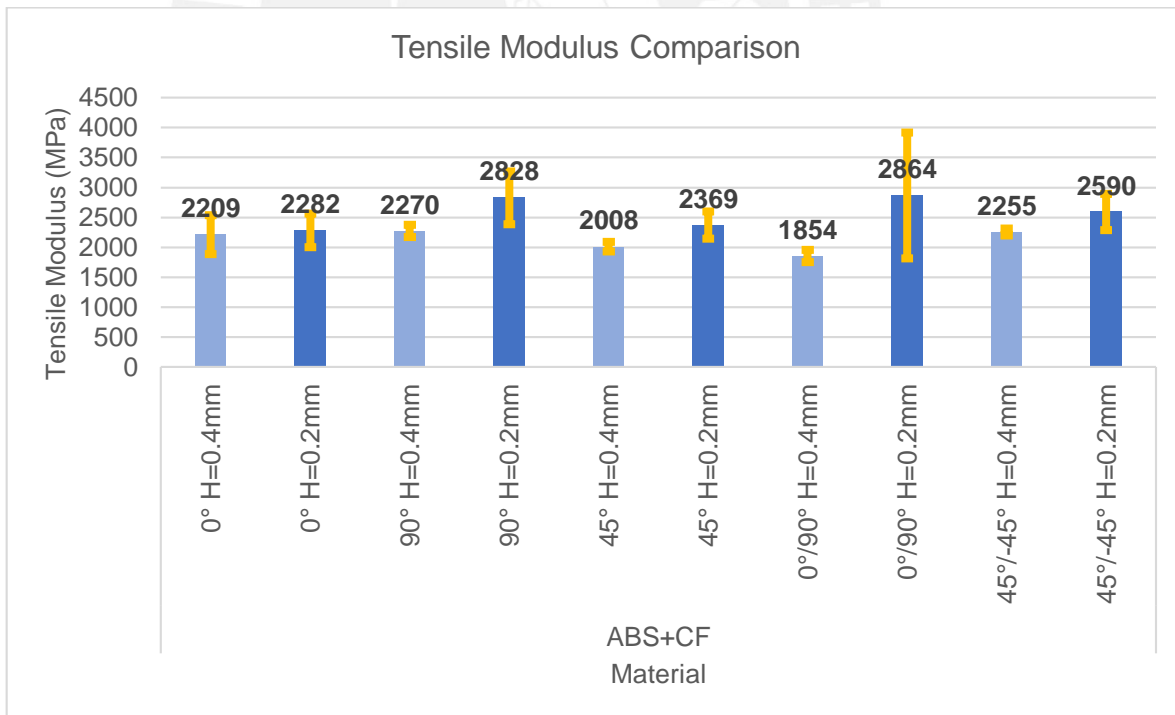
Figure 45. Tensile modulus of FDM ABS/mCF for the selection of the parameters to study (0.4mm layer height in light blue and 0.2mm layer height in blue)

In the elongation, results show that samples deposited with 0.2 mm layer height have a higher elongation that than the 0.4mm ones. This because of the heat introduced for each sample is around four times higher which allows the threads deposited have a better adherence and a lower surface tension between each other [66].

On the ABS/CNT (Figure 47), the highest elongation was found for layer heights of 0.2 mm and orientations of printing of 90°, 45°, 0°/90° and 45°/-45°.

On the ABS/mCF (Figure 48), the highest elongation was found for layer heights of 0.2 mm and orientations of printing of 90°, 45°, 0°/90° and 45°/-45°.
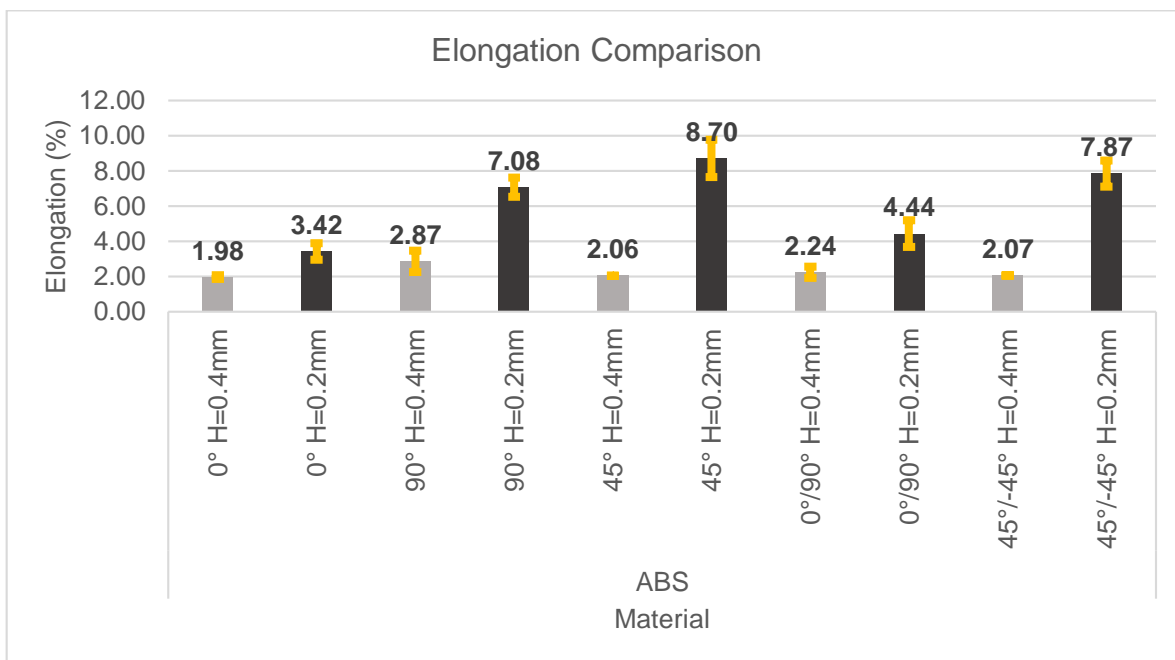
Figure 46. Elongation of FDM ABS for the selection of the parameters to study (0.4mm layer height in gray and 0.2mm layer height in black)
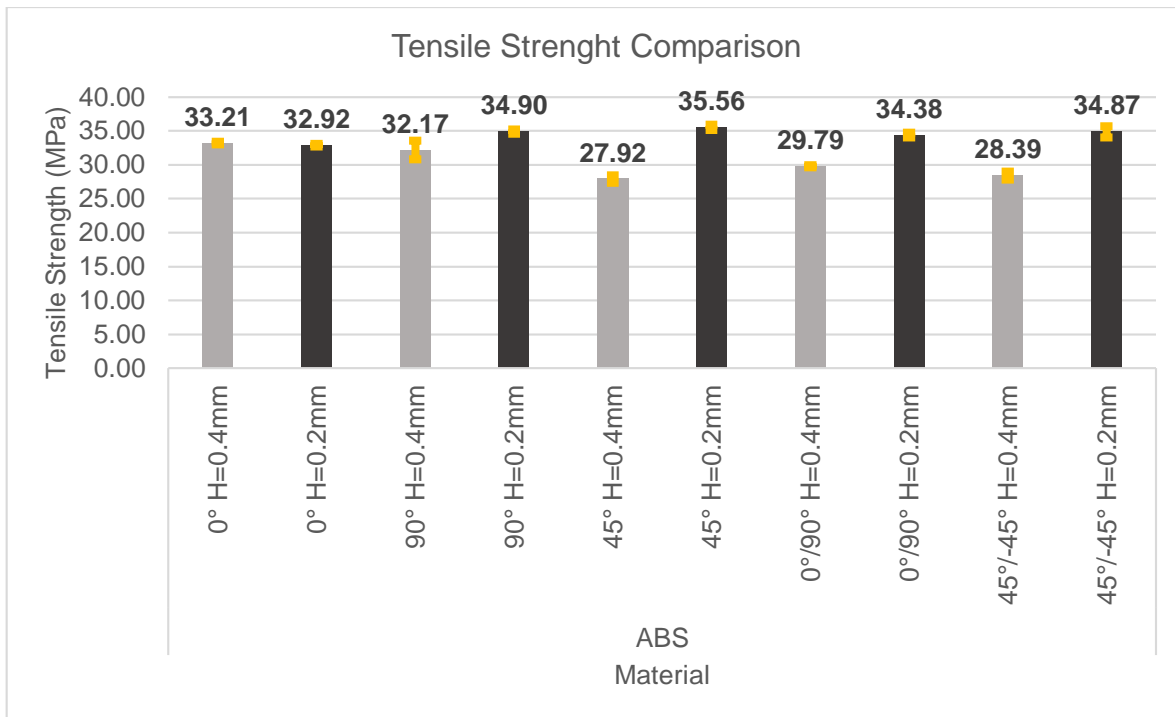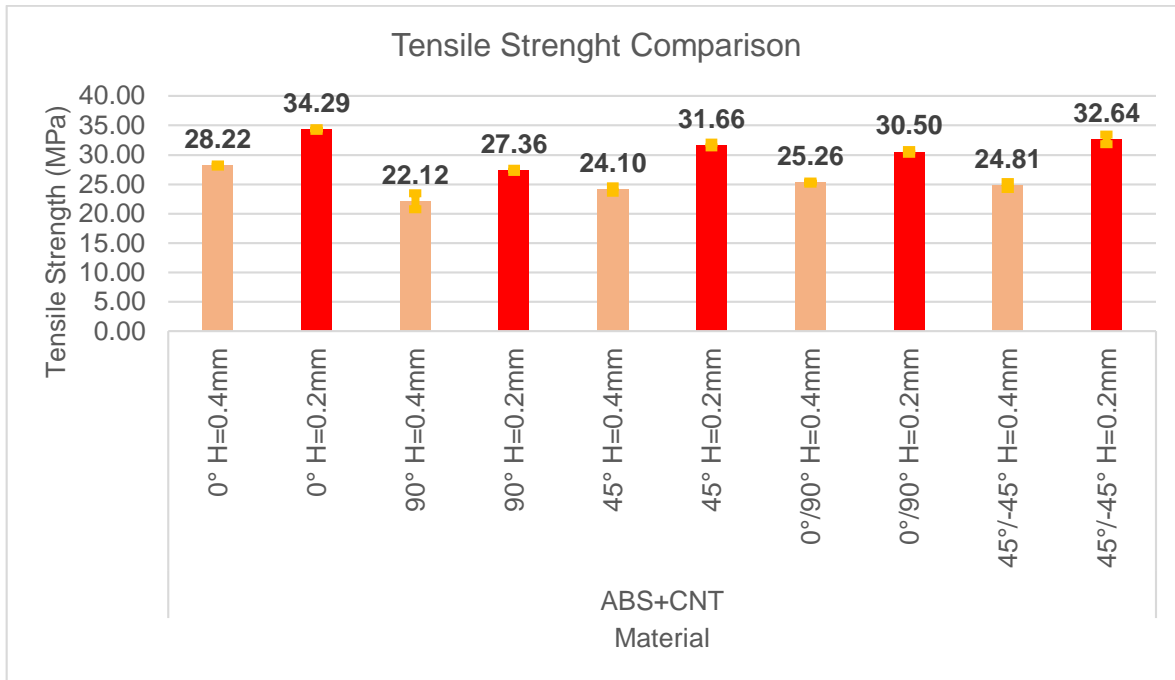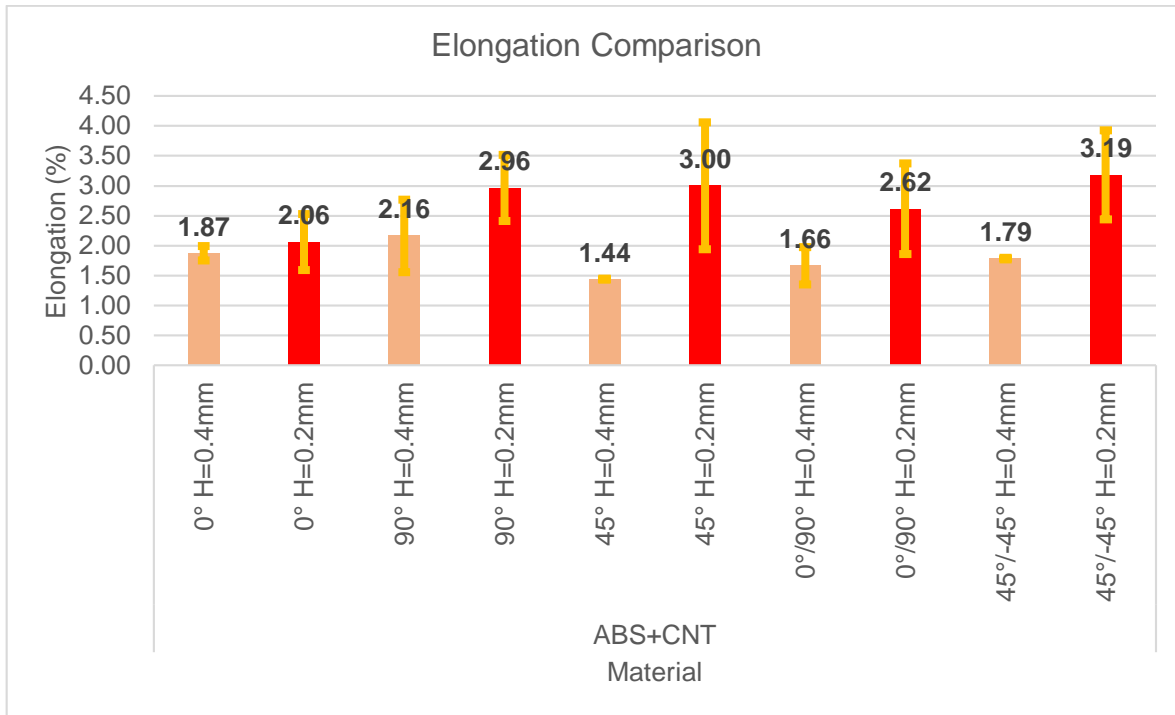
Figure 47. Elongation of FDM ABS/CNT for the selection of the parameters to study (0.4mm layer height in pink and 0.2mm layer height in red)
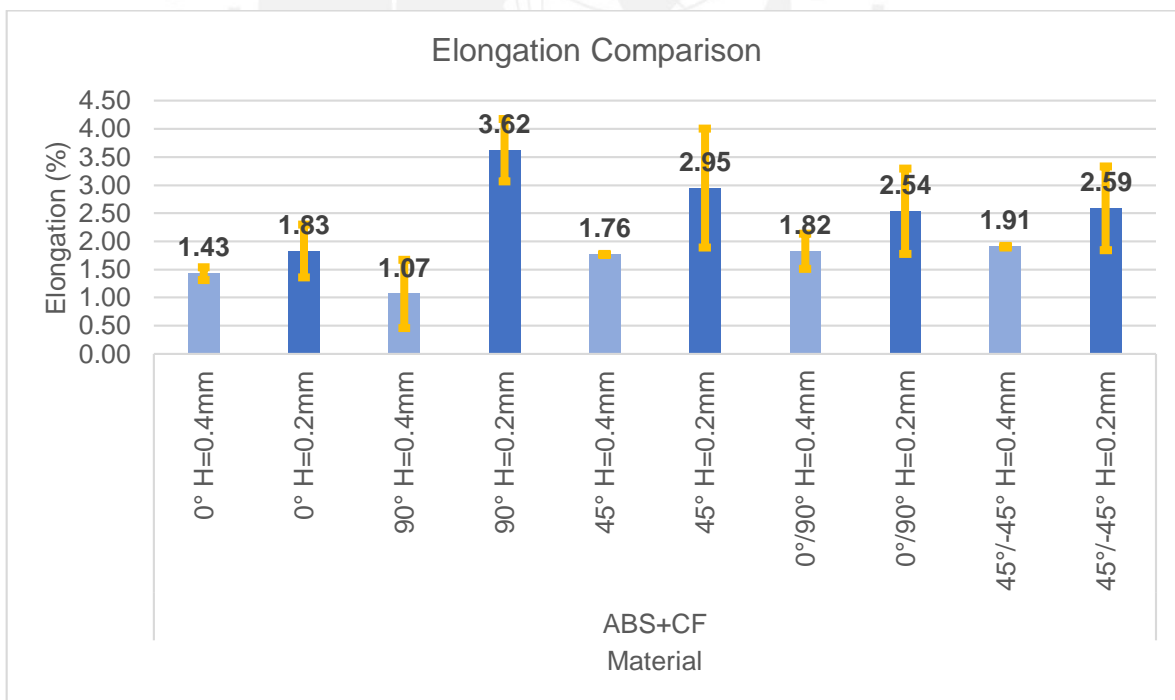
Figure 48. Elongation of FDM ABS/mCF for the selection of the parameters to study (0.4mm layer height in light blue and 0.2mm layer height in blue)

5.3.2 Selection by surface roughness analysis

To analyze the influence of the layer height on the surface finish a roughness analysis was made on pure ABS FDM samples printed with moisture exposed filaments with a layer printing orientation of 45° in the two layer heights in comparison: 0.4 mm and 0.2 mm.

The analysis was made by a lineal roughness analysis in the laser scanning microscope (LSM) which requests the drawing of a line on the image displayed in which the laser make a sweep in a chosen depth range.

The area in analysis for the 0.4 mm layer height specimen is displayed in Figure 49. The roughness was measured along the line drawn by making 45° with the X axis to measure the greatest amount of variation passing over all the deposited threads as can be seen in Figure 50. The spectrum that the analysis generates is shown in Figure 51 and the roughness calculated was 72.26 µm in arithmetical average units (Ra).
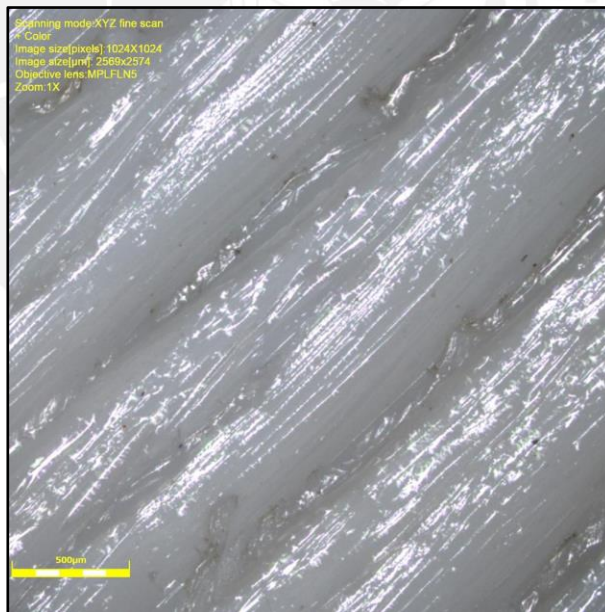
Figure 49. LSM intensities image of 0.4 mm layer height ABS specimen surface
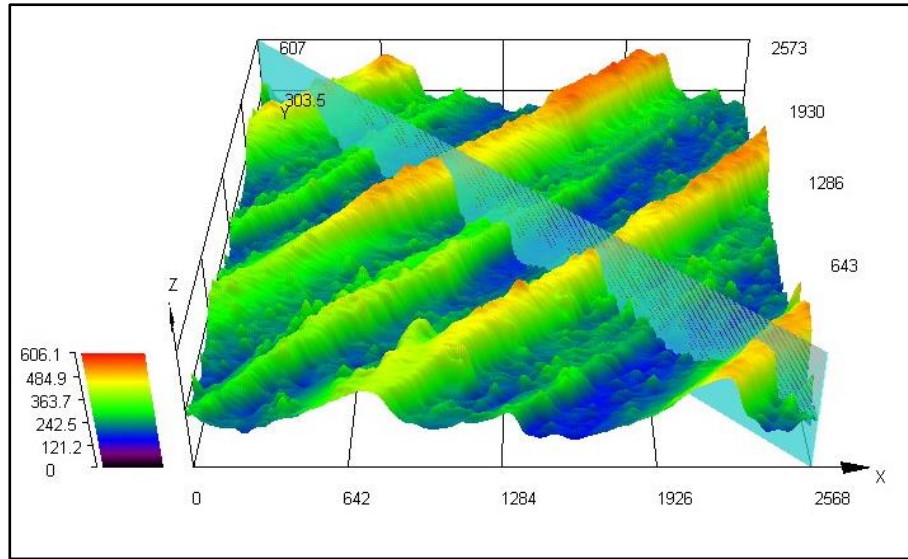
Figure 50. 3D image of the roughness line in analysis of 0.4 mm layer height ABS specimen in microns
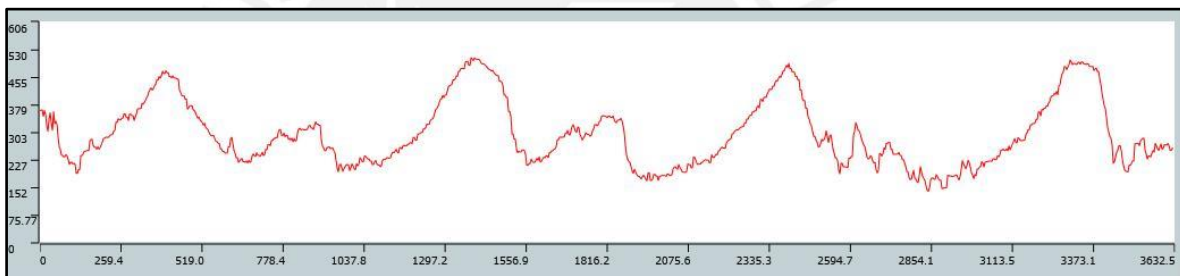
Figure 51. Lineal roughness spectrum of FDM 0.4 mm layer height ABS specimens printed with moisture exposed filament

For the 0.2 mm layer height specimen the test set-up was the same: with the area in analysis displayed in Figure 52 and the roughness line drawn for the analysis displayed in a 3D heights image on Figure 53. The spectrum that the analysis generates is shown in Figure 54 and the roughness calculated was 23.96 µm in arithmetical average units (Ra).

66
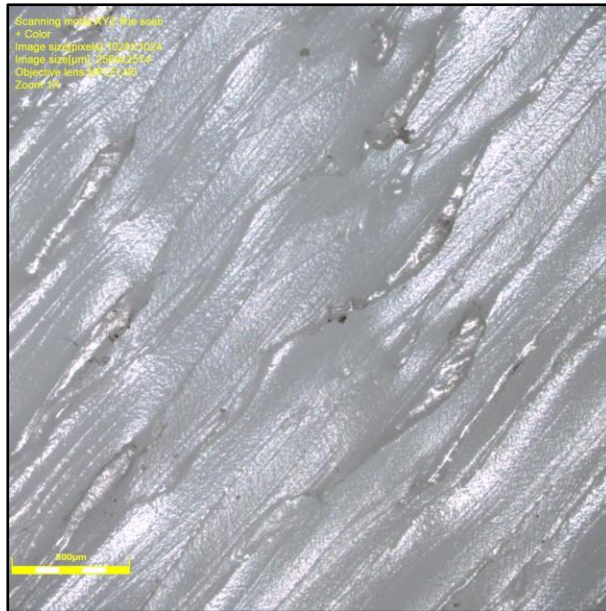
Figure 52. LSM intensities image of 0.2 mm layer height ABS specimen surface
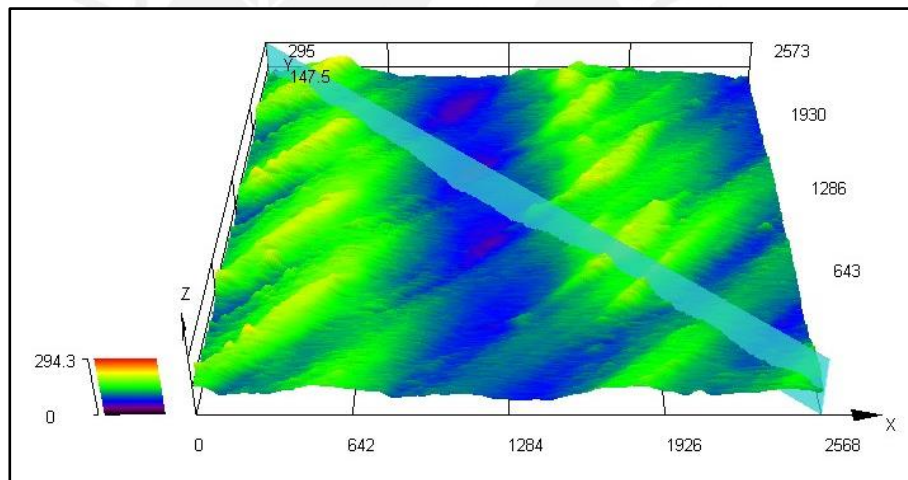
Figure 53. 3D image of the roughness line in analysis of 0.2 mm layer height ABS specimen in microns
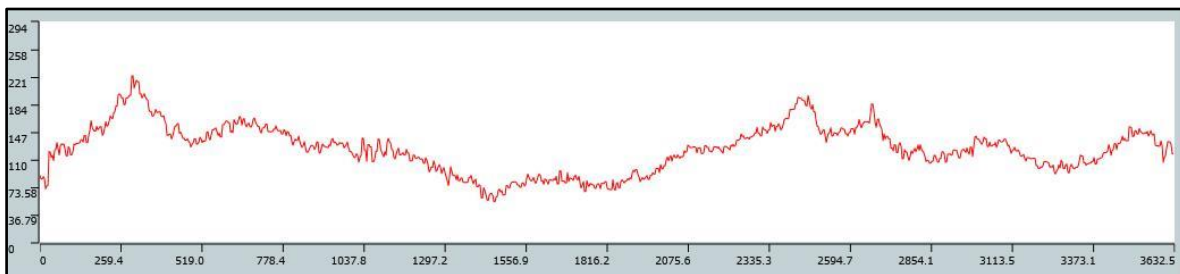
Figure 54. Lineal roughness spectrum of FDM 0.2 mm layer height ABS specimens printed with moisture exposed filament

5.3.3 Layer height and layer printing orientations selection

With the results presented of the tensile properties and the roughness analysis it was decided to study in detail only the layer height of 0.2 mm, which clearly exhibits better tensile properties and also a better surface finishing.

The layer printing orientations selected for the study in detail were 0°, 45° and 45°/-45°, this not only based on the results from the tensile test analysis but also considering the desire of studying the reinforcement alignment and the related literature [56][57].

5.4 Influence of anisotropy and humidity on FDM

With the overtime exposure of the filaments to the atmosphere moisture in the search for the optimal parameters for printing, it was found that these materials can absorb water and this could be perceived because the water absorbed made bubble blasts appear during the extrusion on 3D printing.

For this reason, it was decided to study the influence of the humidity, with the filaments in the dry and moisture exposed conditions, in addition to the study of the anisotropy in the specimens very important to study how the mechanical behavior change in a 3D printing object given the test direction.

5.4.1 Analysis of water absorbed from the moisture exposure

To quantify the moisture exposure of the filaments it was decided to measure the water absorption by the ASTM standards for plastics (ASTM D570 [62]).

Results from the water absorption analysis, detailed on Table 6, shows that the moisture exposition of the filaments can lead to an important percentage of absorption on the ABS based filaments in study, similar to a water immersion for around 2 hours.

Also is important to mention that the ASTM standard used suggest the measurement of the water absorbed after 24 hours of immersion, being this the water saturation time for the material. In this case it can be noticed that in both ABS composites the water absorbed from the moisture is around the 50% of this saturation calculated [45].

68

Table 6. Water absorption analysis of ABS based filaments

Material (Filament)	Moisture exposed (weight %)	2h in water immerse (weight %)	24h in water immerse (weight %)
ABS	0.58	0.73	1.13
ABS/CNT	0.34	0.30	0.69
ABS/mCF	0.40	0.50	0.65

5.4.2 Influence of anisotropy and humidity on the tensile properties

Tensile test specimens were immediately printed with both filament conditions, dry and moisture exposed, for each layer printing orientation on the layer height selected for the study (layer orientations 0°, 45° and 45°/-45° and layer height of 0.2mm).

The tensile properties and behavior of the FDM samples printed with moisture exposed filaments and with dry filaments were compared.

To analyze the influence on the tensile properties a tensile test analysis was made in five samples for each configuration and the mean of the three more representative tests are shown in the following diagrams (Figure 55 to Figure 60) as the ASTM standards specify [63]

The comparison was made in the same layer orientation and layer height specimens printed with filaments moisture exposed having specimens for each ABS based material printed with dry filaments (D) or filaments after moisture exposition (M) all with layer height of 0.2 mm.

On the FDM ABS/CNT (Figure 55) the tensile strength was not really influenced by the anisotropy of the layer orientations or the water absorbed by the filament with a maximum variation not greater than 5% by changing the layer printing orientations between 0° and 45° and not greater than 2% between specimens printed with dry or moisture exposed which was presented in the 45° layer printing orientation specimens.

It was not the same for the FDM ABS/mCF (Figure 56), where the tensile strength was strongly influenced by the anisotropy of the layer orientations and the water absorbed by the filament. The maximum variation due to the layer printing orientations was around 23% between 0° and 45° and the maximum variation due to humidity influence was around 54% which was presented in the 0° layer printing orientation specimens.
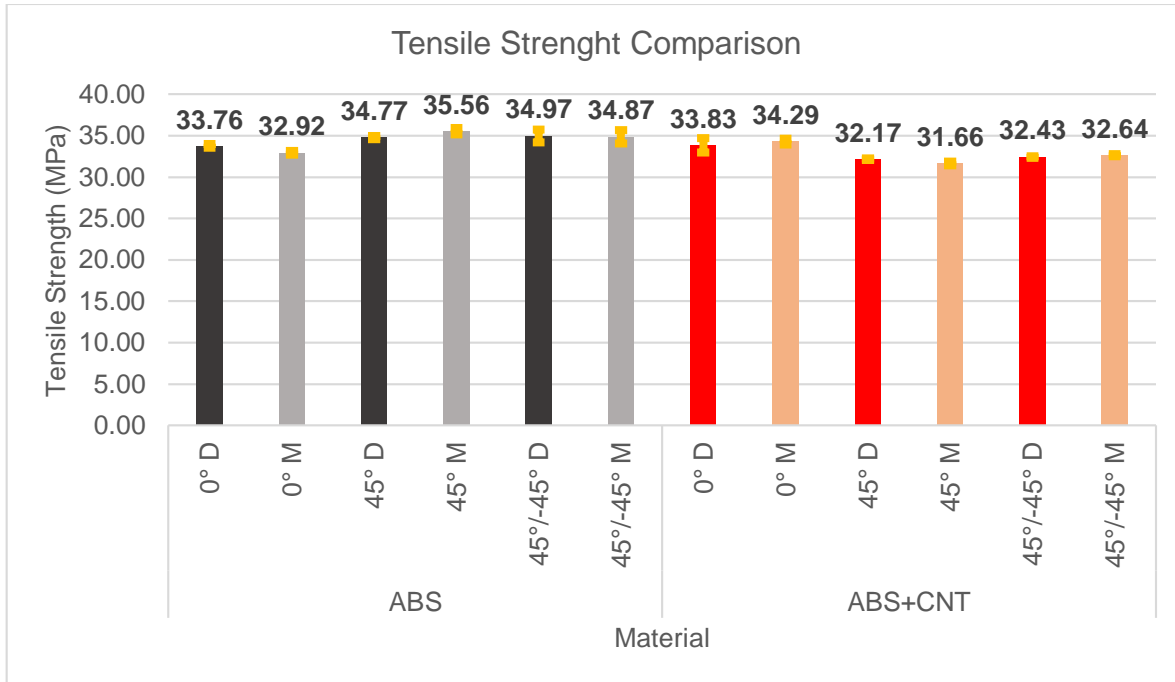
Figure 55. Tensile strength of FDM ABS (black and gray) and ABS/CNT (red and pink) specimens with dry and moisture exposed filaments
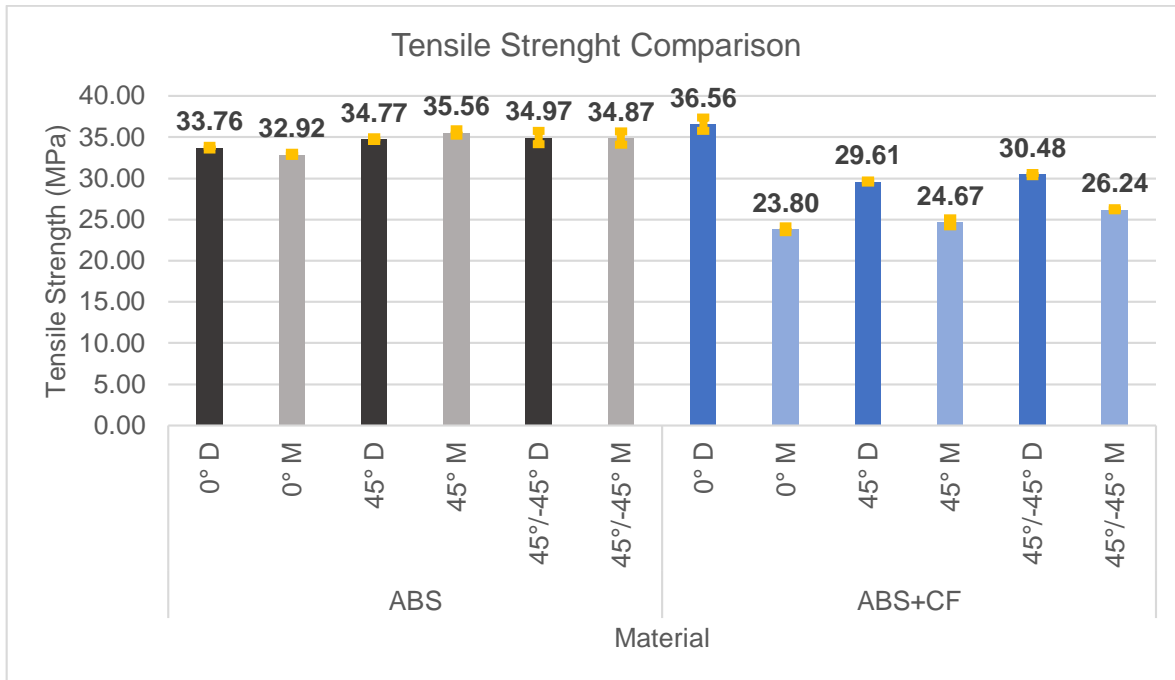
Figure 56. Tensile strength of FDM ABS (black and gray) and ABS/mCF (blue and light blue) specimens with dry and moisture exposed filaments

The influence of the anisotropy and humidity on the tensile modulus of the FDM ABS/CNT (Figure 57) could not be safely stated because of the variance of the results. But generally speaking it can be seen that the FDM samples printed with dry filaments have a little higher average and lower variance.

Almost the same behavior is presented on the ABS/mCF (Figure 58), with only one notable difference in the 0° layer printing orientation specimens. The maximum increase from the 0° specimens printed with dry filaments in comparison to the other layer printing orientations also printed with dry filaments was around 58% between 0° and 45°/-45°, and the maximum increase in comparison with the 0° specimens printed with moisture exposed filament was around 69%. This drastic change could be attributed to the alignment of the micro fiber reinforcement (Figure 67) and also because of the adherence between the reinforcement and the matrix (Figure 68 and Figure 69), analysis which is detailed below.
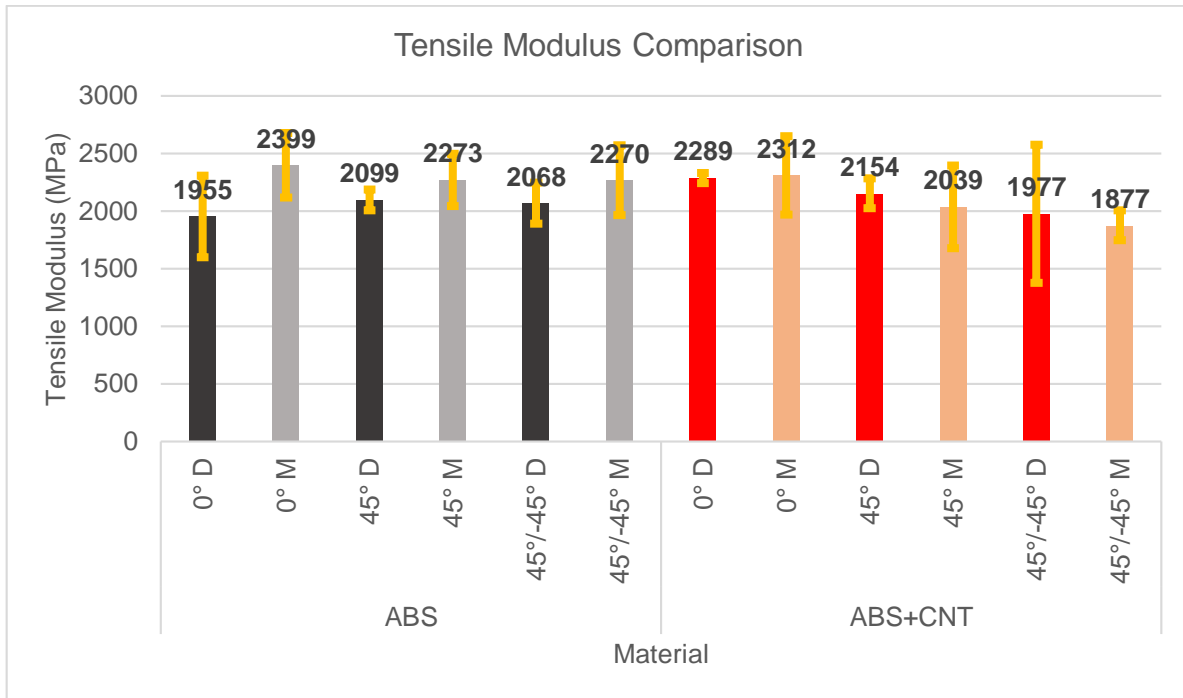
Figure 57. Tensile modulus of FDM ABS (black and gray) and ABS/CNT (red and pink) specimens with dry and moisture exposed filaments
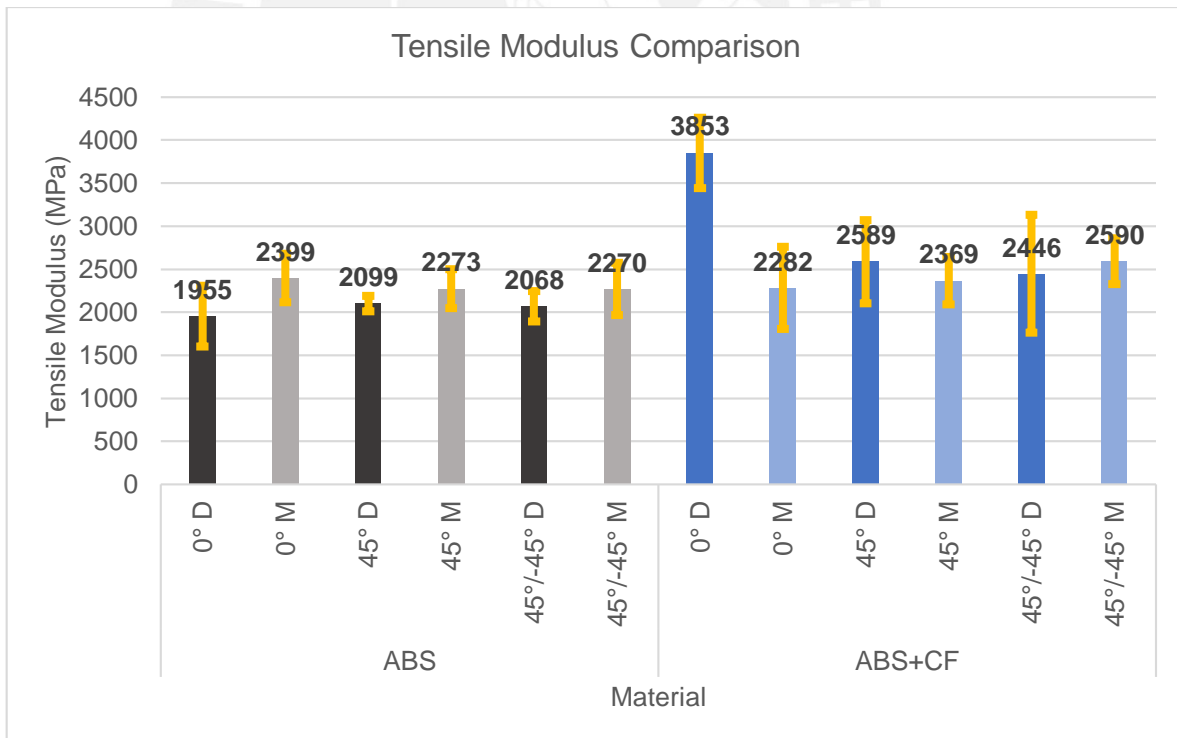
Figure 58. Tensile modulus of FDM ABS (black and gray) and ABS/mCF (blue and light blue) specimens with dry and moisture exposed filaments

72

According to the literature, reinforcements in polymers almost always leads to a loss of plasticity even more when the reinforcements are of high rigidity like carbon nanotubes and the micro carbon fibers [13][14][15][17][18][20][21][22]. That is corroborated in the results presented.

On the ABS/CNT (Figure 59) the elongation is not highly influenced by the anisotropy being the most remarkable change from 2.06% to 3.19% for the 0° and 45°/-45° specimens printed with moisture exposed filaments. The humidity is also not very influential presenting the most remarkable change on the 45° specimens with a variation between 2.39% for the specimens printed with dry filaments and 3% for the specimens printed with moisture exposed ones.

On the ABS/mCF (Figure 60) the elongation is also not highly influenced by the anisotropy being the most remarkable change from 1.06% to 2.86% for the 0° and 45°/-45° specimens printed with moisture exposed filaments. Similar is the case of the humidity influence, presenting the most remarkable change on the 0° specimens with a variation between 1.06% for the specimens printed with dry filaments and 1.83% for the specimens printed with moisture exposed ones.

Something interesting to notice is that, in all cases in which the variance allows to affirm, specimens printed with moisture exposed filaments undergo an increase in the maximum elongation. This increase can be attributed to the internal porosity according to the literature [57].
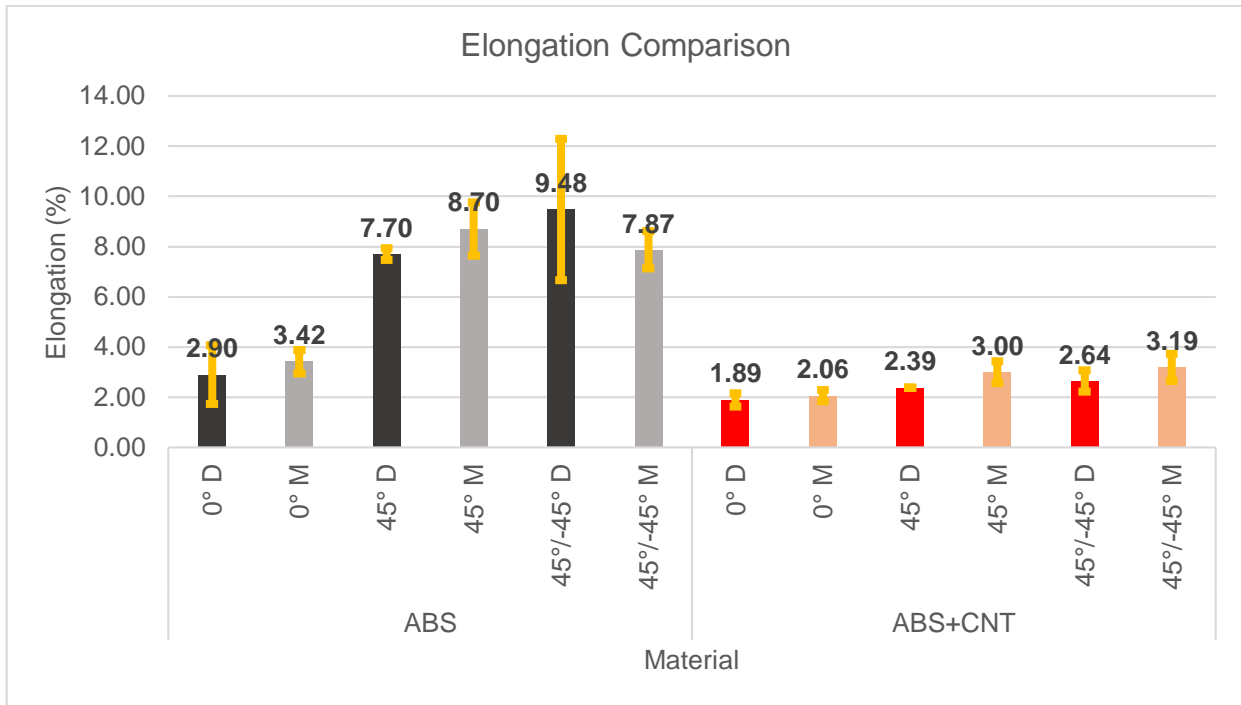
Figure 59. Elongation of FDM ABS (black and gray) and ABS/CNT (red and pink) specimens with dry and moisture exposed filaments
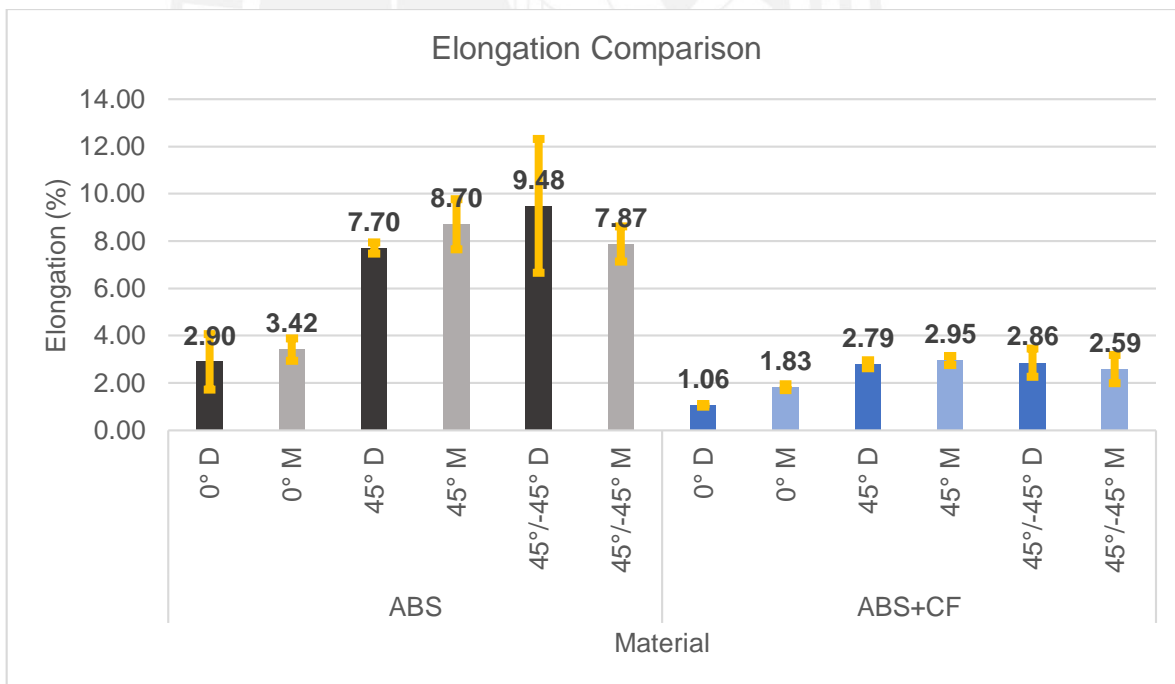
Figure 60. Elongation of FDM ABS (black and gray) and ABS/mCF (blue and light blue) specimens with dry and moisture exposed filaments

Figure 61 through Figure 63 show stress-strain diagrams for specimens with different printing orientation and humidity conditions. To select the most representative diagrams from each condition, the shown curves correspond to the essay from each group which result were closest to the mean.
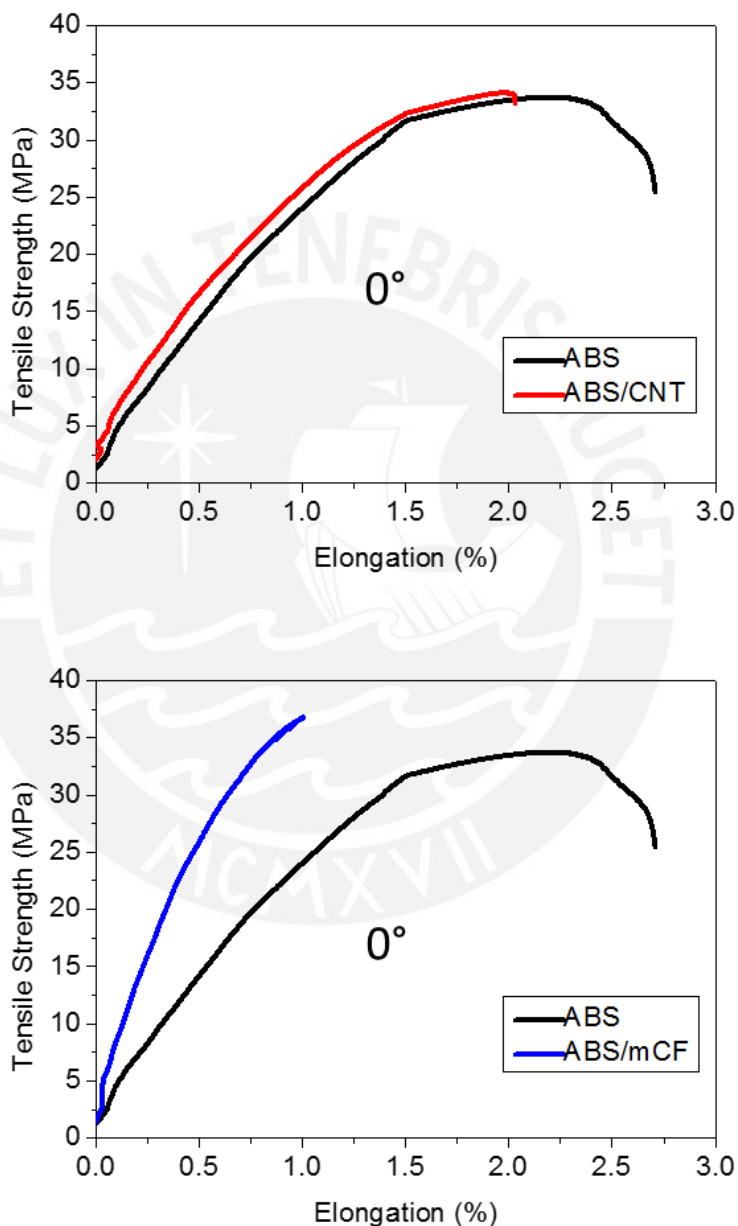
Figure 61. Stress-strain diagrams of 0° FDM ABS (black) ABS/CNT (red) and ABS/mCF (blue)
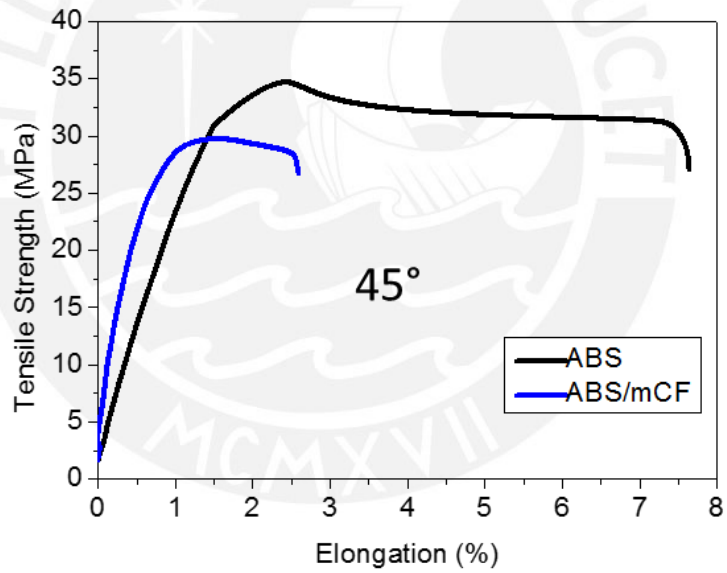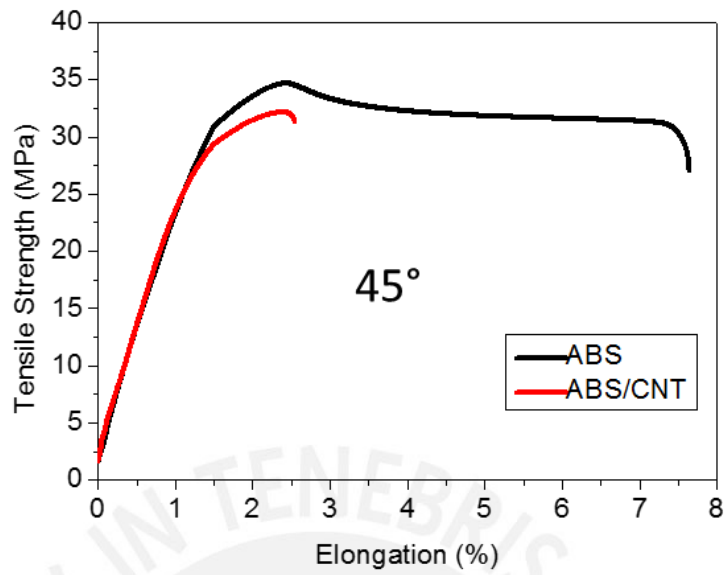
Figure 62. Stress-strain diagrams of 45° FDM ABS (black) ABS/CNT (red) and ABS/mCF (blue)
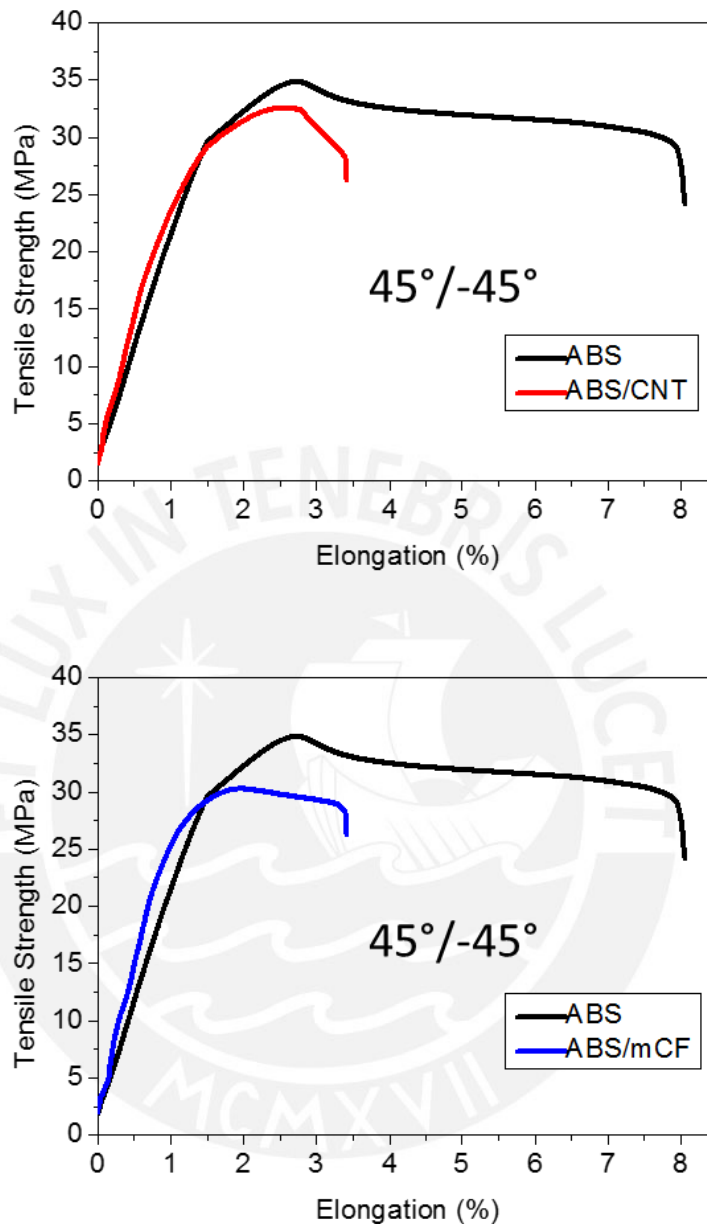
Figure 63. Stress-strain diagrams of 45°/-45° FDM ABS (black) ABS/CNT (red) and ABS/mCF (blue)

SEM and LSM analysis was conducted on the failure surfaces of FDM specimens of each ABS based material in study to analyze the arrangement of the threads deposited, the arrangement of the reinforcements, the interaction between the reinforcements and the ABS matrix and also the porosity of the specimens. This, looking for an explanation on the changes achieved in mechanical properties.

FDM ABS/CNT experience a remarkable loss of elongation in comparison with the pure FDM ABS, even if the temperature of printing was higher for the nanocomposite material.

Comparing the SEM images from the tensile surface of failure of FDM ABS and the ABS/CNT (Figure 64 and Figure 65), it can be seen that the pure ABS specimen present a ductile failure in comparison to the brittle failure of the nanocomposite. Also, it can be seen that the FDM ABS/CNT do not shown good adherence between the threads deposited being able to easily recognize each deposited thread in comparison to the FDM ABS.

This can corroborate what literatures attribute to this loss of elongation by adding multiwalled carbon nanotubes: the interference that the nano reinforcements could represent to the unfolding of the polymer chains during a tension and that the high thermal conductivity from the carbon nanotubes could quickly cool the treads deposited not allowing the formation of a continuous structure [66][67].
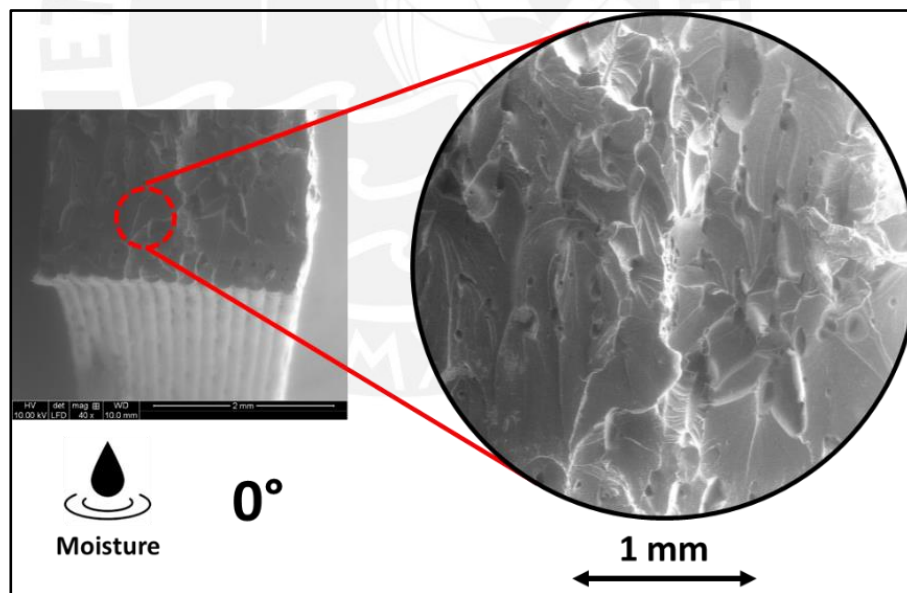
Figure 64. SEM imaging from the failure surface of FDM pure ABS specimen printed with moisture exposed filament (0° layer printing orientation and 0.2 mm layer height)
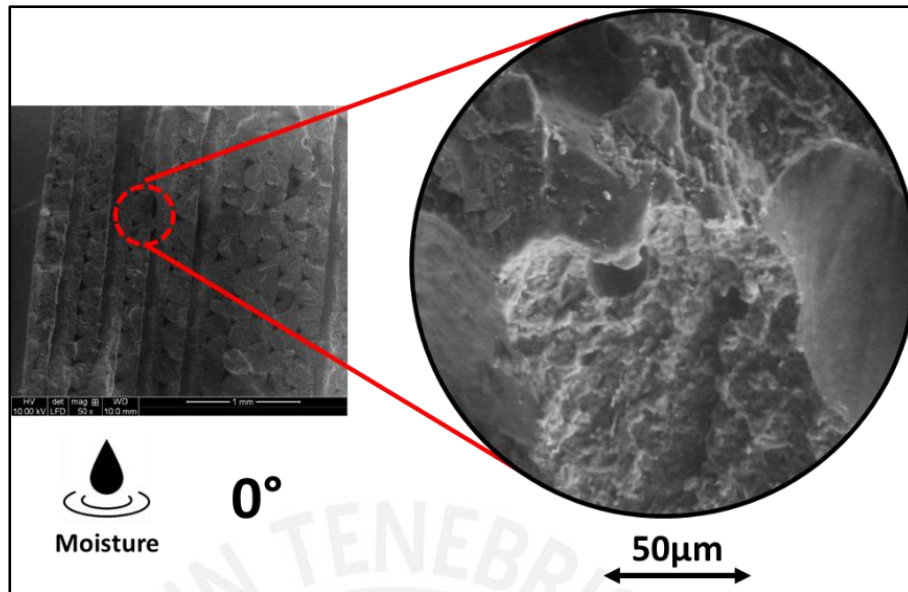
Figure 65. SEM imaging from the failure surface of FDM ABS/CNT specimen printed with moisture exposed filament (0° layer printing orientation and 0.2 mm layer height)

FDM ABS/mCF experiment a significant variation on the tensile properties because of the anisotropy and humidity.

To analyze the anisotropy and humidity influence, LSM imaging from specimens' failure surface which behavior was closest to the mean were analyzed.

Analyzing the LSM imaging from each layer printing orientation it can be seen on Figure 67 that a pattern of alignment occurs and this pattern in which the micro fibers are aligned for each case depend on the threads deposition orientation, this given the size of the reinforcement and the pressure involved in the process although is not much [57]. For example, on the 0° layer orientation samples failure surface is mostly seen the head of the failure given the extrusion in a parallel direction to the traction unlike the 45° and 45°/-45° alignments where more area from the fibers can be seen.

In Figure 66 and Figure 67 it can be seen that both, for ABS and ABS/mCF, the humidity has an influence on the porosity of the solid interior, appearing in both cases voids because of the water removal process that takes place during the extrusion in the form of vapor bubble blasts. Because of this, it was decided to do an analysis in

higher resolution, particularly in the case of ABS/mCF. On Figure 67 the voids are circled in red.
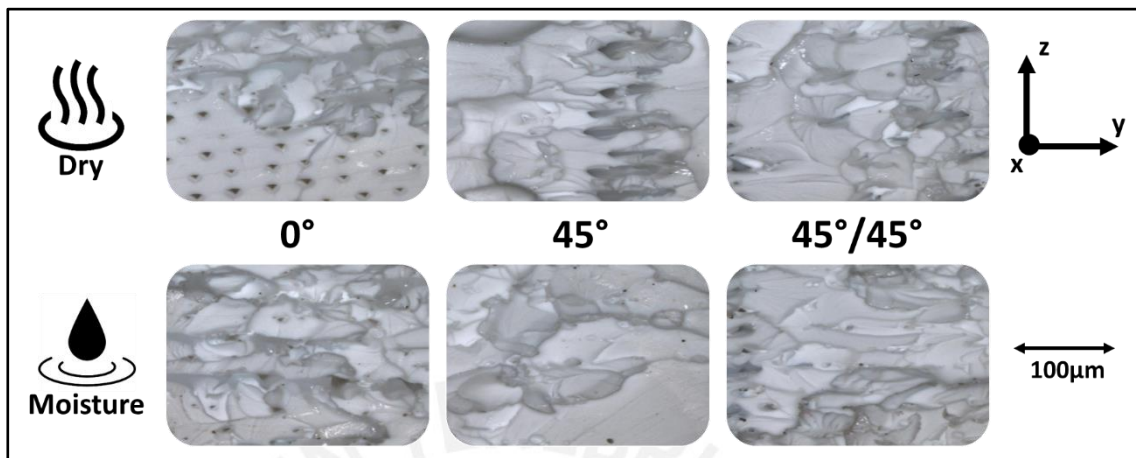
Figure 66. LSM imaging from the failure surface of FDM pure ABS specimens printed with dry and moisture exposed filaments (layer height of 0.2 mm)
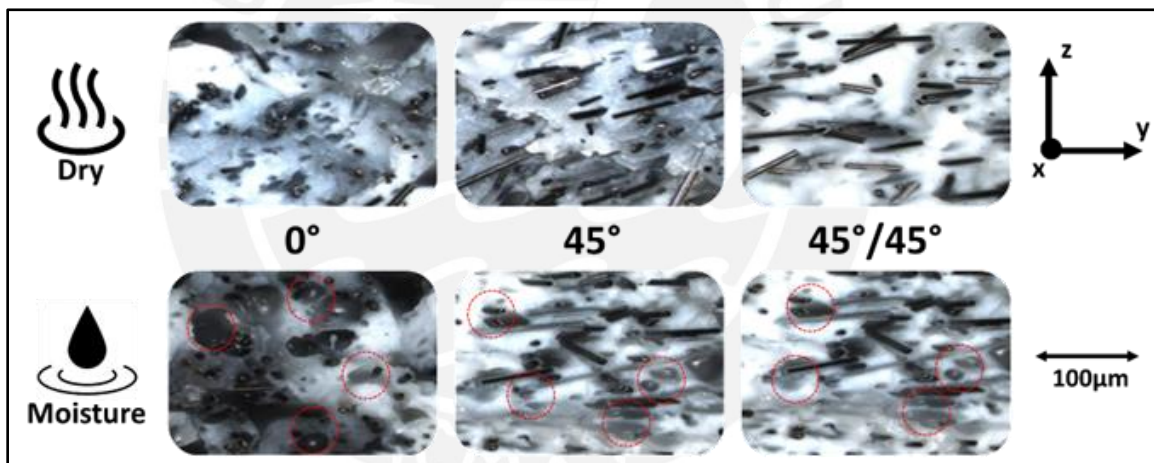
Figure 67. LSM imaging from the failure surface of FDM ABS/mCF specimens printed with dry and moisture exposed filaments (layer height of 0.2 mm)

An analysis of the interaction between the short carbon fibers and the ABS matrix was made with a higher resolution also by LSM imaging.

As can be seen on Figure 68, the interaction between the micro fibers and the ABS matrix on threads deposited from dry ABS/mCF filaments has no voids or discontinuities, thus having a correct adhesion.

This is not the case for the interaction between the micro reinforcements and the matrix on the threads deposited from moisture exposed filaments. As can be seen on Figure 69, the humidity not only is removed by the vapor bubble blasts but also around the fibers themselves, impoverishing even more the adherence between the fibers and the matrix.

With this analysis it is evidenced the main reason for the poor mechanical behavior of the FDM ABS/mCF specimens printed with moisture exposed filaments, in which the poor adhesion between the matrix and the reinforcements makes the fibers work more like pores than like reinforcement.
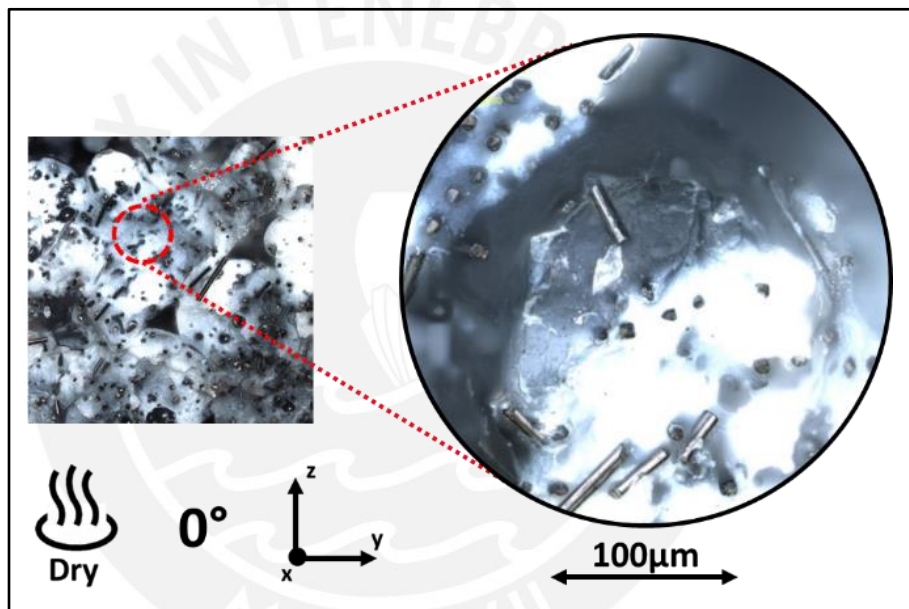
Figure 68. LSM imaging from the failure surface of FDM ABS/mCF specimen printed with dry filament and focus in the reinforcement interaction (0° layer printing orientation and layer height of 0.2 mm)
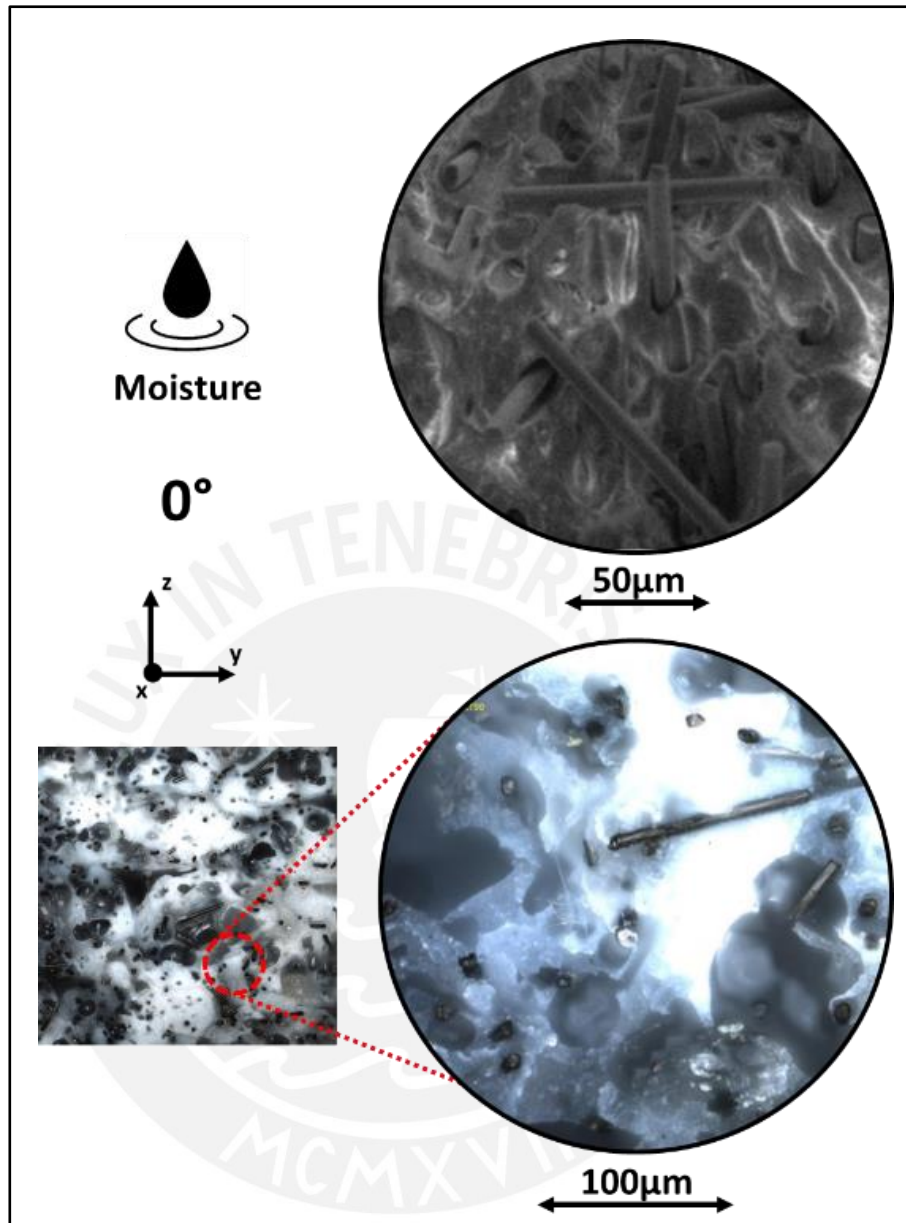
Figure 69. LSM and SEM imaging from the failure surface of FDM ABS/mCF specimen printed with moisture exposed filament and focus in the reinforcement interaction (0° layer printing orientation and layer height of 0.2 mm)

This weak adherence between the mCF and the ABS can be also demonstrated in the SEM images of the failure surface from the FDM ABS/mCF tensile specimens.

As can be seen in Figure 70 the micro carbon fibers continue with lengths of around 100 μm and the diameter of around 7 μm the same dimensions from the filament raw materials (Figure 36) demonstrating the failure of the adherence before the failure of the fibers.

82
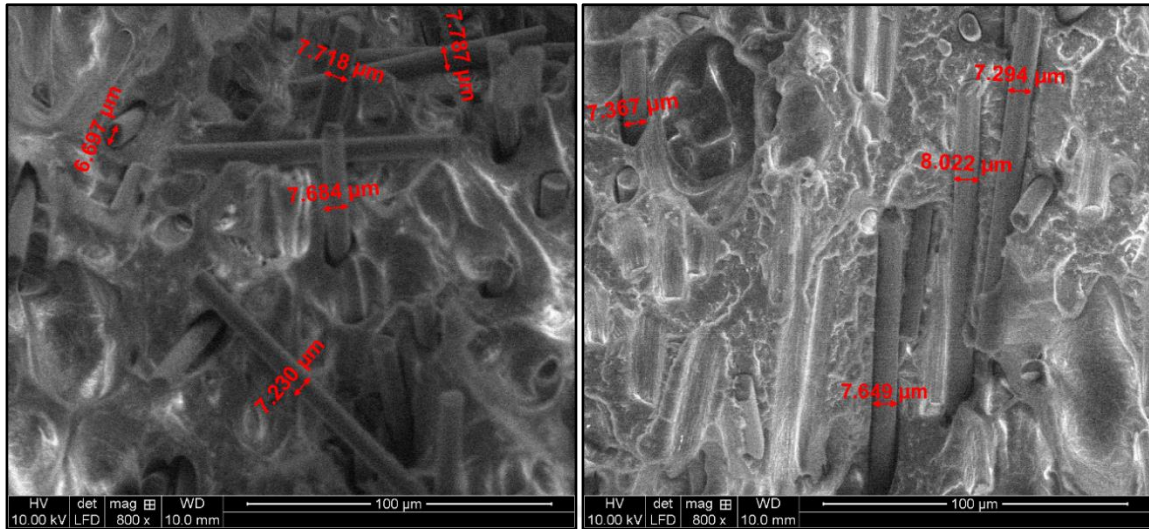
Figure 70. SEM imaging from the failure surface of FDM ABS/mCF printed with moisture exposed filament pointing the diameters of the fibers exposed (0° and 45° layer printing orientations from left to right and layer height of 0.2 mm)

5.4.3 Influence of anisotropy and humidity on electrical volume resistivity

Electrical resistivity was analyzed on FDM specimens for each ABS base material in study. This according to the essay methodology described in section 4.2.8.

Because of the high resistivity of the pure ABS and the ABS/mCF materials, it was impossible to measure the values by the test described. Theoretically, the resistivity of ABS is between 1.4×10^{16} to 1.7×10^{16} Ω.cm [45] which makes this polymer an electrical insulator for being above 10×10^9 Ω.cm [65].

It was not the case for the ABS/CNT where multiwall carbon nanotubes decrease the resistance making it possible to use the methodology described earlier. The resistance was obtained and results are presented for each layer printing orientation in study on Figure 71.
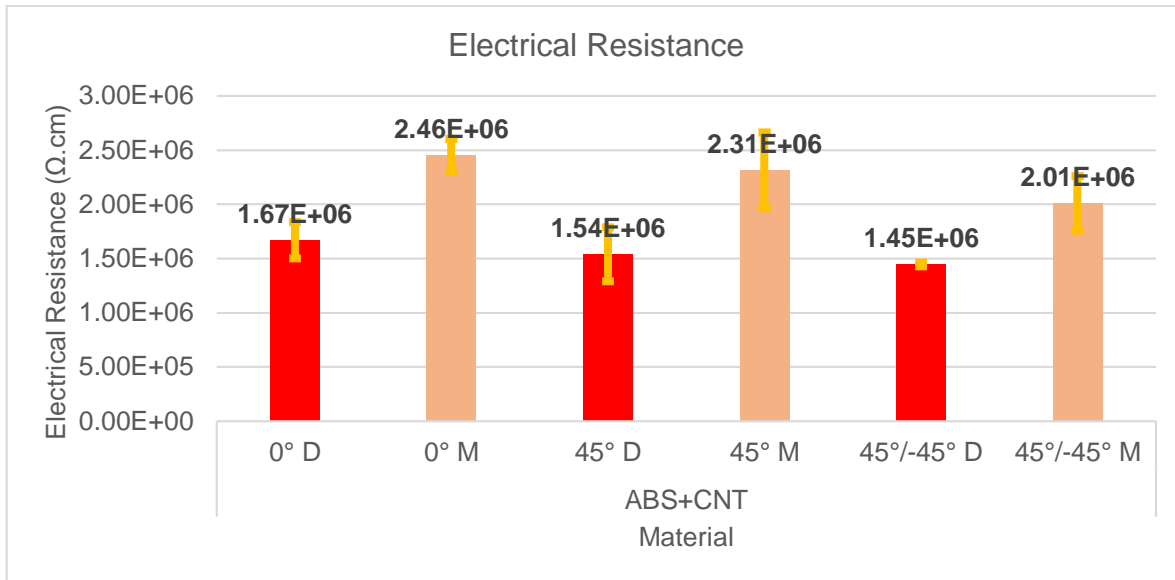
Figure 71. Electrical Resistance from FDM ABS/CNT specimens printed with dry (red) and moisture exposed (pink) filaments (0.2 mm layer height)

Results presented shown that the ABS reduces its volume resistivity by adding 10wt% of mutiwalled carbon nanotubes (ABS/CNT) from around 10^{16} Ω.cm to 10^6 Ω.cm, changing the electrical behavior of the polymer from an insulator material to a semiconductor for being between 10^5 Ω.cm to 10^9 Ω.cm [65].

Analyzing the influence of the humidity, it can be notice that the water absorption of the filaments leads to an increase the volume resistivity value in all the ABS/CNT layer orientations specimens, impoverishing the electrical conductivity. This can be attributed to the less uniform structure the specimens printed with moisture exposed filaments have because of the steam explosions while printing, as discussed before.

Analyzing the influence of anisotropy, no greater influence on the volume resistivity was found due to layer printing orientation. The main reason is because of the volume resistivity test principle which measure the resistance the material have to conduce electrons throw a volume which is delimitated by the area of the cooper plates and the height of the specimens or the height of all the layers deposited (see Figure 28).

The dispersion and functionalization of the carbon nanotubes are essential to study and take into account to achieve special properties on polymer-based

84

nanocomposites but those variables should be decided and applied while extruding the FDM filaments [71].

The diagrams from the essay and all the values can be seen in the annexes 8.3.

5.4.4 Influence of anisotropy and humidity in surface roughness

To analyze the influence of the humidity on the surface finishing a roughness analysis was made on pure ABS FDM samples printed with an orientation of 45° and a layer height of 0.2 mm, in the two humidity conditions in study: samples printed with dry filaments and printed with moisture exposed ones.

The analysis was mas by a lineal roughness analysis in the laser scanning microscope (LSM) which requests the drawing of a line on the image displayed in which the laser make a sweep in a chosen depth range.

The area of analysis for specimens printed with a dry filament is displayed in Figure 72. The roughness was measured along the line drawn by making 45° with the X axis to measure the height variation passing over all the deposited threads as can be seen in Figure 73. The spectrum that the analysis generates is shown in Figure 74 and the roughness calculated was 29.68 µm in arithmetical average units (Ra).
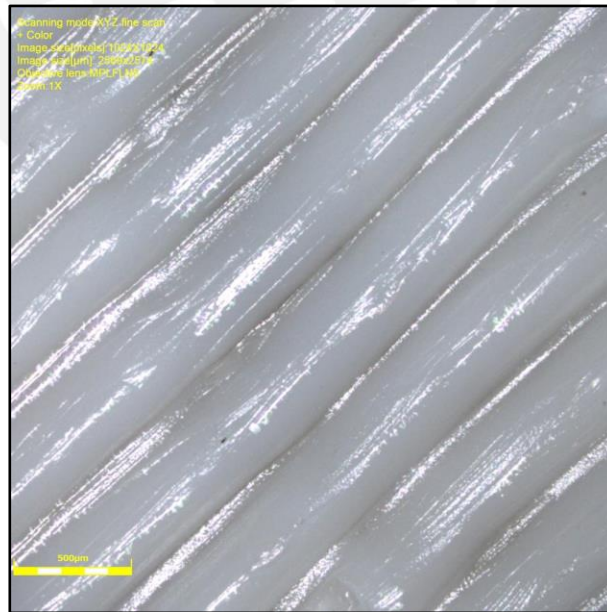
Figure 72. LSM intensities image of FDM ABS specimen printed with dry filament surface

85
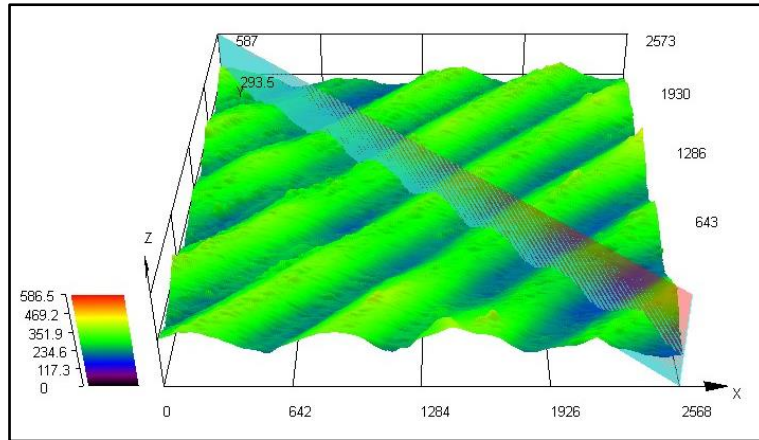
Figure 73. 3D image of the roughness line in analysis of FDM ABS specimen printed with dry filament in microns
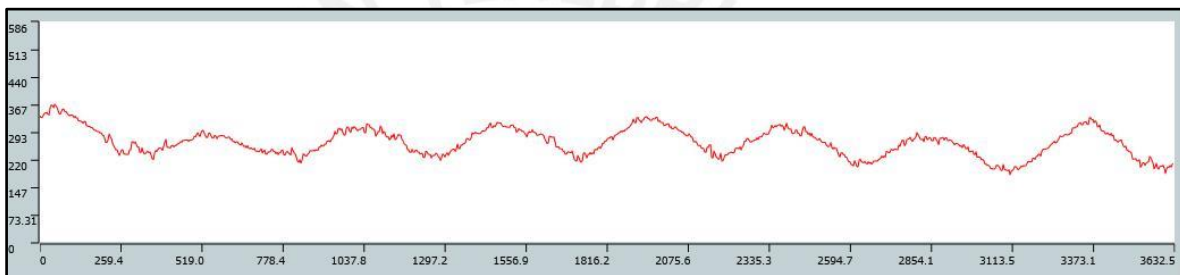
Figure 74. Lineal roughness spectrum of FDM ABS specimen printed with dry filament

On the specimens printed with a moisture exposed filaments the test set-up was the same: with the area in analysis displayed in Figure 75 and the roughness line drawn for the analysis displayed in a 3D heights image on Figure 76. The spectrum that the analysis generates is shown in Figure 77 and the roughness calculated was 23.96 µm in arithmetical average units (Ra).
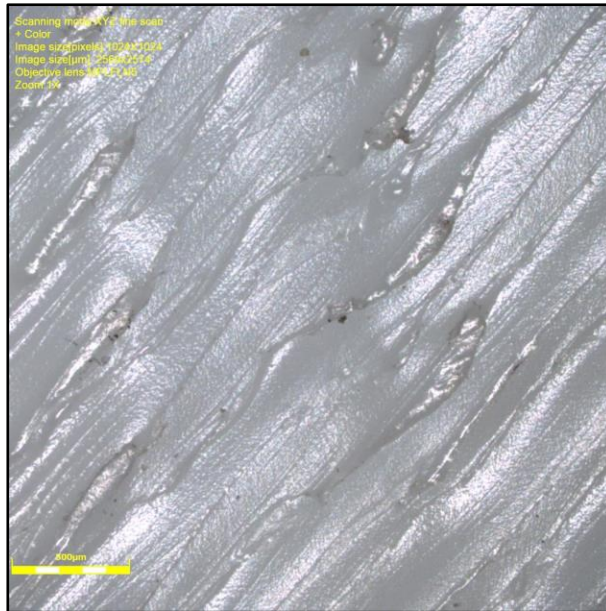
Figure 75. LSM intensities image of FDM ABS specimen printed with moisture exposed filament surface
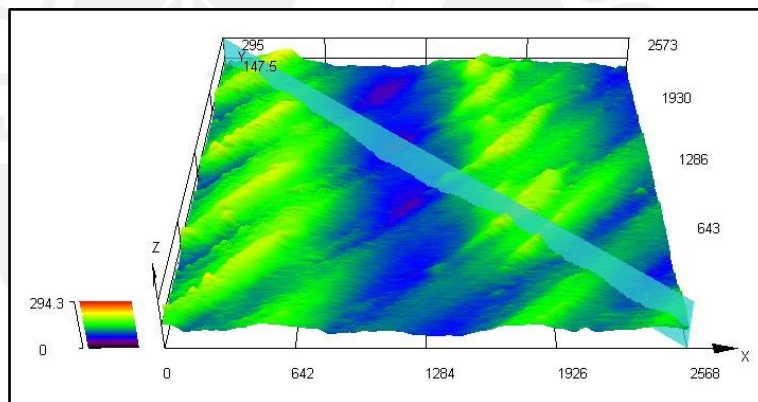
Figure 76. 3D image of the roughness line in analysis of FDM ABS specimen printed with moisture exposed filament in microns
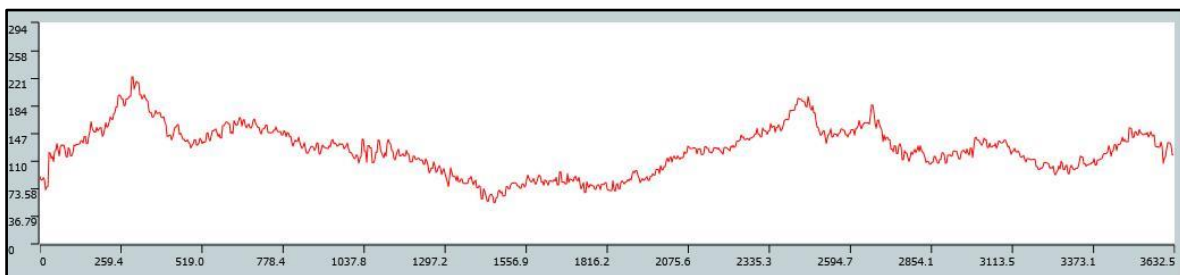
Figure 77. Lineal roughness spectrum of FDM ABS specimen printed with moistures exposed filament

Results show that specimens printed with a dry filament exhibit a uniform surface finishing, where each thread can be recognized. On the other hand, the specimens printed with a moisture exposed filament have a lower value of roughness. The smoother surface in the specimens printed with moisture exposed filaments lies on the fact that the humidity in the filaments is removed during the thread extrusion process as steam explosions. This effect distort the dimensions of the threads deposited generating an overlap between them (as seen in Figure 75), filling the typical concavities observed in FDM 3D printing as a result of depositing two threads of circular section one to the side of another (as seen in Figure 72).

6. Conclusions

An investigation was conducted to evaluate the effect of anisotropy and humidity on the mechanical properties, electrical conductivity, and surface finishing, of ABS based composite materials fabricated by 3D printing using the FDM process. Three filaments were used for the study: pure ABS, ABS with micro carbon fibers, and ABS with carbon nanotubes.

The filaments were structurally characterized by a FTIR, DSC/TG and SEM/FESEM analysis concluding the following:

- Pure ABS filament corresponds to 100 wt% ABS.
- The ABS/CNT filament composition correspond to 90 wt% ABS and 10 wt% multiwalled carbon nanotubes (diameter 10nm to 20nm).
- The ABS/mCF filament composition correspond to 85 wt% ABS and 15 wt% micro carbon fibers (diameter 6µm to 7µm).

A mechanical characterization of the filaments was conducted by tensile test under ASTM standards, this to have a base of comparison regarding to the resistance the FDM samples can achieve.

ABS filament maximum strength was 34.9 MPa, ABS/CNT reached a maximum strength of 33.38 MPa losing around 4% compared to the ABS resistance and ABS/mCF reached a maximum strength of 37.69 MPa increasing the resistance of the ABS by around 8%. The tensile modulus on the pure ABS filament was 1686 MPa, ABS/CNT had a tensile modulus of 1794 MPa increasing the rigidity in comparison with the ABS in around 6% and ABS/mCF also increase the rigidity but in this case the increase was of around 152% presenting a tensile modulus of 4254 MPa. The elongation reached for the pure ABS was 5.56%, both composites could not reach similar values having a mean elongation of 1.89% for the ABS/CNT and 1.23% the ABS/mCF.

To determine which layer height and layer printing orientations were going to be convenient to study in detail for the present thesis, a tensile and roughness analysis was made concluding that for higher properties and a better surface finish it would

89

be more convenient to study only 0.2 mm layer height in the layer printing orientations of 0°, 45° and 45°/-45° (in relation to the direction of the tensile stresses) (see section 5.3).

To analyze the anisotropy and humidity influence on the fused deposition modelling specimens (FDM), the tensile behavior and SEM/LSM imaging from the failure surfaces were compared between the different layer printing orientations and the two humidity conditions in study for the filaments (dry and moisture exposed).

It was concluded that anisotropy does not have a considerable influence on the FDM ABS/CNT, with a maximum variation by changing the layer printing orientations from 33.83 MPa for 0° to 32.17 MPa for 45° in the tensile strength, from 2289 MPa for 0° to 1977 MPa for 45°/-45° in the tensile modulus and from 2.64% for 45°/-45°to 1.89% for 0° in the elongation reached.

That was not the case for the FDM ABS/mCF, were anisotropy has a significant influence on the mechanical properties because most of the micro carbon fibers are aligned in the direction of the threads deposition and this alignment influences on the adherence/performance of the reinforcements. Tensile properties can vary by changing the layer printing orientations from 36.56 MPa for 0° to 29.61 MPa for 45° in the tensile strength, from 3853 MPa for 0° to 2589 MPa for 45° in the tensile modulus and from 2.86% for 45°/-45°to 1.06% for 0° in the elongation reached.

Humidity influence on the ABS/CNT was also not very significant. The maximum variation comparing the moisture conditions of the filament in each layer printing orientation was from 32.17 MPa to 31.66 MPa in the tensile strength on the 45° specimens, from 2154 MPa to 2039 MPa in the tensile modulus on the 45° specimens and from 2.39% to 3% in the elongation on 45° specimens also.

On the ABS/mCF the humidity has a significant influence because the adhesion between the micro fibers and the matrix is affected by internal voids which generates the removal of the moisture from the filaments during the threads deposition. The maximum variation comparing the moisture conditions of the filament in each layer

90

printing orientation was from 36.56 MPa to 23.80 MPa in the tensile strength on the 0° specimens, from 3853 MPa to 2282 MPa in the tensile modulus on 0° specimens and from 1.06% to 1.83% in the elongation also on 0° specimens.

It was also concluded that in all the cases in which the variance allows to affirm, specimens printed with moisture exposed filaments exhibited an increase in the maximum elongation reached. This increase can be attributed to the internal porosity revealed by the microscopic imaging analysis on the failure surface.

In general, the behavior of the ABS/CNT and ABS/mCF, in comparison with the pure ABS, is fragile, with remarkable loss of elongation. The main reason of this low ductility is the obstacle that both high modulus reinforcements represent to the unfolding of the polymer chains. For the ABS/CNT despite of using a higher temperature of extrusion, the most fragile behavior was observed because of the high thermal conductivity of the nanotubes which quickly cool the thread deposited not allowing the formation of a continuous structure being able to easily recognize each one [66][67].

Anisotropy influence is very significant in the case of ABS/mCF because the alignment of the reinforcement depends on the layer orientation of printing; the more parallel are the fibers in comparison to the tensile forces, the better is the performance of the reinforcement. The humidity absorbed by the filament is not only removed by vapor bubble blasts, but also around the fibers themselves, impoverishing even more the adherence between the fibers and the matrix.

On the electrical resistance, ABS/mCF and ABS could not be essayed by the described methodology because of its high resistivity as insulate materials (1.4×10^{16} to 1.7×10^{16} Ω/cm) [45].

Not the same for ABS/CNT which reduces ABS volume resistivity by adding 10wt% of multiwalled carbon nanotubes from around 10^{16} Ω.cm to 10^{6} Ω.cm, changing the electrical behavior of the polymer from an insulator material to a semiconductor.

91

Analyzing the humidity influence it was concluded that the moisture exposure of the filaments increases the resistivity of the ABS/CNT FDM samples from 1.45×10^6 - 1.67×10^6 Ω.cm to 2.01×10^6 - 2.46×10^6 Ω.cm, this due to the less uniform structure the specimens printed with moisture exposed filaments have because of the steam explosions. The anisotropy of the layers does not have a significant influence on the electrical properties.

On the surface finishing, specimens printed with dry filaments have a more uniform surface structure where each thread can be recognized in comparison with specimens printed with moistures exposed filaments where the removal of the moisture as steam explosions distort the dimensions of each threads deposited generating an overlap between themselves filling the typical concavities and generating a smoother surface.

92

7. Future Work

Given the high impact resistance that characterizes ABS, a future analysis of how nano and micro reinforcements in study (ABS/CNT and ABS/mCF) influence on this mechanical property would be necessary.

The micro or short carbon fibers are characterized not only by having a high modulus but also by having an excellent thermal stability. For this reason, a thermo-mechanical analysis by tests such as vicat softening point or heat deflection temperature and dynamic mechanical analysis would be more than interesting to conduct.

Carbon nanotubes have numerous unique properties. Based on this, not only electrical test as the resistivity measured on the present thesis should be performed. Also essays such as thermal conductivity, heat diffusion, vibration dissipation and fatigue should be conducted to expand the properties study.
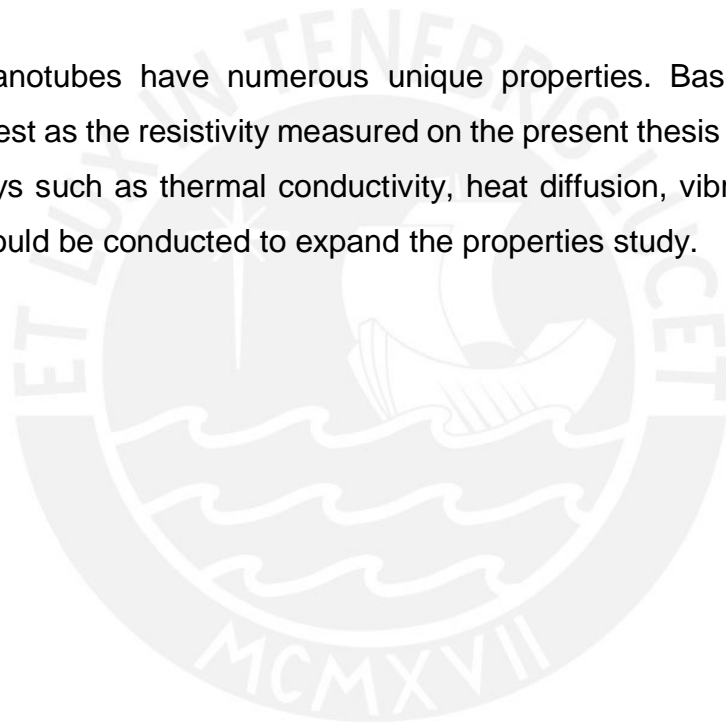
8. Annexes

8.1 Complete Tensile Results

Table 7. Tensile test analysis in ABS based filaments

Material (Filament)	Tensile Strength (MPa)	Tensile Modulus (MPa)	Elongation (%)
ABS	34.90 ± 0.86	1686 ± 36	5.56 ± 2.80
ABS+CNT	33.38 ± 0.59	1794 ± 40	1.89 ± 0.27
ABS+mCF	37.69 ± 1.88	4254 ± 142	1.23 ± 0.30

Table 8. Tensile test in ABS based FDM 3D printed specimens with moisture exposed filaments for layer height of 0.4mm

Material (h=0.4)	Layer Orientation (°)	Tensile Strength (MPa)	Tensile Modulus (MPa)	Elongation (%)
ABS	90°	31.84 ± 1.70	2016 ± 1736	2.89 ± 0.64
	0°	32.74 ± 0.74	2114 ± 427	2.34 ± 1.42
	45°	27.86 ± 0.57	1638 ± 268	2.06 ± 0.01
	0°/90°	29.13 ± 1.70	1752 ± 521	2.20 ± 0.40
	45°/-45°	28.13 ± 0.95	1531 ± 273	2.08 ± 0.04
ABS+CNT	90°	22.52 ± 1.30	1682 ± 627	2.31 ± 0.24
	0°	27.70 ± 3.26	1987 ± 879	1.77 ± 0.52
	45°	24.39 ± 1.52	1717 ± 300	1.44 ± 0.11
	0°/90°	25.36 ± 0.33	1999 ± 1393	1.73 ± 0.16
	45°/-45°	25.21 ± 1.10	1960 ± 563	1.79 ± 0.03
ABS+mCF	90°	18.30 ± 0.38	2188 ± 267	1.11 ± 0.23
	0°	18.93 ± 0.87	2209 ± 633	1.41 ± 0.19
	45°	19.22 ± 0.47	2278 ± 600	1.76 ± 0.02
	0°/90°	18.42 ± 1.10	2058 ± 631	1.79 ± 0.07
	45°/-45°	19.72 ± 0.37	2428 ± 348	1.88 ± 0.15

Table 9. Tensile test in ABS based FDM 3D printed specimens with moisture exposed filaments for layer height of 0.2mm

Material (h=0.2)	Layer Orientation (°)	Tensile Strength (MPa)	Tensile Modulus (MPa)	Elongation (%)
ABS	90°	34.71 ± 1.30	2232 ± 649	7.68 ± 0.95
	0°	32.83 ± 1.01	2166 ± 481	3.54 ± 0.51
	45°	35.21 ± 1.01	2052 ± 482	8.29 ± 1.87
	0°/90°	34.42 ± 0.62	2193 ± 1182	4.70 ± 1.33
	45°/-45°	34.53 ± 1.23	2046 ± 553	6.79 ± 2.56
ABS+CNT	90°	27.65 ± 1.94	1537 ± 511	3.16 ± 1.38
	0°	34.23 ± 0.95	2173 ± 597	2.13 ± 0.57
	45°	31.76 ± 0.97	2059 ± 489	3.29 ± 0.72
	0°/90°	30.70 ± 0.50	2008 ± 480	2.41 ± 0.37
	45°/-45°	32.42 ± 0.51	1818 ± 394	3.38 ± 0.79
ABS+mCF	90°	22.21 ± 0.85	2654 ± 646	3.59 ± 0.58
	0°	23.33 ± 1.65	2326 ± 971	1.85 ± 0.36
	45°	25.04 ± 0.93	2370 ± 281	3.03 ± 0.78
	0°/90°	23.45 ± 0.54	2752 ± 725	2.68 ± 0.36
	45°/-45°	26.18 ± 0.19	3861 ± 1574	2.66 ± 0.72

Table 10. Tensile test in ABS based FDM 3D printed specimens with dried filaments for layer height of 0.2mm

Material (h=0.2)	Layer Orientation (°)	Tensile Strength (MPa)	Tensile Modulus (MPa)	Elongation (%)
ABS	0°	33.76 ± 0.26	1955 ± 357	2.90 ± 1.24
	45°	34.77 ± 0.24	2099 ± 103	7.70 ± 0.27
	45°/-45°	34.97 ± 0.84	2068 ± 182	9.48 ± 3.25
ABS+CNT	0°	33.83 ± 0.99	2289 ± 46	1.89 ± 0.29
	45°	32.17 ± 0.12	2154 ± 148	2.39 ± 0.01
	45°/-45°	32.43 ± 0.12	1977 ± 606	2.64 ± 0.47
ABS+mCF	0°	36.56 ± 0.90	3853 ± 467	1.06 ± 0.05
	45°	29.61 ± 0.13	2589 ± 520	2.79 ± 0.20
	45°/-45°	30.48 ± 0.23	2446 ± 690	2.86 ± 0.63
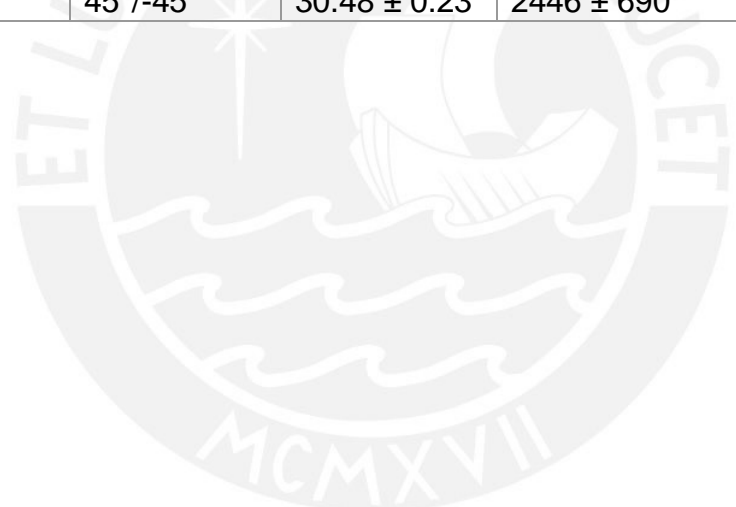
8.2 Complete Density Results

Table 11. Density analysis in ABS based Filaments

Material (Filament)	Density (g/cm^3)
ABS	1.031 ± 0.006
ABS+CNT	1.039 ± 0.007
ABS+mCF	1.016 ± 0.008

Table 12. Density analysis in ABS based 3D printed specimens with layer height of 0.4 mm

Material (h=0.4)	Layer Orientation (°)	Density (g/cm^3)
ABS	90°	0.954 ± 0.031
	0°	0.957 ± 0.027
	45°	0.942 ± 0.018
	0°/90°	0.936 ± 0.057
	45°/-45°	0.935 ± 0.043
ABS+CNT	90°	0.947 ± 0.034
	0°	0.962 ± 0.039
	45°	0.957 ± 0.028
	0°/90°	0.931 ± 0.076
	45°/-45°	0.939 ± 0.073
ABS+mCF	90°	0.896 ± 0.028
	0°	0.796 ± 0.114
	45°	0.877 ± 0.020
	0°/90°	0.841 ± 0.083
	45°/-45°	0.879 ± 0.043

Table 13. Density analysis in ABS based 3D printed specimens with layer height of 0.2 mm

Material (h=0.2)	Layer Orientation (°)	Density (g/cm³)
ABS	90°	1.008 ± 0.044
	0°	0.980 ± 0.041
	45°	1.006 ± 0.035
	0°/90°	1.000 ± 0.031
	45°/-45°	0.999 ± 0.030
ABS+CNT	90°	0.967 ± 0.058
	0°	0.953 ± 0.037
	45°	0.977 ± 0.042
	0°/90°	0.975 ± 0.045
	45°/-45°	0.991 ± 0.051
ABS+mCF	90°	0.982 ± 0.026
	0°	0.910 ± 0.025
	45°	0.973 ± 0.019
	0°/90°	0.953 ± 0.020
	45°/-45°	0.982 ± 0.021

8.3 Flows of Electrical Resistance

Table 14. ABS+CNT electrical resistance

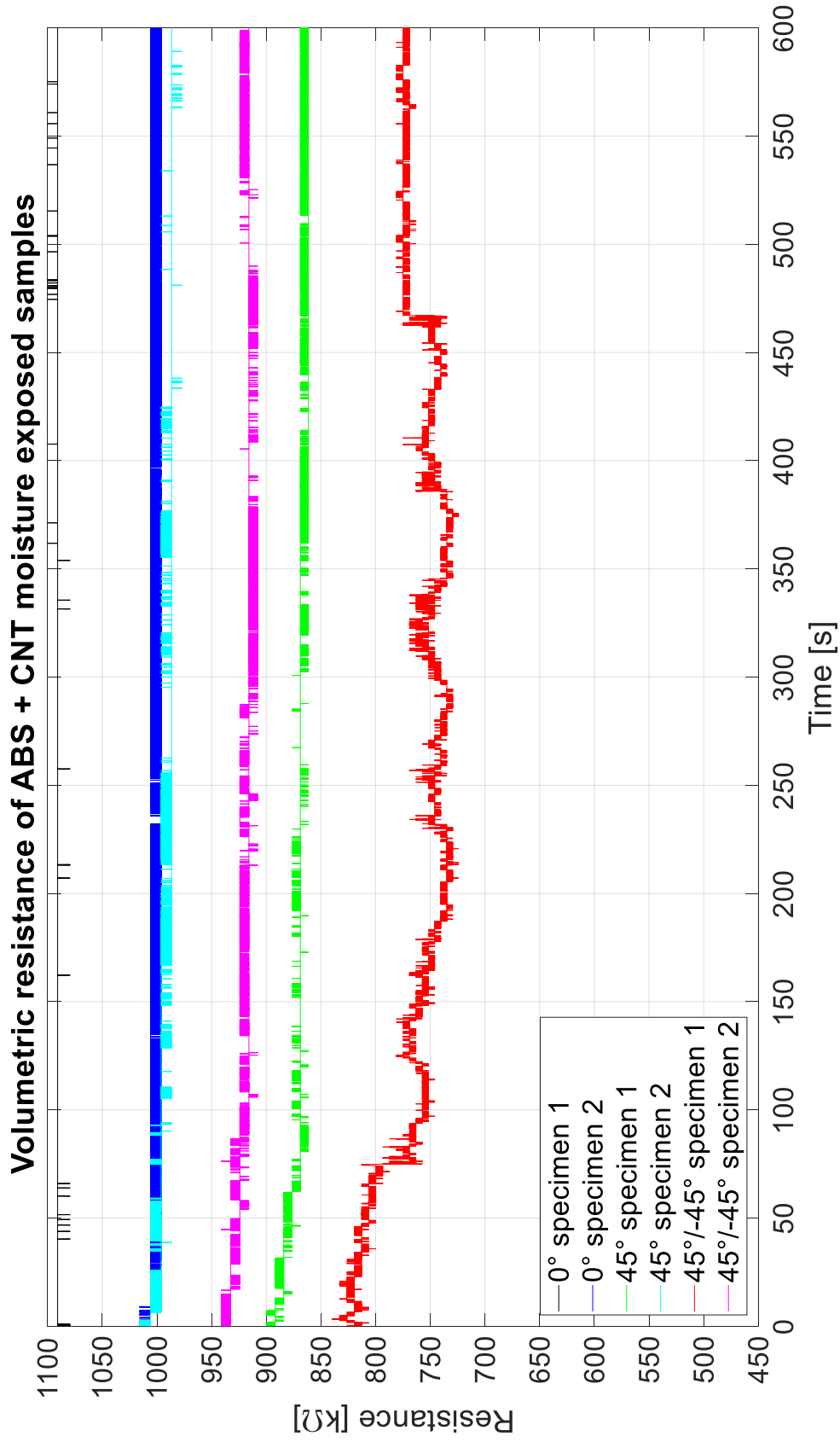| Specimens of ABS+CNT		Resistance (Ω)	Resistance (Ω.cm)
Moisture exposed filament	H^L=0.2mm O°=0°	1.00×10^6 – 1.09×10^6	2.35×10^6 – 2.56×10^6
	H^L=0.2mm O°=45°	0.88×10^6 – 1.09×10^6	2.07×10^6 – 2.56×10^6
	H^L=0.2mm O°=45°/-45°	0.78×10^6 – 0.93×10^6	1.83×10^6 – 2.19×10^6
Dry filament	H^L=0.2mm O°=0°	0.66×10^6 – 0.76×10^6	1.55×10^6 – 1.79×10^6
	H^L=0.2mm O°=45°	0.58×10^6 – 0.73×10^6	1.36×10^6 – 1.72×10^6
	H^L=0.2mm O°=45°/-45°	0.61×10^6 – 0.62×10^6	1.43×10^6 – 1.46×10^6

Figure 78. Electrical resistance of specimens printed by FDM with ABS+CNT moisture exposed filament with layer height of 0.2 mm and printing orientations of 0°, 45° and 45°/-45°
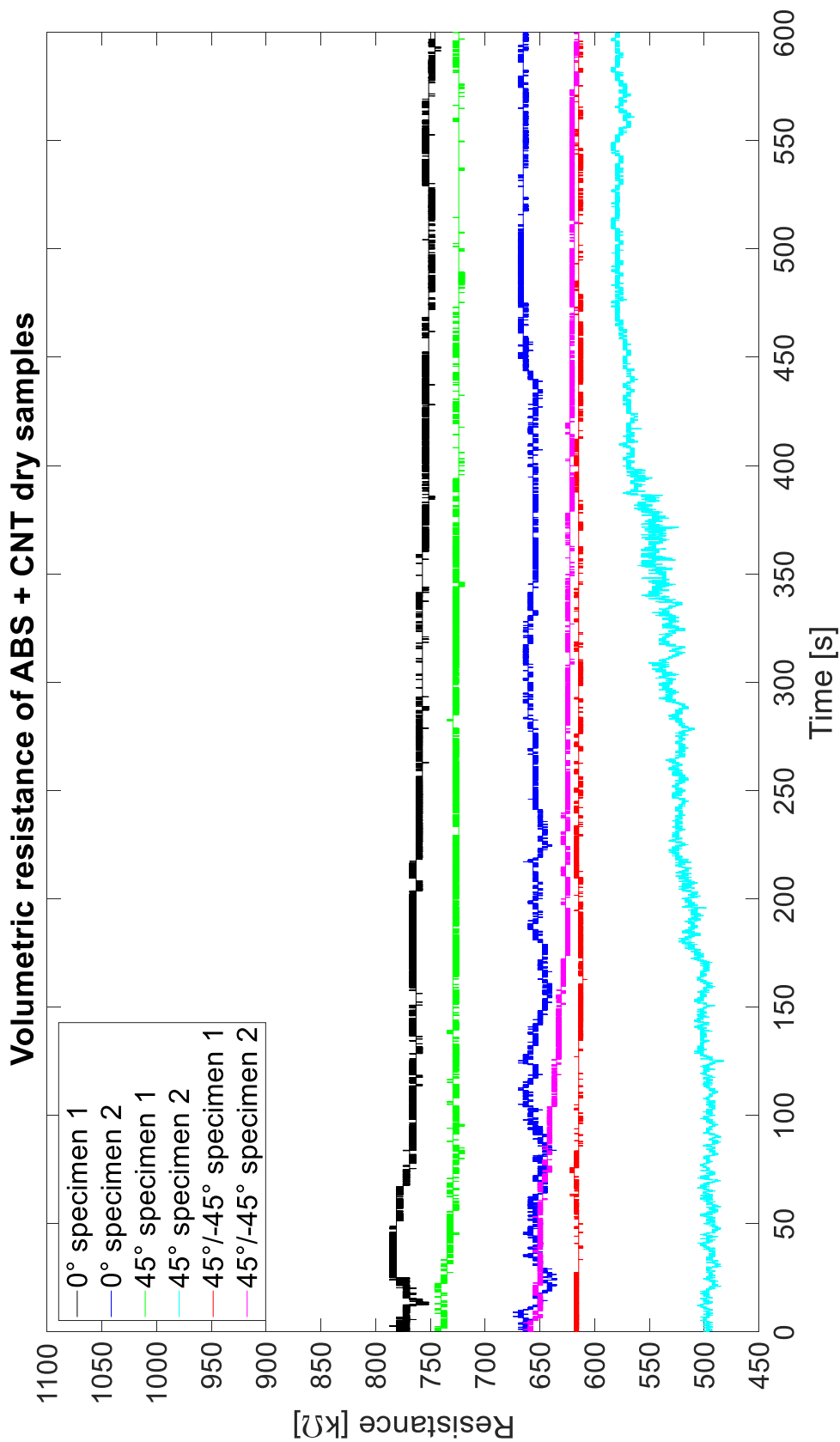
Figure 79. Electrical resistance of specimens printed by FDM with ABS+CNT dried filament with layer height of 0.2 mm and printing orientations of 0°, 45° and 45°/-45°

9. References

[1] ASTM F2792-10-1. (2010). Standard terminology for additive manufacturing technologies. ASTM International.

[2] Berman, B. (2012). 3-D printing: The new industrial revolution. Business horizons, 55(2), 155-162.

[3] Durgun, I., & Ertan, R. (2014). Experimental investigation of FDM process for improvement of mechanical properties and production cost. Rapid Prototyping Journal, 20(3), 228-235.

[4] Ivanova, O., Williams, C., & Campbell, T. (2013). Additive manufacturing (AM) and nanotechnology: promises and challenges. Rapid Prototyping Journal, 19(5), 353-364.

[5] Lipson, H., & Kurman, M. (2013). Fabricated: The new world of 3D printing. John Wiley & Sons, 1-24.

[6] Gebler, M., Uiterkamp, A. J. S., & Visser, C. (2014). A global sustainability perspective on 3D printing technologies. Energy Policy, 74, 158-167

[7] Wittbrodt, B. T., Glover, A. G., Laureto, J., Anzalone, G. C., Oppliger, D., Irwin, J. L., & Pearce, J. M. (2013). Life-cycle economic analysis of distributed manufacturing with open-source 3-D printers. Mechatronics, 23(6), 713-726.

[8] Singh, R., & Singh, S. (2014). Development of nylon based FDM filament for rapid tooling application. Journal of The Institution of Engineers (India): Series C, 95(2), 103-108.

[9] Rahman, K. M., Letcher, T., & Reese, R. (2015, November). Mechanical Properties of Additively Manufactured PEEK Components Using Fused Filament Fabrication. In ASME 2015 International Mechanical Engineering Congress and Exposition (pp. V02AT02A009-V02AT02A009). American Society of Mechanical Engineers.

[10] Bernasconi, R., Natale, G., Levi, M., & Magagnin, L. (2015). Electroless Plating of PLA and PETG for 3D Printed Flexible Substrates. ECS Transactions, 66(19), 23-35.

[11]   Hill, N., & Haghi, M. (2014). Deposition direction-dependent failure criteria for fused deposition modeling polycarbonate. Rapid Prototyping Journal, 20(3), 221-227.

[12]   Shim, J. H., Won, J. Y., Sung, S. J., Lim, D. H., Yun, W. S., Jeon, Y. C., & Huh, J. B. (2015). Comparative efficacies of a 3D-printed PCL/PLGA/β-TCP membrane and a titanium membrane for guided bone regeneration in beagle dogs. Polymers, 7(10), 2061-2077.

[13]   Dul, S., Fambri, L., & Pegoretti, A. (2016). Fused deposition modelling with ABS–graphene nanocomposites. Composites Part A: Applied Science and Manufacturing, 85, 181-191.

[14]   Ning, F., Cong, W., Qiu, J., Wei, J., & Wang, S. (2015). Additive manufacturing of carbon fiber reinforced thermoplastic composites using fused deposition modeling. Composites Part B: Engineering, 80, 369-378.

[15]   Perez, A. R. T., Roberson, D. A., & Wicker, R. B. (2014). Fracture surface analysis of 3D-printed tensile specimens of novel ABS-based materials. Journal of Failure Analysis and Prevention, 14(3), 343-353.

[16]   Gibson, R. F. (2016). Principles of composite material mechanics. CRC press.

[17]   Plymill, A., Minneci, R., Greeley, D. A., & Gritton, J. (2016). Graphene and Carbon Nanotube PLA Composite Feedstock Development for Fused Deposition Modeling.

[18]   Postiglione, G., Natale, G., Griffini, G., Levi, M., & Turri, S. (2015). UV-assisted three-dimensional printing of polymer nanocomposites based on inorganic fillers. Polymer Composites.

[19]   Compton, B. G., & Lewis, J. A. (2014). 3D-printing of lightweight cellular composites. Advanced Materials, 26(34), 5930-5935.

[20]   Zhong, W., Li, F., Zhang, Z., Song, L., & Li, Z. (2001). Short fiber reinforced composites for fused deposition modeling. Materials Science and Engineering: A, 301(2), 125-130.

[21]   Wang, Z. J., Kwon, D. J., Gu, G. Y., Kim, H. S., Kim, D. S., Lee, C. S., ... & Park, J. M. (2013). Mechanical and interfacial evaluation of

CNT/polypropylene composites and monitoring of damage using electrical resistance measurements. Composites Science and Technology, 81, 69-75.

[22]   Tehrani, M., Boroujeni, A. Y., Hartman, T. B., Haugh, T. P., Case, S. W., & Al-Haik, M. S. (2013). Mechanical characterization and impact damage assessment of a woven carbon fiber reinforced carbon nanotube–epoxy composite. Composites Science and Technology, 75, 42-48.

[23]   Rezaei, F., Yunus, R., & Ibrahim, N. A. (2009). Effect of fiber length on thermomechanical properties of short carbon fiber reinforced polypropylene composites. Materials & Design, 30(2), 260-263.

[24]   Wang, X., Jiang, Q., Xu, W., Cai, W., Inoue, Y., & Zhu, Y. (2013). Effect of carbon nanotube length on thermal, electrical and mechanical properties of CNT/bismaleimide composites. Carbon, 53, 145-152.

[25]   Latibari, S. T., Mehrali, M., Mottahedin, L., Fereidoon, A., & Metselaar, H. S. C. (2013). Investigation of interfacial damping nanotube-based composite.Composites Part B: Engineering, 50, 354-361.

[26]   F42 Committee. (2012). Terminology for Additive Manufacturing Technologies. ASTM International.

[27]   Conner, B. P., Manogharan, G. P., Martof, A. N., Rodomsky, L. M., Rodomsky, C. M., Jordan, D. C., & Limperos, J. W. (2014). Making sense of 3-D printing: Creating a map of additive manufacturing products and services.

[28]   Kreiger, M., & Pearce, J. M. (2013). Environmental life cycle analysis of distributed three-dimensional printing and conventional manufacturing of polymer products. ACS Sustainable Chemistry & Engineering, 1(12), 1511-1519.

[29]   Gebler, M., Uiterkamp, A. J. S., & Visser, C. (2014). A global sustainability perspective on 3D printing technologies. Energy Policy, 74, 158-167.

[30]   Gao, W., Zhang, Y., Ramanujan, D., Ramani, K., Chen, Y., Williams, C. B., ... & Zavattieri, P. D. (2015). The status, challenges, and future of additive manufacturing in engineering. Computer-Aided Design, 69, 65-89.

[31]   Kalsoom, U., Nesterenko, P. N., & Paull, B. (2016). Recent developments in 3D printable composite materials. RSC Advances, 6(65), 60355-60371.

[32]   Gibson, I., Rosen, D., & Stucker, B. (2014). Additive manufacturing technologies: 3D printing, rapid prototyping, and direct digital manufacturing. Springer.

[33]   Bose, S., Vahabzadeh, S., & Bandyopadhyay, A. (2013). Bone tissue engineering using 3D printing. Materials Today, 16(12), 496-504.

[34]   Murphy, S. V., & Atala, A. (2014). 3D bioprinting of tissues and organs. Nature biotechnology, 32(8), 773-785.

[35]   Inzana, J. A., Olvera, D., Fuller, S. M., Kelly, J. P., Graeve, O. A., Schwarz, E. M., ... & Awad, H. A. (2014). 3D printing of composite calcium phosphate and collagen scaffolds for bone regeneration. Biomaterials, 35(13), 4026-4034.

[36]   Vorndran, E., Moseke, C., & Gbureck, U. (2015). 3D printing of ceramic implants. MRS Bulletin, 40(02), 127-136.

[37]   Nyberg, E. L., Farris, A. L., Hung, B. P., Dias, M., Garcia, J. R., Dorafshar, A. H., & Grayson, W. L. (2017). 3D-printing technologies for craniofacial rehabilitation, reconstruction, and regeneration. Annals of biomedical engineering, 45(1), 45-57.

[38]   Dodziuk, H. (2016). Applications of 3D printing in healthcare. Kardiochirurgia i Torakochirurgia Polska, 13(3), 283-293.

[39]   Osswald, T. A., & Menges, G. (2012). Materials science of polymers for engineers. Carl Hanser Verlag GmbH Co KG.

[40]   Ashby, M. F., & Johnson, K. (2013). Materials and design: the art and science of material selection in product design. Butterworth-Heinemann.

[41]   Fried, J. R. (2003). Polymer science and technology. Pearson Education. Second Edition. 391,393-394.

[42]   Matsuo, M. (1969). Fine structures and fracture processes in plastic/rubber two-phase polymer systems. II. Observation of crazing

behaviors under the electron microscope. Polymer Engineering & Science, 9(3), 206-212.

[43]   Whelan, A. (2012). Polymer technology dictionary. Springer Science & Business Media. 14-15

[44]   Campo, E. A. (Ed.). (2015). Industrial polymers. Carl Hanser Verlag GmbH Co KG.

[45]   Ellis, B., & Smith, R. (Eds.). (2008). Polymers: a property database. CRC Press.

[46]   Ashby, M. F. (2004). Materials Selection in Mechanical Design. Third Edition, Butterworth-Heinemann. 54.

[47]   Ashby, M. F. (2009). Material and Process Charts. Granta Design. Version 1. Engineering Department, Cambridge University. 9

[48]   Lipson, H., & Kurman, M. (2013). Fabricated: The new world of 3D printing. John Wiley & Sons.

[49]   Guo, N., & Leu, M. C. (2013). Additive manufacturing: technology, applications and research needs. Frontiers of Mechanical Engineering, 8(3), 215-243.

[50]   Saito, R., Dresselhaus, G., & Dresselhaus, M. S. (1998). Physical properties of carbon nanotubes (Vol. 35). London: Imperial college press.

[51]   Amin, M. S., El-Gamal, S. M. A., & Hashem, F. S. (2015). Fire resistance and mechanical properties of carbon nanotubes–clay bricks wastes (Homra) composites cement. Construction and Building Materials, 98, 237-249.

[52]   Wang, X., Jiang, Q., Xu, W., Cai, W., Inoue, Y., & Zhu, Y. (2013). Effect of carbon nanotube length on thermal, electrical and mechanical properties of CNT/bismaleimide composites. Carbon, 53, 145-152.

[53]   Gardea, F., & Lagoudas, D. C. (2014). Characterization of electrical and thermal properties of carbon nanotube/epoxy composites. Composites Part B: Engineering, 56, 611-620.

[54]   3DX Tech EDS filament. www.3dxtech.com/3dxstat-esd-abs-3d-printing-filament/

[55]   Plymill, A., Minneci, R., Greeley, D. A., & Gritton, J. (2016). Graphene and Carbon Nanotube PLA Composite Feedstock Development for Fused Deposition Modeling.

[56]   Kalsoom, U., Nesterenko, P. N., & Paull, B. (2016). Recent developments in 3D printable composite materials. RSC Advances, 6(65), 60355-60371.

[57]   Ning, F., Cong, W., Qiu, J., Wei, J., & Wang, S. (2015). Additive manufacturing of carbon fiber reinforced thermoplastic composites using fused deposition modeling. Composites Part B: Engineering, 80, 369-378.

[58]   http://www.3dxtech.com/bright-white-abs-filament/

[59]   http://www.3dxtech.com/3dxstat-esd-abs-3d-printing-filament/

[60]   http://www.3dxtech.com/carbonx-carbon-fiber-abs-3d-printing-filament/

[61]   Maz, H. (2016). Estudio de las propiedades mecánicas de materiales compuestos de matriz polimérica fabricados mediante impresión 3D. Tesis de Bachiller. Pontificia Universidad Católica del Perú, Banco de Tesis, Ingeniería Mecánica.

[62]   ASTM D570-98(2010)e1, Standard Test Method for Water Absorption of Plastics, ASTM International, West Conshohocken, PA, 2010, www.astm.org

[63]   ASTM D638-14 (2010), Standard Test Method for Tensile Properties of Plastics, ASTM International, West Conshohocken, PA, 2014, www.astm.org

[64]   ASTM D7205 / D7205M-06 (2016), Standard Test Method for Tensile Properties of Fiber Reinforced Polymer Matrix Composite Bars, ASTM International, West Conshohocken, PA, 2016, www.astm.org

[65]   ASTM D257 (1993), Standard Test Methods for DC Resistance or Conductance of Insulating Materials, ASTM International, West Conshohocken, PA, 1993, www.astm.org

[66]   Lee, B. H., Cho, J. W., & Kim, K. H. (2017). Crystallization, orientation, and mechanical properties of laser-heated photothermally drawn

polypropylene/multi-walled carbon nanotube fibers. European Polymer Journal.

[67]   Rostami, A., Masoomi, M., Fayazi, M. J., & Vahdati, M. (2015). Role of multiwalled carbon nanotubes (MWCNTs) on rheological, thermal and electrical properties of PC/ABS blend. RSC Advances, 5(41), 32880-32890.

[68]   Zhang, W., Blackburn, R. S., & Dehghani-Sanij, A. (2007). Electrical conductivity of epoxy resin–carbon black–silica nanocomposites: effect of silica concentration and analysis of polymer curing reaction by FTIR. Scripta materialia, 57(10), 949-952.

[69]   Kaplan, R. S. (1983). Measuring manufacturing performance: a new challenge for managerial accounting research. In Readings in accounting for management control (pp. 284-306). Springer US.

[70]   Dul, S., Fambri, L., & Pegoretti, A. (2016). Fused deposition modelling with ABS–graphene nanocomposites. Composites Part A: Applied Science and Manufacturing, 85, 181-191.

[71]   Ma, P. C., Siddiqui, N. A., Marom, G., & Kim, J. K. (2010). Dispersion and functionalization of carbon nanotubes for polymer-based nanocomposites: a review. Composites Part A: Applied Science and Manufacturing, 41(10), 1345-1367.